ANA MARÍA VILLARREAL BARRERA

PHOSPHORUS ADSORPTION AND FERTILIZER POTENTIAL OF MG/AL-LAYERED DOUBLE HYDROXIDE-DOPED BIOCHAR

LAVRAS – MG
2025

ANA MARÍA VILLARREAL BARRERA

PHOSPHORUS ADSORPTION AND FERTILIZER POTENTIAL OF MG/AL-LAYERED DOUBLE HYDROXIDE-DOPED BIOCHAR

Thesis presented to the Federal University of Lavras, as part of the requirements of the Graduate Program in Soil Science, concentration area Soil Fertility and Plant Nutrition, to obtain the title of Doctor.

Advisor
Prof. Dr. Leônidas Carrijo Azevedo Melo

LAVRAS - MG
2025

Ficha catalográfica elaborada pelo Sistema de Geração de Ficha Catalográfica da Biblioteca Universitária da UFLA, com dados informados pelo(a) próprio(a) autor(a).

Villarreal Barrera, Ana María
Phosphorus adsorption and fertilizer potential of Mg/Al-layered double hydroxide-doped biochar / Ana María Villarreal Barrera. 2025.
114 p.

Orientador: Leônidas Carrijo Azevedo Melo.

Tese (Doutorado) - Universidade Federal de Lavras, 2025.
Bibliografia.

1. Phosphorus recovery. 2. Biochar-LDH composites. 3. Ball milling. 4. Maize plants. 5. Slow-release fertilizer. I. A. Carrijo Melo, Leônidas. II. Universidade Federal de Lavras. III. Título.

ANA MARÍA VILLARREAL BARRERA

ADSORÇÃO DE FÓSFORO E POTENCIAL FERTILIZANTE DE BIOCHAR DOPADO COM HIDRÓXIDO DUPLO EM CAMADAS DE MG/AL

PHOSPHORUS ADSORPTION AND FERTILIZER POTENTIAL OF MG/AL-LAYERED DOUBLE HYDROXIDE-DOPED BIOCHAR

Thesis presented to the Federal University of Lavras, as part of the requirements of the graduate program in Soil Science, area of concentration in Soil Fertility and Plant Nutrition, to earn the title of Doctor.

Approved on Jan 29, 2025
Dr. Leônidas A. Carrijo Melo UFLA
Dr. Carlos Alberto Silva UFLA
Dr. Maria Lígia de Souza Silva UFLA
Dr. José Ferreira Lustosa Filho UnB
Dr. Edson Marcio Matiello UFV

Dr. Leônidas A. Carrijo Melo
Advisor

LAVRAS, MG
2025

To God,
To my wonderful children Alejandra and Alex,
To my life partner Alex,
To my parents Lucy and Uly,
To my siblings Ana Isabel, Nilka and Ulises and to my beloved nephews,
I DEDICATE.

ACKNOWLEDGMENTS

I would like to thank all the people who supported me and were part of my PhD:

To the Federal University of Lavras, to the Faculty of Agricultural Sciences of Lavras and, especially, to the Department of Soil Sciences.

To the Coordination for the Improvement of Higher Education Personnel (CAPES) for providing the student scholarship.

To the National Council for Scientific and Technological Development (CNPq) and the Minas Gerais Research Support Foundation (FAPEMIG Grant APQ-01159-21) for their financial support.

To the National Secretariat of Science, Technology and Innovation (SENACYT) of Panama for their financial support for my studies.

To the University of Panama (UP) for giving me the opportunity to improve my academic development in another country.

To my advisor at UFLA, Prof. Dr. Leônidas Carrijo Azevedo Melo.

To all the professors of the Department of Soil Sciences of the Federal University of Lavras.

To Prof. Dr. Jairo Tronto, Federal University of Viçosa.

All the laboratory technicians, especially Lívia Botelho, Mariene Duarte, Aline Mesquita and Geila Carvalho.

To the city of Lavras for the welcome.

My research group, colleagues and friends: Aline Leite, Evanise Penido, Thiago Pereira, Isabela Durães, Daniela Queiroz, Thiago Viana, Andrés Montes, Felipe Sarto, Julian Sandoval and Giovanna Fontes.

Resumo Geral

O fósforo (P) é um nutriente essencial para o crescimento das plantas, e sua recuperação de fontes alternativas oferece uma estratégia sustentável para reciclar esse elemento crítico dentro de uma economia circular. O biochar, derivado da pirólise de biomassa, serve como matriz promissora para adsorção de P de águas residuais. No entanto, sua eficiência é limitada, exigindo funcionalização com metais para criar locais de adsorção eficazes. Hidróxidos Duplos Lamelares (LDHs), particularmente Mg/Al LDH, exibem excelente capacidade de adsorção de P devido à sua estrutura em camadas. Compósitos de biochar e LDH são materiais promissores que ganharam atenção considerável nos últimos anos. Este estudo examinou os efeitos da dopagem de biochar com Mg/Al LDH, via moagem com moinho de bolas, na capacidade de adsorção e dessorção de P em soluções aquosas e seu desempenho como fertilizante em solos tropicais. Biochars foram produzidos a partir de serragem de eucalipto impregnada com $Mg(OH)_2$ e pirolisada a 300 °C (BC300), 600 °C (BC600) e 900 °C (BC900). LDHs com razões molares Mg/Al de 1:1 (LDH1), 2:1 (LDH2), 3:1 (LDH3) e 4:1 (LDH4) foram sintetizados, e compósitos foram preparados usando 80% de biochar e 20% de LDH4 via moagem de bolas. A caracterização incluiu pH, condutividade eletrica (CE), umidade, teor de cinzas, teor total de nutrientes e carbono, análises de espectroscopia de infravermelho por transformada de Fourier (FTIR), difração de Raios-X (DRX), análise termogravimétrica (TG), microscopia eletrônica de varredura (MEV-EDS) e espectroscopia de fotoelétrons de Raios-X (XPS), cinética de adsorção e isotermas. BC300 e BC600 atingiram as maiores capacidades de adsorção de P (53,8 e 56,4 mg g^{-1}) em uma dose de 10 g L^{-1}, enquanto LDH4 exibiu adsorção superior (272 mg g^{-1}) em 1 g L^{-1}. A dopagem de BC300 com LDH4 aumentou a adsorção de P em 48,5%, e BC600 em 18,7%. O mecanismo mais provável de remoção de P foi a formação de complexo de superfície, conforme observado por XPS. O biochar dopado com $Mg(OH)_2$ adsorveu principalmente P por meio da precipitação de fosfato de Mg. Experimentos em casa de vegetação demonstraram que os compostos de biochar carregado com P e biochar-LDH aumentaram significativamente o crescimento do milho e o acúmulo de P em tecidos vegetais em comparação com LDH carregado com P. No segundo cultivo, BC300-LDH produziu 28% mais materia seca que o superfosfato triplo. A análise do solo revelou melhorias no pH, Mg e disponibilidade de P, juntamente com aumento da saturação de bases (V%), soma de bases (SB) e P remanescente (P-rem). Isso demostra que esses compósitos de biochar-LDH carregados com P tem potencial como fertilizantes de liberação lenta e podem apresentar eficiência aumentada em solos tropicais. Concluindo, a dopagem a seco do biochar com Mg/Al LDH via moinho de bolas provou ser um método simples e eficaz para a produção de compósitos visando aumentar a capacidade de adsorção de P. Além disso, os compósitos de biochar-LDH carregados com P mostraram-se promissores como fertilizantes alternativos, oferecendo uma abordagem sustentável para reduzir a dependência de fertilizantes de P totalmente solúveis.

Palavras-chave: recuperação de fósforo, compostos biochar-LDH, moagem de bolas, plantas de milho, fertilizante de liberação lenta

General Abstract

Phosphorus (P) is an essential nutrient for plant growth, and its recovery from alternative sources offers a sustainable strategy to recycle this critical element within a circular economy. Biochar, derived from biomass pyrolysis, is a promising matrix for P adsorption from wastewater. Nevertheless, its efficiency is limited, requiring functionalization with metals to create effective adsorption sites. Double layer hydroxides (LDHs), particularly Mg/Al LDH, exhibit excellent P adsorption capacity due to their layers structure. Biochar and LDH composites are promising materials that have gained considerable attention in recent years. This study examined the effects of biochar doping with Mg/Al LDH, through ball milling on the adsorption and desorption capacity of P in aqueous solutions and their performance as fertilizer in tropical soils. Biochars were produced from eucalyptus sawdust impregnated with $Mg(OH)_2$ and pyrolyzed at 300 °C (BC300), 600 °C (BC600) and 900 °C (BC900). LDHs with Mg/Al molar ratios of 1:1 (LDH1), 2:1 (LDH2), 3:1 (LDH3) and 4:1 (LDH4), and composites were prepared using 80% biochar and 20% LDH4 via ball milling. Characterization included pH, electrical conductivity (CE), humidity, ash content, total nutrient and carbon content, Fourier-transform infrared spectroscopy (FTIR), X-ray diffraction (DRX), thermogravimetric analysis (TG), scanning electron microscopy (SEM-EDS) and X-ray photoelectron spectroscopy (XPS) analyses, adsorption kinetics and isotherms. BC300 and BC600 achieved the highest P adsorption capacities (53.8 and 56.4 mg g^{-1}) at a 10 g^{-1} dose, while LDH4 displayed upper adsorption (272 mg g^{-1}) at 1 g^{-1}. Doping BC300 with LDH4 increased P adsorption by 48.5%, and BC600 in 18.7%. The most likely P-removal mechanism was the formation of surface complex as observed by XPS. Biochar doped with $Mg(OH)_2$ adsorbed P primarily through the precipitation of Mg phosphate. Greenhouse experiments showed that P-loaded biochar and biochar-LDH composites significantly enhanced maize growth and P accumulation in plant tissues compared to P-loaded LDH. In the second cultivation cycle, BC300-LDH produced 28% more dry matter than triple superphosphate. Soil analysis showed improvements in pH, Mg and P availability, along with increased base saturation (V%), bases (SB) and P remaining (P-rem). This demonstrates that these P-loaded biochar-LDH composites have potential as slow-release fertilizers and may exhibit increased efficiency in tropical soils. In conclusion, the dry doping of biochar with Mg/Al ldh via ball milling proved to be a simple and effective method for composites production to increase P adsorption capacity. Furthermore, P-loaded biochar-LDH composites showed promise as alternative fertilizers, offering a sustainable approach to reduce reliance on fully soluble P fertilizers.

Keywords: phosphorus recovery, biochar-LDH composites, ball milling, maize plants, slow-release fertilizer

Indicadores de Impacto

O fósforo é um elemento essencial para a vida, pois faz parte do DNA, membranas celulares e é fundamental no armazenamento e transferência de energia nos seres vivos. Sua presença é vital para o crescimento das plantas e, portanto, para a produção de alimentos. No entanto, atualmente enfrenta uma situação crítica devido à superexploração de suas fontes não renováveis, principalmente rochas fosfóricas. Portanto, a reciclagem de fósforo na agricultura se torna fundamental para preservar esse recurso escasso e garantir a segurança alimentar futura. Este estudo avaliou a eficiência de um biochar a partir da serragem do eucalipto dopado com hidróxido de dupla camada de Mg/Al na recuperação de fósforo e subsequente uso como fertilizante com base em P. Os impactos sociais e econômicos são evidentes na promoção do uso práticas ou materiais ecológicos sustentáveis, com um efeito bilateral: melhoria da fertilidade do solo e da qualidade da água; e um menor custo de produção. A reciclagem do P, através desse tipo de materiais ecológicos (resultante da transformação de resíduos) pode reduzir a dependência de fontes solúveis de P, reduzindo os custos de produção, fornecendo valor agregado à fertilidade do solo. Do ponto de vista ambiental, os resultados obtidos mostram que esses compósitos biochar-LDH da serragem de eucalipto são eficientes como fontes de P. Isso sugere que, culturas como milho, respondem positivamente a essas fontes ecológicas de P, reduzindo a pressão das fontes convencionais desse nutriente e os impactos negativos que os carregam.

Embora seus efeitos sejam claramente observáveis no campo experimental, os resultados deste estudo têm alto potencial de expansão, especialmente quando se integra em iniciativas de extensão rural e transferência tecnológica. A disseminação desse conhecimento pode incentivar a implementação de práticas agrícolas responsáveis no cultivo do milho, alcançando um equilíbrio entre eficiência produtiva, proteção do ambiente natural e segurança alimentar.

Os impactos deste estudo são divididos em três áreas temáticas da Política Nacional de Extensão: Meio Ambiente, prometendo o uso de tecnologias amigáveis ao meio ambiente; Tecnologia e produção, sugerindo o uso dos compostos biochar-LDH como fontes de fertilizantes de P; e Trabalho, permitindo que técnicos e agricultores melhorem as condições de trabalho no campo. Além disso, contribui para sete dos 17 Objetivos de Desenvolvimento Sustentável (ODS) da ONU: ODS 2. Fome Zero e Agricultura Sustentável, promovendo práticas agrícolas ecológicas sustentáveis e produtivas SDG 6. Água potável e saneamento, contribuindo para a descontaminação das águas; ODS 9. Inovação e infraestrutura, aplicando tecnologias inovadoras e replicáveis; ODS 12. Consumo e produção responsáveis, reduzindo a pressão sobre fontes completamente solúveis de P; ODS 13. Ação contra as mudanças climáticas globais, capturando C através do biochar e reciclando de forma limpa do P; ODS 14. Vida na água, limpando as águas, permitindo o equilíbrio deste Recurso SDG 15. Vida terrestre, contribuindo para a segurança alimentar.

Impacts Indicators

Phosphorus is an essential element for life as it is part of DNA, cell membranes and is fundamental in storage and energy transfer in living beings. Its presence is vital for plant growth and therefore for food production. However, it currently faces a critical situation due to the overexploitation of its non-renewable sources, especially phosphoric rocks. Therefore, phosphorus recycling in agriculture becomes fundamental to preserve this scarce resource and ensure future food security. This study evaluated the efficiency of a biochar from eucalyptus sawdust doped with Mg/Al-layered double hydroxide in the recovery of phosphorus and

subsequent use as a P-based fertilizer. Social and economic impacts are evident in promoting sustainable ecological use, with a bilateral effect: improving soil fertility and water quality; and a lower cost of production. P recycling, through this type of ecological materials (resulting from waste transformation) can reduce dependence on P-sources of P, reducing production costs, providing value added to soil fertility. From an environmental point of view, the results show that these biochar-LDH composites of eucalyptus sawdust are efficient as P sources. This suggests that crops such as maize respond positively to these ecological sources of P, reducing pressure from the conventional sources of this nutrient and the negative impacts that carry them. Although its effects are clearly observable in the experimental field, the results of this study have high expansion potential, especially when it is part of rural extension and technological transfer initiatives. The dissemination of this knowledge can encourage the implementation of agricultural practices responsible for corn cultivation, reaching a balance between productive efficiency, natural environment protection and food safety.

The impacts of this study are divided into three thematic areas of the National Extension Policy: Environment, promising the use of environmental technologies; Technology and Production, suggesting the use of Biochar-LDH compounds as s sources of P fertilizers; and Work, allowing technicians and farmers to improve working conditions in the field. In addition, it contributes to seven of the 17 United Nations Sustainable Development Goals (SDGs): SDG 2. Zero hunger and sustainable agriculture, promoting sustainable and productive agricultural practices SDG 6. Drinking water and sanitation, contributing to water decontamination; SDG 9. Innovation and Infrastructure, applying innovative and replicable technologies; SDG 12. Responsible consumption and production, reducing pressure on completely soluble sources of P; SDG 13. Action against global climate change, capturing C through biochar and cleanly recycling P; SDG 14. Life in water, cleaning the waters, allowing the balance of this resource SDG 15. Earthly life, contributing to food safety.

SUMMARY

FIRST PART 13
GENERAL INTRODUCTION 13
REFERENCES 17
SECOND PART - ARTICLES 21
CHAPTER 1 – Facile MgAl-layered double hydroxide doping enhances phosphorus adsorption capacity in eucalyptus sawdust biochar 21
1 INTRODUCTION 23
2 MATERIAL AND METHODS 25
2.1 Biomass sampling and biochar preparation 25
2.2 LDH synthesis 26
2.3 Biochar-LDH composites 27
2.4 Adsorbents characterization 28
2.5 Adsorption experiments 30
2.5.1. Adsorption isotherms 30
2.5.2. Adsorption kinetics 31
3 STATISTICAL ANALYSIS 31
4 RESULTS 31
4.1 Effects of LDH on forming composites 31
4.1.1 BET Surface Area 31
4.1.2 Other properties related to adsorption 33
4.1.3 Scanning electron microscopy 34
4.1.4 Thermogravimetric analysis (TGA) and Fourier-transform infrared spectroscopy (FTIR) 37
4.1.5 X-ray diffraction (XRD) 39
4.2 Phosphorus adsorption 42
4.2.1 Adsorption kinetics 42
4.2.2 Adsorption isotherms 45
4.2.3 XPS analysis 48
5 CONCLUSION 50
REFERENCES 52
SUPPLEMENTARY MATERIAL 61

CHAPTER 2 - Phosphorus-loaded MgAl-LDH-biochar composites as a potential phosphate fertilizer for maize growth in acidic soil 76
1 INTRODUCTION 78
2 MATERIALS AND METHODS 81
2.1 Adsorbents preparation 81
2.2 Adsorption-Desorption study 81
2.3 Pot experiment 82
3 DATA ANALYSIS STATISTICS 84
4 RESULTS AND DISCUSSION 85
4.1 Desorption study 85
4.2 Greenhouse experiment 87
5 CONCLUSION 100
REFERENCES 101
SUPPLEMENTARY MATERIAL 111
CONCLUDING REMARKS 11

FIRST PART

General Introduction

Biochar is a carbon-rich material produced through pyrolysis; a thermal decomposition process carried out at relatively low temperatures (300–700 °C) under limited oxygen conditions (Lehmann et al., 2024). This process prevents complete combustion, allowing carbon to be locked into a more persistent and solid form rather than being released as carbon dioxide or other greenhouse gases (Brown, 2021). Biochar can be derived from a wide range of natural and waste feedstocks, including forest and agricultural residues, industrial by-products, animal manure, and municipal solid waste (Ponnusamy et al., 2020; Yi et al., 2020). The feedstock type and pyrolysis conditions play a crucial role in determining the physicochemical characteristics of the resulting biochar, including its carbon content, surface area, pore structure, and chemical composition (Zhang et al., 2017).

Due to its unique physicochemical properties, such as high surface area, porosity, acid buffering capacity, cation exchange capacity, and enriched surface functional groups, biochar holds significant potential for diverse applications. In agriculture, biochar is widely recognized as a soil amendment that improves soil fertility, enhances water retention, and reduces nutrient leaching, ultimately leading to increased crop yields (Alkharabsheh et al., 2021). Its ability to sequester carbon in soils for extended periods makes it a valuable tool in mitigating climate change (Lehmann et al., 2021). In environmental remediation, biochar has shown promise in adsorbing heavy metals, organic pollutants, and excess nutrients from wastewater, thereby contributing to water purification and pollution control (Chabi et al., 2020; Liu et al., 2019; Wang et al., 2018). In addition, biochar can serve as a feedstock for bioenergy production, supporting sustainable energy systems (Lee et al., 2020). Its role in biomass waste management also helps reduce environmental burdens by converting organic waste into a stable and valuable product. Overall, biochar represents a versatile and sustainable material with significant contributions to agriculture, environmental protection, renewable energy, and climate change mitigation efforts.

Given the abundance of potential feedstocks, low biodegradability, and low environmental risk, biochar emerges as a valuable material with exceptional adsorption qualities (Singh et al., 2024).

Forest production in Brazil is 10,2 million hectares planted with eucalyptus, pine trees and other species (IBÁ, 2024). Minas Gerais represents more than 2.3 million hectares of trees planted nationwide, of which 96.8% correspond to eucalyptus plantations (AMIF, 2023).

The use of biochar produced from eucalyptus residues, which is an abundant and easily acquired material in several countries (Heidari et al., 2019) and due to its high efficiency and rapid growth, especially in Brazilian plantation conditions, eucalyptus plays a prominent role in biochar research. In addition to traditional uses such as paper, construction and furniture, wood can be used with high efficiency in bioenergy generation, with important by-products such as biochar (Maia, et al., 2021).

While traditionally used for soil remediation and amendment, there is a growing number of studies exploring the application of biochar for the removal of pollutants from water, largely due to its cost-effectiveness and sustainability (Choudhary et al., 2020). The role of biochar in wastewater treatment aligns with the principles of circular economy, which focuses on resource efficiency, waste minimization, reduced raw material consumption, and environmental protection, all while generating economic benefits (Morseletto, 2020). Thus, biochar can be specifically designed for water remediation and subsequently reintegrated into production systems, contributing to a sustainable and closed-loop economic model.

Phosphorus (P) is an essential nutrient for all living organisms. However, its natural sources are finite, increasingly scarce, and irreplaceable. The rising global population drives a higher demand for food production and, consequently, for phosphate-based fertilizers (Desmidt et al., 2014). This growing dependency may lead to the depletion of easily accessible P reserves (Iwaniec et al., 2016). Additionally, the extraction and processing of phosphate rock are energy-intensive and environmentally damaging, contributing to habitat destruction and pollution (Fayiga and Nwoke, 2016). As a result, P recycling is becoming increasingly critical to sustain agricultural productivity while minimizing environmental pollution.

A significant portion of P is lost through improper waste and wastewater disposal, contributing, along with nitrogen (N), to the eutrophication of aquatic ecosystems, which leads to algal blooms, oxygen depletion, and loss of aquatic biodiversity (Cai et al., 2019). Furthermore, inefficient fertilizer application practices exacerbate these losses, reducing the overall efficiency of P use in agriculture (Bindraban et al., 2020). In tropical agricultural systems, P dynamics are particularly complex due to the unique characteristics of tropical soils. These soils are often highly weathered, acidic, and rich in iron (Fe) and aluminum (Al) oxides, which strongly bind P, making it largely unavailable to plants (Gérard, 2016). Even with substantial P fertilizer inputs, a significant fraction becomes immobilized through adsorption

onto soil mineral surfaces or precipitation as insoluble compounds (Zhu et al., 2018). Furthermore, tropical regions frequently experience intense rainfall, which accelerates soil erosion and P runoff, leading to substantial nutrient losses from agricultural fields and contributing to downstream eutrophication (Lucas et al., 2023). Inefficient fertilizer application practices, such as overuse, poorly timed application, and reliance on soluble phosphate fertilizers, exacerbate these losses, reducing P use efficiency and increasing environmental risks (Bindraban et al., 2020). To address these challenges, sustainable P management strategies tailored to tropical soil conditions are essential, including the use of slow-release fertilizers, organic amendments, precision agriculture techniques, and innovative materials like biochar to minimize losses, and enhance crop uptake efficiency.

Recovering P from wastewater using biochar is a promising and sustainable approach to facilitate P recycling and reuse in agriculture. Additionally, biochar-based P recovery systems can be integrated into wastewater treatment plants, providing an economically viable and environmentally friendly solution. This approach not only reduces dependency on finite phosphate rock reserves but also mitigates water pollution, supporting a circular economy model in nutrient management. The surface of biochar, however, can be predominantly characterized by negative charges, primarily due to a high pH and the presence of oxygen-containing functional groups. This results in a low adsorption capacity for phosphate ions ($H_2PO_4^-$ or HPO_4^{2-}) from aqueous solutions (Takaya et al., 2016; Shepherd et al., 2016). Additionally, the adsorption of phosphate ions on biochar is influenced by factors such as biochar feedstock, pyrolysis temperature, and the chemical composition of the resulting biochar surface. For example, biochars produced at higher pyrolysis temperatures tend to have a higher degree of carbonization, leading to a decrease in surface functional groups, which further reduces their ability to bind phosphate anions (Li et al., 2017).

An effective approach to enhance the specific surface area, pore volume, and pore structure of biochar for various environmental applications is through chemical or physical modifications that improve its physicochemical properties. Chemical treatments, such as impregnation with metal ions (e.g., magnesium, iron, or aluminum), or physical treatments, such as thermal activation, have been shown to significantly increase phosphate adsorption capacity by introducing positively charged adsorption sites (Shin et al., 2020). In this context, the combination of biochar and Layered Double Hydroxides (LDHs) emerges as a promising strategy to overcome these limitations.

Layered double hydroxides (LDHs) are a class of crystalline materials characterized by a layered structure composed of positively charged metal hydroxide sheets and interlayer spaces

containing charge-balancing anions and water molecules (Hassani et al., 2017; Gao et al., 2020). These materials have gained significant attention due to their wide range of applications, particularly in water treatment. The combination of LDHs with biochar as composite materials has shown significant improvements in physicochemical properties, including increased specific surface area, enhanced surface functional groups, structural heterogeneity, stability, and superior adsorption performance (Chen et al., 2018; Meili et al., 2019). The production of biochar-LDH composites is a sustainable and cost-effective alternative with exceptional efficiency in removing various toxic pollutants. Moreover, their high reusability can significantly reduce the overall cost of water treatment processes. The porous biochar structure acts as an ideal support matrix, providing a large reactive surface area for effective LDH deposition while preventing LDH aggregation (He et al., 2019). However, further studies are needed to fully understand the underlying adsorption mechanisms and to evaluate how this material would function as a P fertilizer in tropical soils. Moreover, most studies combining biochar and LDH (Chen and Qu, 2004; Zhang et al., 2013, Yang et al., 2019) have relied on wet processes, which pose significant challenges for large-scale production. To address this limitation, we propose, for the first time, the evaluation of a dry synthesis method using ball milling to produce biochar–LDH composites, aiming to simplify the process and enhance scalability. A deeper understanding of this approach is presented in the next two chapters, which explore the mechanisms of phosphorus (P) adsorption by biochar–LDH composites and, following P recovery from aqueous solutions, assess their potential as phosphate fertilizers under tropical soil conditions.

This research was guided by the following questions:

- Can Mg-enriched eucalyptus sawdust biochar doped with LDH improve P adsorption compared to unmodified biochar? Under which pyrolysis and LDH doping conditions does this improvement occur?
- Do biochar–LDH composites have potential as P fertilizers? How do they influence maize growth? Can they fully or partially replace conventional soluble P fertilizers?

In Chapter 1, we hypothesize that doping biochar with LDH to form biochar–LDH composites enhances P adsorption capacity. In Chapter 2, we hypothesize that maize dry matter production and other growth parameters will be improved when using biochar–LDH composites produced at lower pyrolysis temperatures.

Dissertation outline

In Chapter 1, we examined the production of biochar and layered double hydroxides (LDHs), along with their individual phosphorus (P) adsorption properties. We then investigated the synthesis of biochar–LDH composites and their mechanisms for P adsorption from aqueous solutions. To achieve this, we applied kinetic and isotherm adsorption studies alongside advanced characterization techniques, including X-ray diffraction (XRD), Fourier-transform infrared spectroscopy (FTIR), scanning electron microscopy coupled with energy-dispersive X-ray spectroscopy (SEM-EDX), and X-ray photoelectron spectroscopy (XPS).

In Chapter 2, we assessed the desorption capacity of P from these materials using different chemical extractants to simulate P release. A greenhouse experiment was then conducted to evaluate the effectiveness of these materials as P sources under tropical soil conditions using maize as the test crop.

References

ASSOCIAÇÃO MINEIRA DA INDÚSTRIA FLORESTAL (AMIF), 2023. **Área plantada por estado brasileiro.** Available in: https://amif.org.br/. Accessed: February 24, 2025

ALKHARABSHEH, H. M., SELEIMAN, M. F., BATTAGLIA, M. L., SHAMI, A., JALAL, R. S., ALHAMMAD, B. A., ALMUTAIRI, K. F., & AL-SAIF, A. M. 2021. **Biochar and Its Broad Impacts in Soil Quality and Fertility, Nutrient Leaching and Crop Productivity: A Review**. Agronomy 11, 993. https://doi.org/10.3390/agronomy11050993

BINDRABAN, P.S., DIMKPA, C.O., PANDEY, R. 2020. **Exploring phosphorus fertilizers and fertilization strategies for improved human and environmental health**. Biol. Fertil. Soils 56, 299–317. https://doi.org/10.1007/s00374-019-01430-2

BROWN, R.C. 2021. **The Role of Pyrolysis and Gasification in a Carbon Negative Economy**. Processes 9, 882. https://doi.org/10.3390/pr9050882

CAI R., WANG X., JI X., PENG B., TAN C., HUANG X. 2019. **Phosphate reclaim from simulated and real eutrophic water by magnetic biochar derived from water hyacinth**. J Environ Manage 187, 212–219. https://doi.org/10.1016/j.jenvman.2016.11.047

CHABI, N., BAGHDADI, M., HALLAJI SANI, A., GOLZARY, A., HOSSEINZADEH, M., 2020. **Removal of tetracycline with Aluminum Boride Carbide and boehmite particles decorated biochar derived from algae**. Bioresour. Technol. 123950. https://doi.org/10.1016/j.biortech.2020.123950

CHEN, S., HUANG, Y., HAN, X., WU, Z., LAI, C., WANG, J., DENG, Q., ZENG, Z., DENG, S. 2018. **Simultaneous and efficient removal of Cr (VI) and methyl orange on LDHs**

decorated porous carbons. Chem. Eng. J. 352, 306–315. https://doi.org/10.1016/j.cej.2018.07.012

CHEN, W., QU, B.J. 2004. **LLDPE/ZnAlLDH-exfoliated nanocomposites: effects of nanolayers on thermal and mechanical properties**. J. Mater. Chem. 14, 1705– 1710. https://doi.org/10.1039/B401790K

CHOUDHARY, M., KUMAR, R., NEOGI, S. 2020. **Activated biochar derived from Opuntia ficus-indica for the efficient adsorption of malachite green dye, Cu^{2+} and Ni^{2+} from water**. J. Hazard. Mater. 392, 12244-12249. https://doi.org/10.1016/j.jhazmat.2020.122441

DESMIDT, E., GHYSELBRECHT, K., ZHANG, Y., PINOY, L., VAN DER BRUGGEN, B., VERSTRAETE, W., RABAEY, K., MEESSCHAERT, B. 2014. **Global Phosphorus Scarcity and Full-Scale P-Recovery Techniques: A Review**. Crit. Rev. Environ. Sci. Technol. *45*, 336–384. https://doi.org/10.1080/10643389.2013.866531

FAYIGA, A.O., NWOKE, O.C. 2016. **Phosphate rock: origin, importance, environmental impacts, and future roles**. Environ.Rev. 24, 403-415. https://doi.org/10.1139/er-2016-0003

GAO, X., PENG, Y., GUO, L., WANG, Q., GUAN, C.-Y., YANG, F., CHEN, Q., 2020. **Arsenic adsorption on layered double hydroxides biochars and their amended red and calcareous soils**. J. Environ. Manage. 271, 111045. https://doi.org/10.1016/j.jenvman.2020.111045

GÉRARD, F. 2016. **Clay minerals, iron/aluminum oxides, and their contribution to phosphate sorption in soils — A myth revisited**. Geoderma 262, 213-226. https://doi.org/10.1016/j.geoderma.2015.08.036.

HASSANI, E.K., BEAKOU, B.H., KALNINA, D., OUKANI, E., ANOUAR, A. 2017. **Effect of morphological properties of layered double hydroxides on adsorption of azo dye Methyl Orange: a comparative study**. Appl. Clay Sci. 140, 124–131. https://doi.org/10.1016/j.clay.2017.02.010

HE, H., ZHANG, N., CHEN, N., LEI, Z., SHIMIZU, K., ZHANG, Z. 2019. **Efficient phosphate removal from wastewater by MgAl-LDHs modified hydrochar derived from tobacco stalk**. Bioresour. Technol. Reports 8, 100348. https://doi.org/10.1016/j.biteb.2019.100348

HEIDARI, A., KHAKI, E., YOUNESI, H., LU, H.R. 2019. **Evaluation of fast and slow pyrolysis methods for bio-oil and activated carbon production from eucalyptus wastes using a life cycle assessment approach**. J Clean Prod 241, 118394. https://doi.org/10.1016/J.JCLEPRO.2019.118394

INDÚSTRIA BRASILEIRA DE ÁRVORES (IBÁ), 2024. **Anual Report**. Available in: https://iba.org/datafiles/publicacoes/relatorios/relatorio2024.pdf. Accessed: February 24, 2025

IWANIEC, D.M., METSON, G.S., CORDELL, D. 2016. **P-FUTURES: towards urban food andamp; water security through collaborative design and impact**. Curr Opin Environ Sustain. 20, 1–7. https://doi.org/10.1016/j.cosust.2016.03.001

LEHMANN, J., COWIE, A., MASIELLO, C.A., KAMMANN, C., WOOLF, D., AMONETTE, J.E., CAYUELA, M.L., CAMPS-ARBESTAIN, M., WHITMAN, T. 2021. **Biochar in climate change mitigation**. Nat. Geosci. 14, 883–892. https://doi.org/10.1038/s41561-021-00852-8

LEHMANN, J., JOSEPH., S (Eds.). 2015. **Biochar for Environmental Management.** London: Routledge, 1–12. doi:10.4324/ 9780203762264

Li, H., Dong, X., Silva, E.B.da., Oliveira, L.M.de., Chen, Y., Ma, L.Q. 2017. **Mechanisms of metal sorption by biochars: Biochar characteristics and modifications.** Chemosphere 178, 466-478. https://doi.org/10.1016/j.chemosphere.2017.03.072.

LIU, W.-J., JIANG, H., YU, H.-Q., 2019. **Emerging applications of biochar-based materials for energy storage and conversion**. Energy Environ. Sci. 12, 1751–1779. https://doi.org/10.1039/C9EE00206E

MEILI, L., LINS, P.V., ZANTA, C.L.P.S., SOLETTI, J.I., RIBEIRO, L.M.O., DORNELAS, C.B., SILVA, T. L., VIEIRA, M.G.A. 2019. **MgAl-LDH/Biochar composites for methylene blue removal by adsorption**. Appl. Clay Sci. 168, 11–20. https://doi.org/10.1016/j.clay.2018.10.012

LEE, M., LIN, Y-L., CHIUEH, P-T., DEN, W. 2020. **Environmental and energy assessment of biomass residues to biochar as fuel: A brief review with recommendations for future bioenergy systems**. J. Clean. Prod. 251, 119714. https://doi.org/10.1016/j.jclepro.2019.119714.

LUCAS, E., KENNEDY, B., ROSWALL, T., BURGIS, C., TOOR, G.S. 2023. **Climate Change Effects on Phosphorus Loss from Agricultural Land to Water: A Review.** Curr. Pollution. Rep. 9, 623–645. https://doi.org/10.1007/s40726-023-00282-7

MAIA, C. M. B. de F., GUIOTOKU, M., PEIXOTO, R. T dos G., VARGAS, L. M. P. Biochar e o eucalipto. *In*: OLIVIERA, E. B. de, PINTO JUNIOR, J. E. (Embrapa). **O eucalipto e a Embrapa: quatro décadas de pesquisa e desenvolvimento**. Brasília, DF: Embrapa, 2021. P. 589-610.

MORSELETTO, P., 2020. **Targets for a circular economy**. RCR Advances. 153, 53-59. https://doi.org/10.1016/j.resconrec.2019.104553

PONNUSAMY, V.K., NAGAPPAN, S., BHOSALE, R.R., LAY, C.-H., DUC NGUYEN, D., PUGAZHENDHI, A., CHANG, S.W., KUMAR, G., 2020. **Review on sustainable production of biochar through hydrothermal liquefaction: physico-chemical properties and applications**. Bioresour. Technol. 310, 123414. https://doi.org/10.1016/j.biortech.2020.123414

SINGH, S., KHAN, N.A., SHEHATA, N., SINGH, J., RAMAMURTHY, P.C. 2024. **Insight into biochar as sustainable biomass: Production methods, characteristics, and environmental remediation**. J. Clean. Prod**.** 475, 143645. https://doi.org/10.1016/j.jclepro.2024.143645.

SHEPHERD, J.G., SOHI, S.P., HEAL, K.V. 2016. **Optimising the recovery and re-use of phosphorus from wastewater effluent for sustainable fertiliser development**. Water Res. 94, 155–165. https://doi.org/10.1016/j.watres.2016.02.038

SHIN, H., TIWARI, D., KIM, D-J. 2020. **Phosphate adsorption/desorption kinetics and P bioavailability of Mg-biochar from ground coffee waste**. J. Water Process Eng. 37, 101484. https://doi.org/10.1016/j.jwpe.2020.101484.

TAKAYA, C.A., FLETCHER, L.A., SINGH, S., ANYIKUDE, K.U., ROSS, A.B. 2016. **Phosphate and ammonium sorption capacity of biochar and hydrochar from different wastes**. Chemosphere 145, 518–527. https://doi.org/10.1016/j.chemosphere.2015.11.052

YANG, F., ZHANG, S., SUN, Y., TSANG, D.C.W., CHENG, K., OK, Y.S. 2019. **Assembling biochar with various layered double hydroxides for enhancement of phosphorus recovery**. J. Hazard. Mater. 365, 665-673. https://doi.org/10.1016/j.jhazmat.2018.11.047

YI, Y., HUANG, Z., LU, B., XIAN, J., TSANG, E.P., CHENG, W., FANG, J., FANG, Z., 2020. **Magnetic biochar for environmental remediation: a review**. Bioresour. Technol. 298, 122468. https://doi.org/10.1016/j.biortech.2019.122468

WANG, T., LI, C., WANG, C., WANG, H., 2018. **Biochar/MnAl-LDH composites for Cu (II) removal from aqueous solution. Colloids Surfaces A Physicochem.** Eng. Asp. 538, 443–450. https://doi.org/10.1016/j.colsurfa.2017.11.034

ZHANG, H., CHEN, C., GRAY, E.M., BOYD, S.E. 2017. **Effect of feedstock and pyrolysis temperature on properties of biochar governing end use efficacy**. Biomass and bioenergy https://doi.org/10.1016/j.biombioe.2017.06.024

ZHANG, M., GAO, B., YAO, Y., INYANG, M. 2013. **Phosphate removal ability of biochar/MgAl LDH ultra-fine composites prepared by liquid-phase deposition**. Chemosphere 92, 1042-1047. https://doi.org/10.1016/j.chemosphere.2013.02.050

ZHU, L., LI, M., WHELAN, M. 2018. **Phosphorus activators contribute to legacy phosphorus availability in agricultural soils: A review**. Sci. Total Environ. 612, 522-537. https://doi.org/10.1016/j.scitotenv.2017.08.095

SECOND PART – ARTICLES

CHAPTER 1

Facile MgAl-layered double hydroxide doping enhances phosphorus adsorption capacity in eucalyptus sawdust biochar

To be submitted to Chemosphere journal

Facile MgAl-layered double hydroxide doping enhances phosphorus adsorption capacity in eucalyptus sawdust biochar

Ana María Villarreal Barrera[a,b], Evanise Silva Penido[a], Aline do Amaral Leite[a], Andres Olaya Montes[a,c], Thiago Costa Viana[a], Daniela Dourado Leal Quiroz[a], Giovana Pereira Nunes[a], Jairo Tronto[d], Leônidas Carrijo Azevedo Melo[a*]

[a] Federal University of Lavras/UFLA – Soil Science Dept., 37203-202, Lavras, Brazil
[b] University of Panama/UP – Soil and Water Dept., 772-9085, Chiriqui, Panama
[c] University of Amazon – Faculty of Engineering, 84358786, Caqueta, Colombia
[d] Federal University of Viçosa/UFA - Institute of Exact and Technological Sciences, Viçosa, Brazil

*corresponding author: leonidas.melo@ufla.br

Abstract

The use of biochar as a matrix for removing phosphate from wastewater is a promising approach for phosphorus (P) recovery within the principles of circular economy, resulting in biochar-based fertilizers. Doping biochar with metals is can create sites for even more effective P adsorption. Layered-double hydroxides (LDH) have shown excellent P adsorption properties, yet their association with biochar to form a composite is still poorly understood, especially through dry methods (e.g., ball milling). This study investigated the effects of doping biochar with Mg-Al-CO_3-LDH through ball milling on P adsorption in aqueous medium. The biochars were produced from eucalyptus sawdust impregnated with $Mg(OH)_2$ and pyrolyzed at 300 (BC300), 600 (BC600) and 900 °C (BC900). Mg/Al-CO_3 LDHs were synthesized in proportions of 1:1 (LDH1), 2:1 (LDH2), 3:1 (LDH3) and 4:1 (LDH4) Mg/Al molar ratios; and composites were prepared with 80% biochar and 20% LDH by 30 min of ball milling. P adsorption kinetics and isotherms were performed. Characterizations included measurements of pH, electrical conductivity, moisture and ash contents, total nutrient contents, total C, point of zero chage (PZC), Fourier transform infrared spectroscopy (FTIR), X-ray diffraction (XRD), thermogravimetric analysis (TGA), scanning electron microscopy (SEM-EDS) and X-ray photoelectron spectroscopy (XPS). The highest P removal by biochar was obtained in BC300 and BC600 (53.8 and 56.4 mg g^{-1}, respectively) at a dose of 10 g L^{-1}. LDH4 showed the highest P adsorption (272 mg g^{-1}) among the LDHs at a dose of 1 g L^{-1}. Doping BC300 with LDH4 increased the P adsorption capacity of by 48.5% and BC600 by 18.7% at the dose of 5 g L^{-1}. This was likely due to the formation of complexes with functional groups containing in LDH as demonstrated by XPS analysis. The main mechanism for P adsorption by biochar doped with Mg was precipitation of magnesium phosphate. The dry doping of biochar with LDH using a ball mill proved to be a straightforward and effective technique for biochar functionalization. In conclusion, biochar doped with Mg/Al-CO_3 LDH is an efficient alternative for enhancing P removal from aqueous solutions. Further studies on the reuse of P-loaded biochar as a fertilizer are crucial not only for closing the P cycle but also for enhancing its economic feasibility.

Keywords: recycling; fertilizer; slow-release; pyrogenic carbon

Highlights

- The Mg/Al molar ratio of 4:1 showed the highest P adsorption capacity for LDHs.

- Low pyrolysis temperature had greater synergy between biochar and LDH for P removal.
- Precipitation of magnesium phosphates was the main adsorption mechanism.
- The formation of P-O complexes with –OH after P adsorption improves P availability

1. Introduction

Phosphorus (P) is an essential element for living organisms, but its supply is limited and irreplaceable. Phosphorus in soil primarily exists in insoluble mineralforms, limiting its bioavailability and thereby restrict-ing plant uptake and utilization (Ringeval et al. 2024).

With global population growth in recent decades, it is crucial to improve the P recycling to ensure adequate food production and minimize the damage caused by its misuse and mismanagement. Misuse examples include the over-application of phosphate fertilizers, leading to nutrient runoff into water bodies, harmful algal blooms, and eutrophication (Huang et al., 2017). The extraction of phosphate rocks to produce soluble fertilizers is expected to increase over time (Scholz et al., 2013), posing risks to agricultural production and, by extension, global food security (Iwaniec et al., 2016). Increasing available P in agricultural soils is essential, as P is a macronutrient critical for plant growth (Tian et al. 2024).

Brazil plays a major role in global agriculture as one of the largest producers and exporters of key agricultural commodities such as soybeans, sugar, coffee, beef, and chicken, significantly contributing to global food security. However, much of its territory consists of soils with a high P fixing capacity due to advanced weathering and the presence of kaolinite and Fe and Al oxyhydroxides in the clay fraction (Roy et al., 2016). This challenge is exacerbated by the dependence on imports for >50% of the industrial phosphate needed for food production (ANDA, 2022). Consequently, there is an urgent need for efficient, economical, and environmentally friendly techniques to recover P, minimizing environmental damage and supporting sustainable global agricultural production.

There are physical, chemical and biological methods to recover phosphorus (Witek-Krowiak et al., 2022). Adsorption-desorption plays a crucial role in influencing phosphorus availability (Wang et al., 2024). Adsorption has emerged as a promising and scalable method for P recovery. This method offers some advantages, including high selectivity, relatively ease to scale, and compatibility with a wide range of adsorbent materials such as activated carbon, biochar, and zeolites (He et al., 2010). These characteristics make it a viable option for sustainable P management (Zhang et al., 2025). However, the main challenge in this technology

is developing low-cost, high-efficiency adsorbents that enable economical and simple phosphate recovery (Zhang et al., 2018). In this regard, biochar is a standout material for P adsorption due to its porous structure and high surface area, which can be prepared to capture and retain P from various sources.

Biochar can be produced from various natural and waste materials, including forest and agricultural residues, industrial by-products, and municipal solid waste (Li et al., 2020; Ponnusamy et al., 2020; Yi et al., 2020). This process not only converts organic matter into a more stable form of carbon but also enhances its potential to improve soil properties, making biochar a valuable amendment for agricultural and environmental applications (Gao et al., 2017; Lehmann and Joseph, 2024).

In 2024, forest production in Brazil was 10,2 million hectares planted with eucalyptus, pine trees and other species (IBÁ, 2024). The state of Minas Gerais represents more than 2.3 million hectares of trees planted nationwide, of which 96.8% correspond to eucalyptus plantations (AMIF, 2023). Thus, eucalyptus residues are abundant and easily acquired materials, not only in Brazil but in several countries (Heidari et al., 2019). In addition to traditional uses such as paper, construction and furniture, wood can be used with high efficiency in bioenergy generation, with important by-products such as biochar (Maia, et al., 2021).

The surface chemistry of biochar usually limit its P adsorption capacity due to its predominantly negative charge, caused by high pH and oxygen-functional groups, hindering its efficiency in removing anionic P ions (Shepherd et al., 2016; Takaya et al., 2016; Zeng et al., 2013). To address this limitation, studies have shown that impregnating biomass with magnesium (Mg) before pyrolysis significantly enhances P adsorption capacity by biochar due to the formation of cationic bridges, improving P adsorption from aqueous media (Akgül et al., 2019; Leite et al., 2023; Nardis et al., 2021; Yao et al., 2013). Additionally, Mg-enriched biochar facilitates the formation of MgO nanoparticles during pyrolysis, which adsorb phosphate (PO_4^{3-}) efficiently via rapid surface binding and slower diffusion into the biochar's interior (Zhu et al., 2020). While Mg-enriched biochar has proven effective for P adsorption, its performance can be further optimized through enrichment with layered double hydroxides (LDHs). LDHs, or anionic clays, consist of positively charged metal hydroxide layers intercalated with anions and water molecules (Alagha et al., 2020; Dan Luo et al., 2025; Gao et al., 2020). Their high anion-exchange capacity, tunable composition, and structural stability make them versatile for applications such as removing heavy metals (e.g., lead, cadmium, and chromium), recovering phosphate to address nutrient pollution, and adsorbing organic pollutants (Mu'azu et al., 2020; Wang and Ohare, 2012). Recent studies suggest that combining

biochar with LDHs can yield synergistic effects, enhancing properties like surface area, stability, and adsorption efficiency (Bian et al., 2023; Buates and Imai, 2021). However, related research has focused on wet synthesis methods for biochar-LDH composites (Rahman et al., 2021), which involve multiple steps and present scalability challenges for practical applications.

To address the challenges associated with using chemical methods to impregnate biochar with LDH, ball milling is emerging as an efficient and simple green method that allows for scalability (Li et al., 2022; Wang et al., 2022). However, its application in producing biochar-LDH composites has not yet been explored. The primary objective of this study was to evaluate the potential use of biochar-LDH composites produced by fast ball milling method for the removal and recovery of P in aqueous solutions and to elucidate the mechanisms of P adsorption by biochar, LDH, and biochar-LDH composites as adsorbents. This innovative approach aimed to improve the adsorption capacity of the biochar-LDH composites, making it a promising solution for mitigating P pollution in aquatic systems. The effectiveness of the composites in removing P was assessed through adsorption experiments and detailed characterization. The results of this study are expected to offer insights into the feasibility of using biochar-LDH composites as a sustainable strategy for P recovery from wastewater.

2. Material and methods

2.1. Biomass sampling and biochar preparation

Eucalyptus sawdust was obtained locally from a sawmill in Lavras, state of Minas Gerais, Brazil. The biomass was washed with deionized water and then dried at 65 °C until a constant weight was achieved. It was subsequently sieved to obtain particles <0.25 mm for further processing. The sawdust was then impregnated with $Mg(OH)_2$ aiming to achieve a target concentration of 10% Mg (w/w) in the final biochar, based on previous tests. Biochar without Mg impregnation was not included in this study as it showed a negligible capacity to adsorb P in previous tests (data not shown).

The final Mg concentration added to the biomass prior to pyrolysis was estimated using biochar yields reported in other studies with similar conditions (Leite et al., 2023), and based on previous tests. Magnesium impregnation was performed in the biomass using a ball mill with a milling time of 30 minutes. The amounts of $Mg(OH)_2$ used for each biochar production were 5.62 g, 3.71 g, and 3.29 g, corresponding to 10% Mg on the final yield of biochars produced at 300 °C, 600 °C, and 900 °C, respectively. $Mg(OH)_2$ was chosen as Mg source based on previous research (Leite et al., 2023).

The pyrolysis process was conducted in a laboratory-scale adapted muffle furnace, with a heating rate of 5 °C per minute and a residence time of one hour. After cooling to room temperature (25 °C), the samples were collected, passed through a 100-mesh sieve, and stored at room temperature. The yields of the biochars produced were 35.9%, 26.6%, and 25.0%, respectively. The resulting biochars were designated as BC300 (biochar produced at 300 °C), BC600 (biochar produced at 600 °C), and BC900 (biochar produced at 900 °C). These temperatures were selected to represent low, intermediate, and high pyrolysis conditions, which are known to significantly influence the final properties of biochar.

2.2. LDH synthesis

The layered double hydroxides (LDHs) used in this study were synthesized as magnesium/aluminum layered double hydroxides intercalated with carbonate anions (Mg-Al-CO_3-LDH), which was prepared using the co-precipitation method (Pavan et al., 2000). Initially, a solution containing magnesium nitrate hexahydrate [$Mg(NO_3)_2 \cdot 6H_2O$] and aluminum nitrate monohydrate [$Al(NO_3)_3 \cdot 9H_2O$] was diluted in deionized water, maintaining Mg/Al ratios of 1:1, 2:1, 3:1, and 4:1. This solution was then added dropwise to a vigorously stirred mixture of sodium hydroxide (NaOH, 3.5 M) and sodium carbonate (Na_2CO_3, 0.943 M) in 1000 mL of water, while controlling the temperature at 35 ºC and the pH level. Following synthesis, the mixture was allowed to sit at room temperature for 18 hours to facilitate precipitation and cooling. The supernatant was then centrifuged, and the resulting solid was washed with distilled water. The LDHs were subsequently placed in a petri dish and dried in a vacuum desiccator with activated silica gel.

After production, the produced LDHs were calcined in the presence of oxygen gas with a flow rate of 150 mL min^{-1} and a temperature of 550 ºC for 4 hours. The calcination process of Mg/Al LDHs leads to the formation of oxides. These materials exhibit a phenomenon known as the "memory effect," which refers to the ability of the calcined derivative to reconstruct the lamellar structure of the LDH upon contact with an aqueous solution (Cavani et al., 1991; Forano et al., 2006). Additionally, the calcined materials have a superior capacity to adsorb P. The yields for each material were 77.4%, 48.5%, 57.5%, and 55.43%, respectively, for Mg/Al ratios of 1:1, 2:1, 3:1, and 4:1. The four LDH samples were passed through a 100-mesh sieve, and after processing they were designated as follows: LDH1 (Mg-Al-CO_3-LDH with a Mg/Al ratio of 1:1), LDH2 (Mg-Al-CO_3-LDH with a Mg/Al ratio of 2:1), LDH3 (Mg-Al-CO_3-LDH with a Mg/Al ratio of 3:1), and LDH4 (Mg-Al-CO_3-LDH with a Mg/Al ratio of 4:1). To assess

the impact of the Mg/Al ratio on P adsorption, experiments were conducted with all LDH formulations using a dosage of 2 g L^{-1} in a P solution containing 500 mg L^{-1}.

2.3. Biochar-LDH composites

To evaluate the effect of pyrolysis temperature on P adsorption, an experiment was conducted using a biochar dose of 10 g L^{-1} and a P concentration of 500 mg L^{-1}. The results showed that biochars produced at 300 ºC and 600 ºC had the highest P adsorption capacities (Table S1), and these were selected for the further preparation of biochar-LDH composites. Subsequently, a second experiment was conducted to assess the effect of biochar dosage on P adsorption. This experiment tested five different biochar doses (1, 2, 5, 10, and 20 g L^{-1}) using the same P concentration of 500 mg L^{-1} in solution, and the doses of 10 g L^{-1} biochar demonstrated the highest P adsorption capacity (Table S3) and was chosen for the subsequent experiments involving biochar-LDH composites. In parallel, an adsorption experiment was performed to investigate the influence of LDH dosage on P adsorption, and four different LDH doses (1, 2, 5, and 10 g L^{-1}) were evaluated under the same P concentration of 500 mg L^{-1}. The results showed that the 1 g L^{-1} of LDH4 exhibited the highest P adsorption capacity (Table S4), making it the optimal candidate for further studies. The influence of the composites dosage on P adsorption was also studied by an adsorption experiment. For composites BC300-LDH4 and BC600-LDH4 four different doses (1, 2, 5, 5 and 10 g L^{-1}) were evaluated using 500 mg L^{-1} P solution. The dose of 5 g L^{-1} LDH4 showed the highest P adsorption capacity (Table S5).

Based on the preliminary experiments, biochar-LDH composites were prepared using biochar produced at 300 ºC and 600 ºC combined with LDH4. The composites were prepared using a ball mill (MA350, Marconi, Brazil) with closed chamber and stainless steel griding tank (235 mL), where 50 mL of volume was filled with the material and one griding sphere of 132 g following 617 vertical strikes per minutes, for 30 minutes. Two distinct mixtures were obtained: BC300-LDH4 (comprising 80% biochar produced at 300 ºC and 20% LDH with a Mg/Al ratio of 4:1) and BC600-LDH4 (comprising 80% biochar produced at 600 ºC and 20% LDH with a Mg/Al ratio of 4:1). Both composites were sieved through a 100-mesh screen and stored in a desiccator to protect them from moisture, ensuring they remained suitable for further characterization and adsorption experiments.

For all adsorption experiments, a stock solution of P was prepared using KH_2PO_4 to achieve P concentration of 1000 mg L^{-1}. The background solution used for all P adsorption experiments was prepared by mixing 0.01 M NaOH with Milli-Q water. From this stock solution, 250 mL was diluted in 500 mL of background solution to obtain a final P concentration of 500 mg L^{-1}.

The samples were stirred continuously for 24 hours, after which the equilibrium pH was measured. Subsequently, the samples were filtered using a 0.45 μm membrane filter (PVDF 25mm). The P concentration in the equilibrium solution was then determined by inductively coupled plasma optical emission spectroscopy (ICP-OES, Blue Germany).

2.4. Adsorbents characterization

In order to evaluate the adsorption characteristics of the materials, several analyses were performed. For the purposes of this research, we will use the term "adsorption" to describe the process of removing P from an aqueous solution, however, in addition to adsorption, other mechanisms may be occurring simultaneously through which P is being removed, including precipitation, absorption, among others.

The surface morphology of biochar, LDH, and biochar-LDH composites was analyzed using scanning electron microscopy (SEM) with an ultra-high-resolution (UHR) FEG scanning electron microscope (Tescan-Clara, Kohoutovice, Czech Republic), coupled with energy dispersive spectroscopy (EDS) using an XFlash 6|60 ex detector (Bruker Nano GmbH, Berlin, Germany). A small portion of each sample was mounted on double-sided carbon tape adhered to the sample holder. Scanning electron microscopy analysis was conducted under a voltage of 20 kV and a working distance of 10 mm to capture detailed surface characteristics.

X-ray powder diffraction (XRD) analysis was performed using a Shimadzu XRD-6000 diffractometer (Osaka, Japan) equipped with a graphite monochromator to filter the Cu Kα radiation (λ = 1.54 Å). Data were collected at a scan speed of 0.02 degrees per second, with a 2θ scanning range from 4º to 70º. This setup allowed for the identification of crystalline phases present in the biochar, LDH, and biochar-LDH composites before and after P adsorption experiments. Crystalline phases were identified using the open crystallography database (COD) and X'Pert Highscore Plus v4.9 (Panalytical, Malvern, UK).

The surface area and pore volume of each sample were determined via N_2 adsorption analysis. Before analysis, the samples were degassed to remove surface impurities. Adsorption isotherms were obtained by measuring the relative pressure (P/Po) and the corresponding amount of N_2 adsorbed ($cm^3\ g^{-1}$ STP). The specific surface area was calculated using the Brunauer-Emmett-Teller (BET) equation, while the Barret-Joyner-Halenda (BJH) method was employed to analyze pore size distribution, providing insights into the average pore width and pore diameter.

Fourier-transform infrared (FTIR) spectroscopy analysis was conducted using a 600-IR spectrometer (Varian, California, USA) equipped with a GladiATR accessory (Pike

Technologies, Wisconsin, USA) for attenuated total reflectance (ATR) measurements. The spectral range was examined from 4000 to 400 cm^{-1}, with a resolution of 4 cm^{-1}. Each spectrum was generated from the average of 32 scans. Thermogravimetric analysis (TGA) was conducted to evaluate the thermal stability of the samples using a Q500 (TA Instruments, New Castle, USA). The analysis was performed under both N_2 and synthetic air atmospheres at a flow rate of 50 mL min^{-1}. The mass loss of the samples was monitored as they were heated from room temperature to 900 °C, employing a heating rate of 10 ºC min^{-1}.

Electrical conductivity (EC) and pH were measured in a suspension prepared by mixing the samples and deionized water at a 1:20 (w/v) ratio (Rajkovich et al., 2012) . The mixture was shaken on a reciprocal shaker for 90 minutes, after which the measurements were taken using a pH meter and EC meter. The ash and moisture content of the biochar and composites were assessed through oven drying at 105 °C to determine moisture content, followed by heating the samples in open crucibles at 750 °C for 6 hours to evaluate ash content. Total element contents were determined according to Enders and Lehmann, (2012). Briefly, 200 mg of each sample were ashed in a compact muffle furnace at 500 °C for eight hours. The ashed samples were then digested in concentrated nitric acid (70%) at 120 °C. To facilitate the oxidation of organic carbon, hydrogen peroxide (30%) was added during the final digestion step. The resulting solutions were diluted to a 5% nitric acid (v/v) solution. The contents were filtered through membranes (<0.45 μm) and the elements were quantified by ICP-OES.

The total C content of biochar and mixtures was determined in a dry combustion carbon analyzer (Elementar, model Vario TOC Cube, Germany). The pH at the point of zero charge (pH_{PZC}) for the biochars, LDHs, and composites was determined using an adapted procedure as described in Amaringo and Hormaza (2013). Briefly, 10 mL of deionized water was added to a 50 mL Erlenmeyer flask. Solutions with pH values of 1, 3, 5, 7, 9, 11, and 13 were prepared by carefully adding quantities of 0.1 M HCl and 0.1 M NaOH. To each of these pH-adjusted solutions, 0.1 g of the respective absorbent material was added. The mixtures were stirred continuously at room temperature for 48 hours, after which the final pH was measured. The pH_{PZC} was identified as the intersection point of the final pH values plotted against the initial pH values on a graph, representing the point where the curve intersects the diagonal line.

X-ray photoelectron spectroscopy (XPS) spectra were analyzed (model K-Alpha, Thermo Scientific) and deconvoluted using the Gaussian–Lorentzian sum function in Casa XPS v. 2.3.18 (Casa Software). A Shirley background correction was applied to remove background noise. Atomic ratios of C, O, Mg, and P were calculated from the peak areas of the C(1s), O(1s),

Mg(1s), and P(2p) peaks, respectively. The XPS results correspond to the average of three independent measurements collected in different regions of each sample.

2.5. Adsorption experiments

2.5.1. Adsorption isotherms

Adsorption isotherms and kinetics were conducted to evaluate the P adsorption capacity of the materials. Isotherm experiments were performed in triplicate by weighing 100 mg of biochar and biochar-LDH composites, and 20 mg of LDHs, and placing them in 50-mL propylene tubes containing 20 mL of P solution. This setup resulted in an adsorbent dose of 5 g L^{-1} for biochar and biochar-LDH composites, and 1 g L^{-1} for the LDHs. The P concentrations tested were 50, 100, 150, 200, 250, 300, 400, and 500 mg L^{-1}. These P concentrations were prepared from 1000 mg L^{-1} stock solution of KH_2PO_4 and a background solution containing 0.01 mol L^{-1} NaOH. The samples were stirred for 24 hours in a horizontal shaker at 120 rpm at room temperature. After this period, the equilibrium pH was measured, and the extracts were filtered through a 0.45 µm membrane. The concentration of P in the equilibrium solution was then determined by ICP-OES.

The adsorption capacity (Qe) of the different adsorbents was calculated by mass balance, as expressed by Equation (1), where V (L) is the volume of the P solution, m (g) represents the mass of the adsorbents, and Ci and Ce (mg L^{-1}) are the initial and equilibrium P concentrations, respectively.

$$Qe\ (mg\ g^{-1}) = \frac{V\ (C_i - C_e)}{m} \qquad \text{(Equation 1)}$$

Langmuir (Equation 2), Freundlich (Equation 3), and Redlich-Peterson (Equation 4) isotherms models were used to describe the P adsorption process.

$$Q = \frac{Qm\,.\,K_L\,.\,C}{1 + K_L\,.\,C} \qquad \text{(Equation 2)}$$

$$Q = K_f \cdot C^{\frac{1}{n}} \qquad \text{(Equation 3)}$$

$$Q = \frac{K_R \cdot C}{1 + a_r \cdot C^g} \qquad \text{(Equation 4)}$$

In which, K_L: Langmuir isotherm constant, *Qm*: maximum adsorption capacity index, K_f: Freundlich isotherm constant, *n*: adsorption intensity, K_R: Redlich–Peterson isotherm

constant, a_r: Redlich–Peterson isotherm constant, g: Redlich–Peterson isotherm exponent, and C: represents the adsorbate concentration.

2.5.2. Adsorption kinetics

For the kinetic experiments, 100 mg of biochar and biochar-LDH composites, along with 20 mg of LDHs, were added to a set of 50 propylene tubes containing 20 mL of solution with a P concentration of 200 mg L^{-1}. The tubes were shaken on a horizontal shaker at 120 rpm for varying durations, ranging from 1 to 1440 minutes. Following the shaking period, the solutions were filtered through a 0.45 µm membrane. The P concentration at equilibrium was measured by ICP-OES.

The kinetic data for P adsorption onto the studied materials were fitted with the Pseudo-first-order (Equation 5) and Pseudo-second-order (Equation 6) models.

$$log\ (q_e\ -\ q_t) = log\ (q_e) - \frac{k_1}{2.303} \cdot t \qquad \text{(Equation 5)}$$

$$\frac{t}{q_t} = \frac{1}{\frac{k}{2} \cdot q_e^2} + \frac{1}{q_e} \cdot t \qquad \text{(Equation 6)}$$

in which q_e: adsorption capacity at equilibrium, q_t: adsorption capacity at time t, k_1: rate constant of the PFO kinetics, k_2: rate constant of the PSO and t is the time.

3. Statistical analysis

All adsorption experiments were conducted with three replicates. Data analysis (using the two-sample t-test) was performed with SPSS Statistics software v. 21 (SPSS Inc., USA). All kinetic and isotherm data were fitted using OriginPro v. 10.0.5.157 (OriginLab Corporation, USA), and the sum of squared residuals (RSS) and the determination coefficient (R^2) values of the fitted equations were determined.

4. Results and discussion

4.1. Effect of LDH on forming composites

4.1.1. BET Surface Area

The specific surface area (SBET) values for BC300 and BC600 were determined to be 0.29 m^2 g^{-1} and 304.1 m^2 g^{-1}, respectively. For the layered double hydroxides (LDHs), the corresponding SBET values were found to be 109.1, 95.86, 60.41, and 69.22 m^2 g^{-1} for LDH1, LDH2, LDH3,

and LDH4, respectively. In the case of biochar combined with LDH Mg/Al at a ratio of 4:1 (biochar-LDH), the SBET values for BC300-LDH4 and BC600-LDH4 were 7.77 and 205.0 m^2 g^{-1}, respectively (Table 1).

Table 1. BET surface area and pore characteristics of biochar and LDH samples.

Samples	S_{BET} values (m^2 g^{-1})	Cumulative Pore Volume (cm^3 g^{-1})	Average pore diameter (Å)	Average pore width (Å)
BC300	0.2955 ± 0.08	0.00996	673	942.8
BC600	304.1 ± 7.4	0.01719	77.4	19.93
LDH1	109.1 ± 0.1	0.57334	194	209.3
LDH2	95.86 ± 0.21	0.70190	285	285.3
LDH3	60.4 ± 0.10	0.41401	265	246.9
LDH4	69.2 ± 0.2	0.45646	242	230.4
BC300-LDH4	7.77 ± 0.22	0.02489	330	98.58
BC600-LDH4	205.0 ± 4.6	0.05903	150	27.44

Note: The mixtures were prepared in the proportion of 80% eucalyptus sawdust biochar and 20% Mg/Al LDH.

The biochar produced at a higher temperature (BC600) demonstrates a significantly greater specific surface area (SBET) when compared with BC300. This difference arises because biochars produced at lower temperatures retain a high content of volatile matter, including partially decomposed cellulose, hemicellulose, and lignin. These volatile components hinder pore formation, thereby limiting the development of a higher surface area at lower pyrolysis temperatures (Leng et al., 2021).

Among the LDHs, the highest SBET value was observed in LDH1, while for the composites, BC600-LDH4 exhibited the highest specific surface area. The SBET values of the biochar-LDH composites increased compared to the unmodified biochar when BC300 was used. Conversely, this value decreased relative to the unmodified biochar when BC600 was used in the composite. The presence of LDH enhanced the accumulated pore volume of the biochars, resulting in the composites achieving pore volumes between 2.5 and 5 times higher than those of the biochars alone (Table 1). These surface area values are consistent with those reported for wood-derived biochar (Wang et al., 2013). Furthermore, the ball milling conditions employed in this study did not appear to significantly enhance the surface area of the materials. Typically, eucalyptus biochars produced under these pyrolysis conditions can achieve surface areas exceeding 400 m^2 g^{-1}, even without ball milling (Fernandes et al., 2020).

4.1.2. Other properties related to adsorption

Other properties of the biochars impregnated with Mg prepared in this study are summarized in Table S2. As the pyrolysis temperature increased, the pH also exhibited a slight rise, with maximum pH values of 11.1 recorded at 600 ºC and 900 °C. It has been reported that increasing the pyrolysis temperature or extending the residence time could increase the pH of biochars (Sun et al., 2017). The pH increase with higher pyrolysis temperatures are explained by the thermal decomposition of lignocellulosic materials and release of vapor and compounds such as CO and CO_2 followed by a formation of a more stable carbonaceous structure with high ash content wich are composed mainly by mineral elements in the form of oxides and carbonates (Muhammad et al., 2022; Sun et al., 2017). In this study, particularly, a high pH is especially due to $Mg(OH)_2$ enrichement.

The pH_{PCZ} is a crucial parameter in adsorption processes, as it represents the pH at which the surface of a solid exhibits no net electrical charge (Feitoza et al., 2022). When the pH of the solution exceeds the pH_{PZC}, the surface of the adsorbent becomes negatively charged, favoring the adsorption of positively charged species. Conversely, when the pH is lower than the pH_{PCZ}, the surface of the adsorbent is positively charged, facilitating the adsorption of negatively charged species (Thue et al., 2017). The pH_{PZC} for BC300 and BC600 was determined to be approximately 10.5 and 10.3, respectively. For the LDHs, the pH_{PZC} value did not vary much, with an approximate value of 12.9. These pH_{PZC} values suggest that the net surface charge will be positive, favoring the adsorption of anionic species for a solution pH lower than 10.5 and 10.3 for BC300 and BC600, respectively, and lower than 12.9 for LDH. This means that the selection or adjustment of the solution pH plays an important role in the adsorption study (Nguyen et al., 2023). In this study, the P solution used for the adsorption analyses had an acidic pH (approximately 5.5), which could justify the phosphate adsorption efficiency of these adsorbents, since the lower pH_{PZC} of the materials increases the possibility of adsorption of anionic species in solutions. Therefore, a higher P adsorption can be expected for this material by electrostatic attraction (protonated functional groups, for example, hydroxyl groups).

At pyrolysis temperatures of 600 °C and 900 °C, the C content was higher (70.2% and 70.3%, respectively) when compared with the lower pyrolysis temperature of 300 °C, which yielded a C content of 55.9%. This increase in C contents with higher pyrolysis temperatures is attributed to the loss of O and H through the cracking of C-H and C-O bonds, resulting in gas release and a higher degree of aromatization (He et al., 2024; Sun et al., 2017). The reduction in O and H functional groups aligns with the observed decrease in yield as pyrolysis temperature increased, with yields of 35.9, 26.6, and 25.0% at 300, 600, and 900 °C, respectively.

Pyrolysis temperature did not significantly affect ash content, which remained in the range of 14.0–14.8%. The ash content of eucalyptus wood biochar is generally low, even at higher pyrolysis temperatures (<1%), consistent with its high C content (Domingues et al., 2017). The slightly higher ash content observed in this study can likely be attributed to the residual Mg content from $Mg(OH)_2$ impregnation.

4.1.3. Scanning electron microscopy

The surface morphology of biochars, biochar-LDH composites, and LDH4 after P adsorption was analyzed for Mg, P, and K mapping (Fig. 1). A distinct morphological difference was observed between the surfaces of the biochars and the LDH. The morphology of the biochar (Fig. S1) is associated with the original eucalyptus structure, which after pyrolysis consists of macroporous particles with the loss of outer layers and the exposure of porous structures (Fernandes et al., 2020). However, the accumulation of ash due to Mg enrichment is responsible for filling the macropores.

Mapping of the samples after P adsorption revealed concentrated spots of Mg and P consistent with studies where Mg impregnation was performed prior to adsorption (Nardis et al., 2021). This is likely due to the formation of Mg-phosphates, as confirmed by XPS analysis (discussed later) of the Mg 1s and P 2p peaks. In contrast, the distribution of K on the surface was more homogeneous, reflecting the solubility of the K-phosphate used. SEM images of the LDH show small particles with a homogeneous distribution. This was further quantified by EDS spectra (Table S7), which indicated a high concentration of Mg and Al compared to the biochars alone (Table S6), and the biochar-LDH composites. These findings align with studies involving LDH samples (Zhang et al., 2013).

The presence of LDH particles was observed on the surfaces of the biochar, which exhibited a more heterogeneous, amorphous, and irregular surface morphology at both temperatures. This was confirmed by the EDS spectra (Fig. S2), which showed the highest Mg concentration peaks, indicating the impregnation of the biochar with this element after the pyrolysis process. The surfaces of the LDH-modified biochar were coated with fine LDH particles (Fig. S3). However, it is unclear whether these LDH particles penetrated deep into the biochar pores or channels. It has been reported that the pore network and surface of biochar can facilitate the dispersion of LDH flakes, thereby enhancing their reaction with phosphate and improving adsorption efficiency (Zhang et al., 2013). However, since the biochars in this study have low pore volumes, this effect may be less pronounced.

Compared to the unmodified biochars, the morphology of the composites appeared more homogeneous, likely due to the 30-minute milling process used during their production. The surface morphology of these composites was further analyzed through EDS spectra (Table S8), which revealed an increased Al concentration relative to the unmodified biochars, while the Mg content showed minimal variation after mixing with LDH. Another study suggests that biochar can be homogeneously intercalated throughout the layers of LDH, which would be favorable for P adsorption due to the positive charges and adsorption properties of LDH (Alagha et al., 2020).

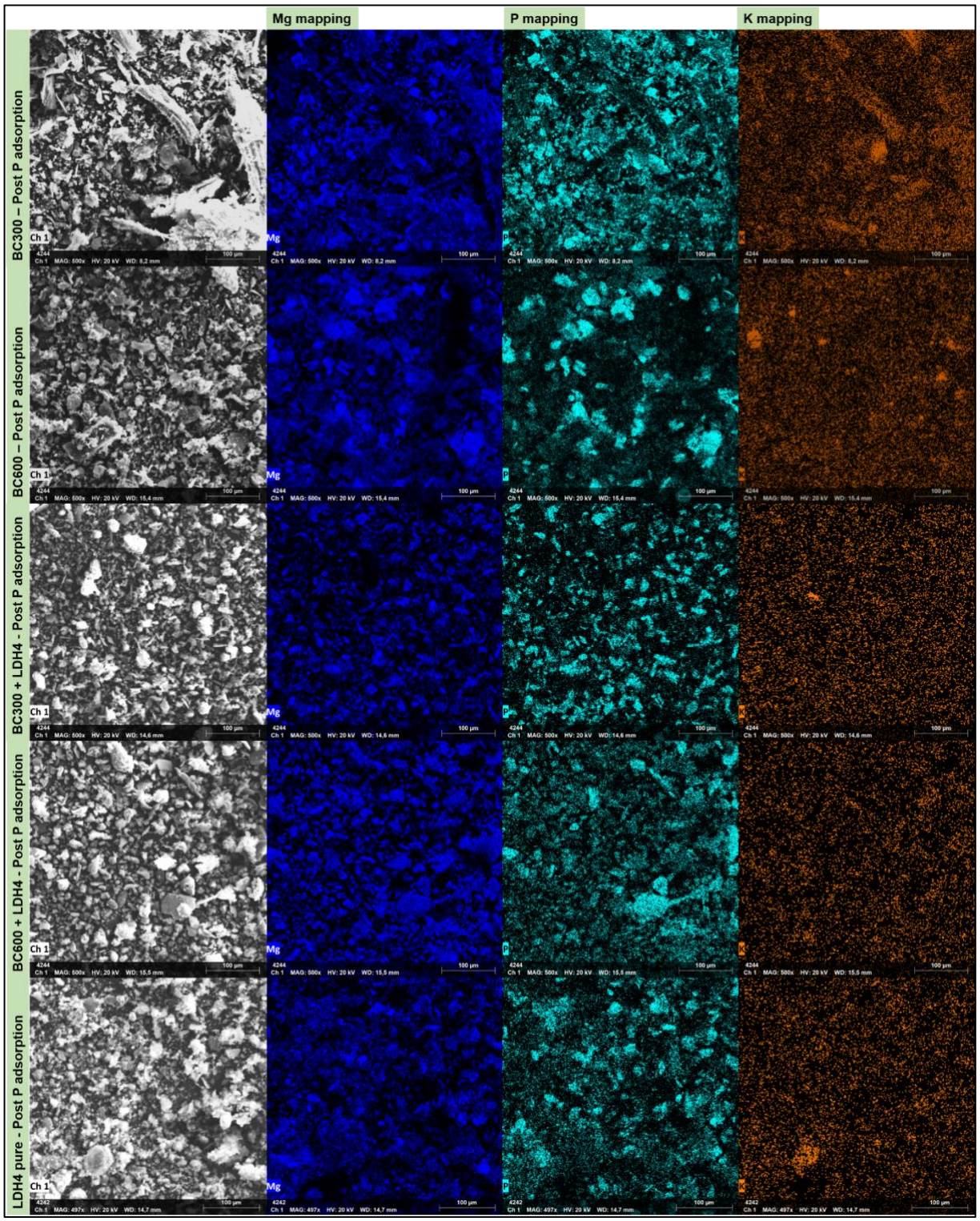

Figure 1. Scanning electron microscopy (SEM) and element mapping (EDS) of biochars, LDH and biochar-LDH composites post P adsorption.

4.1.4 Thermogravimetric analysis (TGA) and Fourier-transform infrared spectroscopy (FTIR)

The thermal stability analysis revealed that biochars exhibit significant mass loss, leaving approximately 18% ash residue (Fig. 2a). Given the low ash content of eucalyptus biochar, the ash remaining after thermal decomposition originates primarily from $Mg(OH)_2$ impregnation. The mass losses correspond to the decomposition of organic compounds present in the biomass (lignocellulosic compounds) and their release as volatile matter. It has been reported that eucalyptus biomass contains approximately 72% volatile matter, which decreases to 24% in biochars upon pyrolysis, while fixed C increases from 22% to 58% (Durango Padilla et al., 2024).

Among the biochars, BC600 demonstrated higher thermal stability, indicating that most of the lignocellulosic compounds were already degraded during pyrolysis. For BC600, the onset of mass loss occurred around 450 °C, a pattern also observed in BC600-LDH4. The degradation temperatures for cellulose, hemicellulose, and lignin range from 210 to 520 °C (Ben Salem et al., 2021) with higher peaks of CO_2 and CO release around 550 °C (Giudicianni et al., 2013). In contrast, the LDHs showed a nearly constant mass loss, retaining about 75–85% of their mass at 800 °C. Among the LDH samples, LDH2 exhibited the lowest overall mass loss. The thermal decomposition of synthetic hydrotalcite (LDH) occurs in several steps: the removal of weakly adsorbed water up to 105 °C, interlayer water from 105 to 200 °C, and, beginning at 310 °C, dehydroxylation, decarbonation, and the removal of interlayer anions. These processes account for approximately 20% mass loss overall (Theiss et al., 2013), consistent with the findings of this study. Individual TG and DTA curves of biochars, LDH, and biochar-LDH composites are found in Fig. S4.

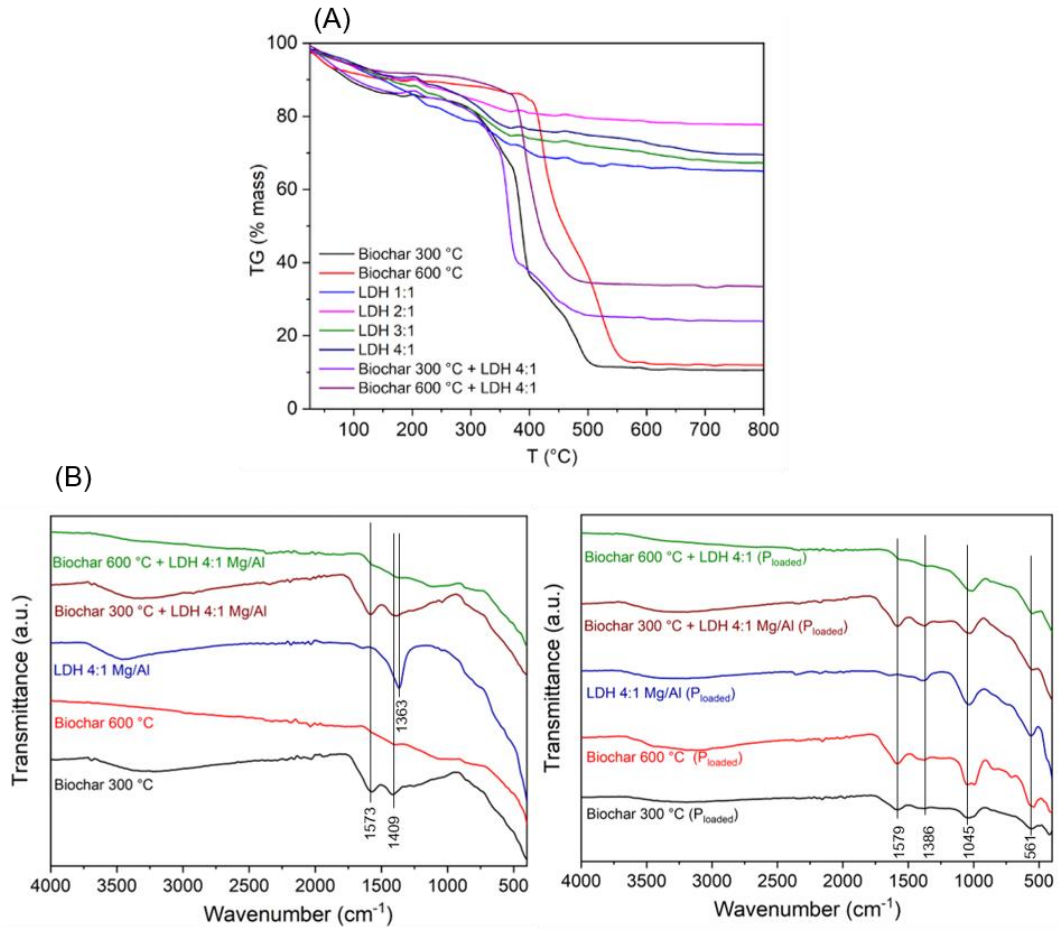

Figure 2. (A) Thermogravimetric analysis (TGA) of the materials under synthetic air atmosphere, (B) FTIR spectra and spectral bands of biochars, LDH and biochar-LDH composites before and after adsorption with P.

The FTIR analysis revealed distinct absorption bands corresponding to various functional groups in the biochar and biochar-LDH composites (Fig. 2b). The strong and broad band around 3421.1 cm^{-1} is the stretching vibration of–NH and –OH (Huang et al., 2020). A prominent band at 1573 cm^{-1} was attributed to the presence of aromatic groups, characteristic of lignocellulosic compounds, and related to C=C stretching of aromatic components as well as C=O stretching in conjugated ketones and quinones (Janu et al., 2021). The band at 1409 cm^{-1} indicated aliphatic C–H bending (Farobie et al., 2022), while the band at 1363 cm^{-1} was associated with small amounts of carbonate (CO_3^{2-}) (Benício et al., 2015; Zhang et al., 2013). A similar aromatic signal appeared at 1579 cm^{-1}, further confirming the presence of lignocellulosic structures. The band at 1386 cm^{-11} was linked to –CH_2- groups (Li et al., 2016) and, after P adsorption, the peak at 1045 cm^{-1} attributed to the bending vibration of adsorbed phosphate P-O and P=O, with higher intensities observed below 1029 cm^{-1}, which sugests complexation with –OH groups (Nardis et al., 2021; Novais et al., 2018) or intercalation of

phosphate into the interlayer space of LDH (Alagha et al., 2020). Additionally, phosphate-related groups such as O-P-O were detected at 561 cm^{-1} and 538 cm^{-1} (Nardis et al., 2021; Novais et al., 2018). Aromatic groups, along with C=C stretching of aromatic components and C=O stretching of conjugated ketones and quinones were identified in BC300, its composite with LDH4, and all P-loaded materials, except for LDH4 alone. Aliphatic C–H bending was detected in BC300, BC600, and BC300-LDH4. A prominent carbonate peak was found in LDH, while the materials loaded with P also exhibited -CH_2- groups. In addition, the functional groups corresponding to carbonates, aliphatic C-H bending and CH_2 groups desapeared or decreased intensity, indicating that the adsorbate interacts with these groups, either transforming them into more oxidezed functional groups or forming complexes (Zhang et al., 2019), which was later confirmed by XPS analysis.

4.1.5. X-ray diffraction (XRD)

The diffractogram in Figure 3 (a) demonstrates the regeneration of the lamellar structure of calcined magnesium-aluminum layered double hydroxide (HDLc) after interacting with a solution containing phosphate ions. For this material, the basal spacing calculated using Bragg's equation was 7.90 nm, a value characteristic of layered double hydroxides (LDHs) intercalated with hydroxyl anions (OH^-) (Benício et al., 2018). It suggests that the "regenerated" structure consists of the phase known as meixnerite (Wan et al., 2017; Zhang et al., 2013). This phase comprises layers intercalated with OH^-, commonly observed in regenerations conducted in aqueous solutions with low ionic strength and without a high concentration of polyvalent anions.

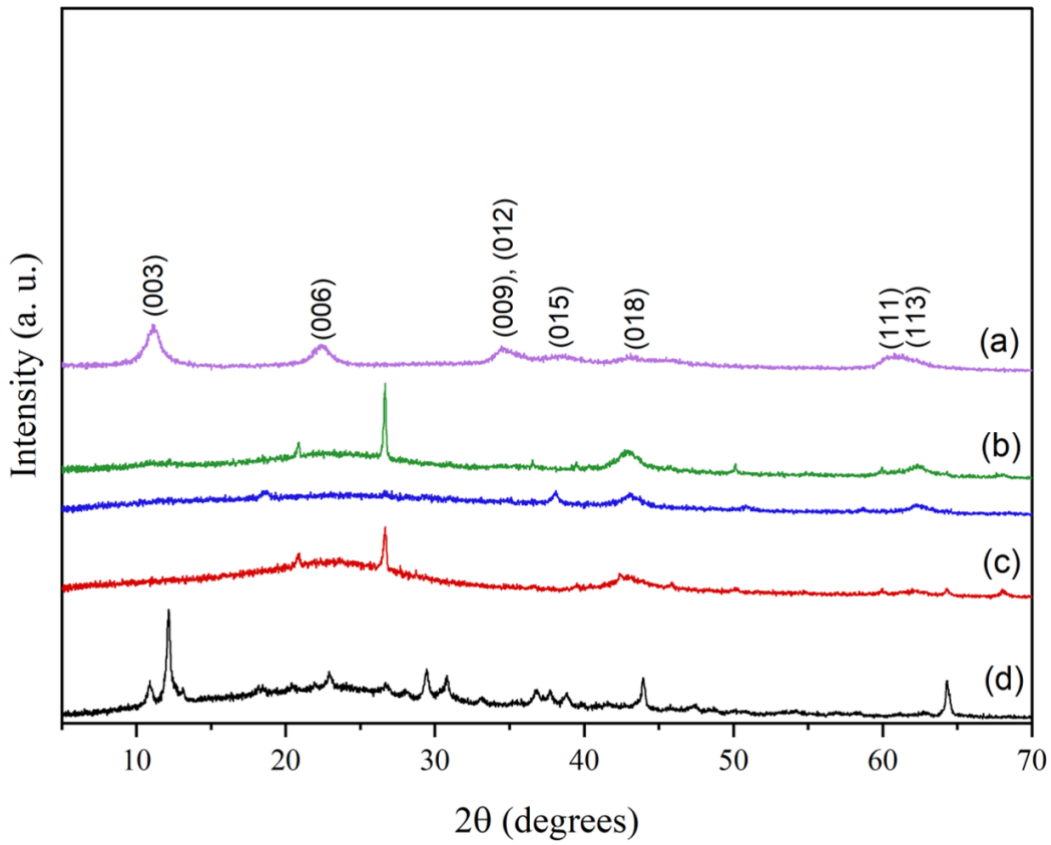

Figure 3. X-ray diffraction and mineral phases identification of biochars, LDH and biochar-LDH composites after P adsorption. (a-LDH; b- BC600-LDH4 and BC300-LDH4, c-BC600, d-BC300).

The behavior observed in the diffractogram can be interpreted from different perspectives. Firstly, the absence of peaks indicating larger spacings suggests that the phosphate ions were not intercalated between the layers in the traditional "upright" orientation, where their dimensions would be perpendicular to the lamellar plane (Benício et al., 2017). This arrangement, frequently observed for bulky and highly hydrated anions, would typically result in basal spacings exceeding 10 nm, depending on the type of interaction established.

The data support the hypothesis of surface adsorption of phosphate ions. In aqueous solutions, phosphate ions are known to exhibit a high affinity for active sites on the surface of metal oxides and LDHs, promoting chemisorption bonds (Gao et al., 2025). This interaction predominantly occurs through hydrogen bonding (Benício et al., 2017) or covalent coordination with the metal groups exposed on the surface of the layers, especially in slightly alkaline environments, where the equilibrium among the different phosphate ion species favors adsorption.

A second possibility to consider is the intercalation of phosphate ions in a parallel orientation to the lamellae (Benício et al., 2015). This arrangement would minimize the impact

on the basal spacing and could explain the observed value of 7.90 nm. Previous studies reported that bulkier anions, such as phosphates, can adopt such a configuration in LDHs, particularly when van der Waals or hydrogen bonding interactions balance the electrostatic force between the layer cation and the intercalated anion. However, this configuration is less common and heavily dependent on specific conditions, such as pH and the relative concentration of anions in the medium (Keyikoglu et al., 2022).

The preferential regeneration of meixnerite, even in a phosphate-containing solution, can be attributed to kinetic and thermodynamic factors. During the regeneration process, the rapid rehydration of the calcined lamellae favors the capture of smaller anions such as OH^{-}, which exhibit higher ionic mobility and lower activation energy for intercalation. The competition between phosphate and OH^{-} anions may have resulted in the former's surface adsorption and the latter's intercalation (Bravo-Suárez et al., 2004).

In Figure 3 (b) the calcined layered double hydroxide (LDHc) regenerated in a phosphate ion-containing solution was mixed with biochar, resulting in a hybrid system. The analysis of the diffractograms indicates the absence of characteristic peaks of the regenerated LDH. This behavior can be attributed to the dilution effect of the biochar matrix, which compromises the intensity of the crystallographic signals from the regenerated LDH.

Biochar, a predominantly amorphous or semicrystalline matrix (Zhang et al., 2020), acts as a dispersing medium for the regenerated LDH, reducing the local concentration of crystalline phases and, consequently, the intensity of the diffraction peaks. Moreover, due to its heterogeneous and disorganized nature (Zhang et al., 2019b), biochar often exhibits a diffractometric pattern with elevated background noise, which can mask low-intensity signals from the regenerated LDH (Ma et al., 2022). The mixing process may also promote the physical dispersion of LDH particles within the biochar matrix. This dispersion reduces the coherent alignment of the crystalline domains of the LDH, which is essential for generating detectable X-ray diffraction peaks. As a result, even if the crystalline phase of the LDH is present, its contribution to the diffractogram will be significantly weakened.

Therefore, the absence of peaks in the diffractogram in Figure 3 (b) can be explained by a combination of the dilution effect caused by the biochar matrix, its amorphous nature, and possible physicochemical interactions between the regenerated LDH and the biochar (Zubair et al., 2023). These results highlight the importance of complementary techniques for more precisely characterizing hybrid systems involving LDHs and heterogeneous matrices.

4.2. Phosphorus adsorption

4.2.1. Adsorption kinetics

The kinetic experiment demonstrated that P adsorption by the biochar-LDH composites and pristine biochars (BC300 and BC600) increased rapidly, reaching equilibrium at around 6 hours, much faster than for LDH alone (Fig. 4). The adsorption process for these materials followed two distinct phases: an initial rapid phase, during which 80-90% of the adsorption occurred within 360 minutes (6 hours), followed by a slower phase as the system approached equilibrium (Fig. 5). The BC300, BC600, the composites BC300-LDH4 and BC600-LDH4, and LDH4 removed more than 89%, 78%, 59%, 94%, and 94% of phosphate from the solution at their equilibrium times, respectively. In contrast, studies have reported that biochar and biochar-LDH composites usually reach equilibrium within 1 hour of contact time or faster (He et al., 2019; Yao et al., 2011). The delayed equilibrium (6 hours) in P adsorption could be due to factors such as surface heterogeneity, limited pore accessibility, higher P concentration, and mass transfer limitations in the biochar-LDH composites.

During the first 6 hours, all adsorbents exhibited a relatively fast adsorption rate, with a marked increase in the adsorption capacity, except for LDH4, which reached equilibrium later. After this period, further time had little effect on the adsorption capacity, with most adsorbents stabilizing (Fig. 4). However, LDH4 showed a delayed equilibrium, requiring 12 hours to reach a stable phase.

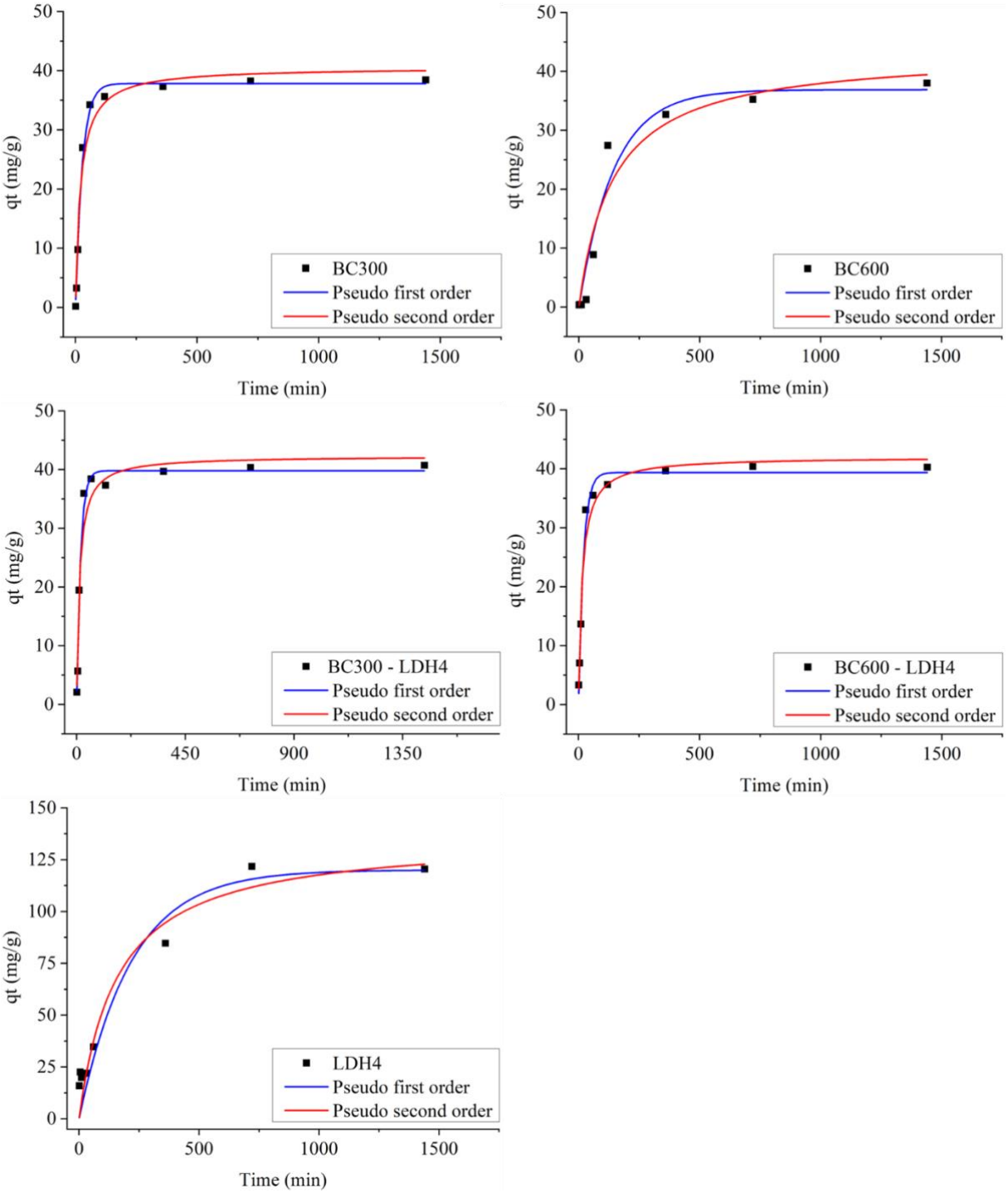

Figure 4. Kinetics of phosphorus adsorption from BC300, BC600, BC300-LDH4, BC600-LDH4 and LDH4. Experimental data was fitted to the pseudo first and pseudo second order equations. The X-axis represents the time (h), and the Y-axis represents the amount of P adsorbed (mg g^{-1}). Note: Kinetics parameters are presented in Table 2.

The commonly used pseudo-first-order, pseudo-second-order, and Elovich models were applied to simulate phosphate adsorption kinetics data. The model parameters fitted to the experimental data were evaluated based on the coefficient of determination (R^2) and the sum of squared residuals (RSS) values, as shown in Table 2. In the P adsorption process, both the

pseudo-first-order and pseudo-second-order kinetic models showed good correlation coefficients, suggesting chemical sorption might be occurring (Robati, 2013). However, the pseudo-first-order model demonstrated higher R^2 values and lower RSS values compared to the pseudo-second-order model for most adsorbents, with Rv > 0.95 (Table 2), except for LDH4, where R^2 for both models was below 0.95. Overall, the pseudo-first-order kinetic model more accurately represented the adsorption process for BC300, BC600, and their composites (BC300-LDH4 and BC600-LDH4).

Table 2. Parameters of the pseudo-first order and pseudo-second order kinetic models for P adsorption on from BC300, BC600, BC300-LDH4, BC600-LDH4 and LDH4.

Material	Pseudo-first order				Pseudo-second order			
	Q_e	k_1	R^2	RSS	Q_e	k_2	R^2	RSS
BC300	37.821	0.0358	0.99	21.30	40.569	0.0012	0.96	67.71
BC600	36.878	0.0069	0.95	98.67	43.303	0.0002	0.94	125.78
BC300-LDH4	39.793	0.0611	0.98	38.29	42.215	0.0019	0.94	95.83
BC600-LDH4	39.367	0.0486	0.99	23.12	42.032	0.0015	0.97	53.92
LDH4	120.015	0.0045	0.91	1109.29	136.350	0.00005	0.93	919.31

Note: Q_e is the adsorption capacity (mg g^{-1}); k_1 e k_2 (mg g^{-1} h^{-1}) are constants of the pseudo-first and second order, respectively; and R^2 are the R-squared values for each model fit.

The pseudo-first-order model is suitable for systems where adsorption occurs rapidly and decreases as the adsorbent surface saturates, meaning that it assumes a linear decrease in the sorption rate with an increase in adsorption capacity. In contrast, the pseudo-second-order model suggests that chemisorption processes involving chemical bonding between the adsorbent active sites and phosphate indicate that adsorption and desorption are in dynamic equilibrium (He et al., 2019; Yang et al., 2014). The pseudo-second-order model provided a more favorable fit for LDH4, evidenced by higher parameter values and lower RSS values. This outcome suggests that the phosphateadsorption process for LDH4 was predominantly controlled by chemical interactions, rather than following the linear sorption rate decrease assumed by the pseudo-first-order model, which is in agreement with studies using LDH materials (Wan et al., 2017).

4.2.2. Adsorption isotherms

The equilibrium adsorption data of biochars and biochar-LDH composites were fitted to the Freundlich, Langmuir, and Redlich-Peterson isotherm models to describe the adsorption characteristics of P. The P adsorption isotherms and the fitting of isotherm models for BC300, BC600, BC300-LDH4, BC600-LDH4, and LDH4 are shown in Figure 5. All models described the isotherm data reasonably well, but the Redlich-Peterson model provided a slightly higher R^2 value (Table 3) than the other models. Among the three isotherm models, Freundlich describes heterogeneous adsorption on surfaces with varied affinities; Langmuir assumes monolayer adsorption on a surface with a finite number of identical sites, and Redlich-Peterson combines features of both to account for the adsorption behavior over a wide range of concentrations (Bolbol et al., 2019; Vikrant et al., 2018). As reported, the Redlich-Peterson model demonstrated the best fit for the P adsorption data, slightly outperforming the Freundlich and Langmuir models in terms of the R^2 coefficient. This suggests that phosphorus adsorption on the adsorbents may be influenced by multiple processes (Wan et al., 2017), which is consistent with the complexity in their surfaces as shown in the characterization of these adsorbents.

Considering the Langmuir model, the maximum P adsorption capacity (Q_{max}) of BC300, BC600, BC300-LDH4, BC600-LDH4, and LDH4 could reach up to 44.34, 55.06, 74.90, 64.11, and 272.53 mg g^{-1}, respectively. The maximum P adsorption capacity decreased in the following order: LDH4 > BC300-LDH4 > BC600-LDH4 > BC600 > BC300. The K_l values for BC300, BC600, BC300-LDH4, BC600-LDH4, and LDH4 were 0.975, 0.388, 0.175, 0.148, and 0.016 L mg^{-1}, respectively (Table 3). The Langmuir constant (K_L) represents the binding energy between the adsorbent and the adsorbate. Lower K_L values generally indicate stronger binding affinities (Luo et al., 2016). In this case, LDH4 stands out with the highest Q_{max} and the lowest K_L, indicating both a high adsorption capacity and strong binding. Following this, BC300-LDH4 and BC600-LDH4 also exhibit significant adsorption capacities, while BC600 and BC300 have lower adsorption capacities compared to the LDH-containing samples. Additionally, the coefficient value of binding energy for biochar-LDH composites was higher than that of raw biochar, suggesting that desorption of P sorbed on biochar-LDH composites would be more difficult and could be retained longer by the sorbent (Soliemanzadeh et al., 2016; Bolbol et al., 2019), reaching the maximum retention in LDH. This suggests that LDH have great capacity to adsorb P but can limit its desorption aiming its recycling as fertilizer in soils.

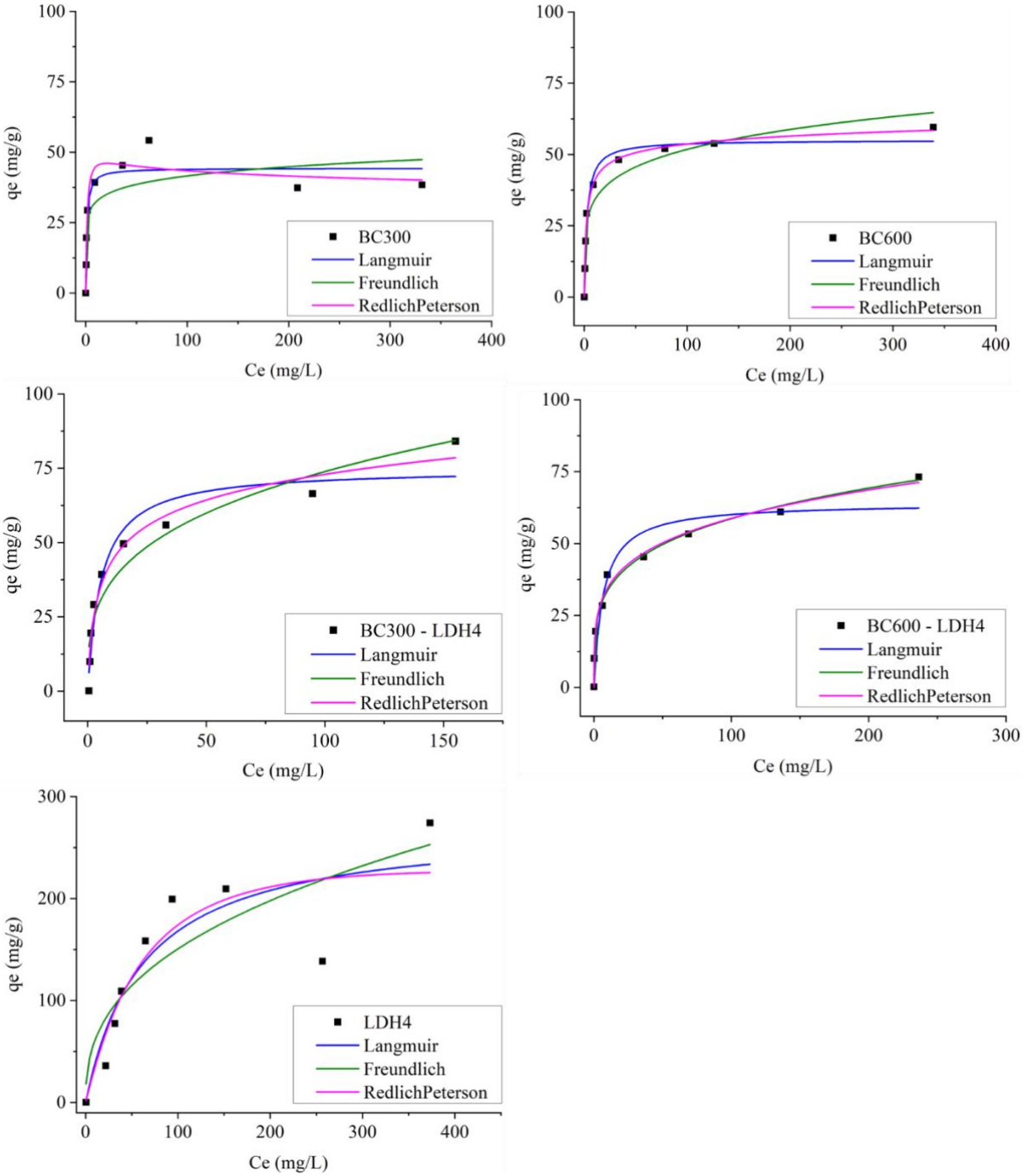

Figure 5. Isotherm of phosphorus adsorption from BC300, BC600, BC300-LDH4, BC600-LDH4 and LDH4. The X-axis represents the time the equilibrium concentration of P in solution (mg L^{-1}), and the Y-axis represents the amount of P adsorbed (mg g^{-1}). Experimental data was fitted to the Langmuir and Freundlich, models. Note: Isotherm parameters are presented in Table 3.

On the other hand, in the Freundlich equation, the *Kf* constant represents the adsorption capacity and strength of adsorption, with higher values indicating a greater ability of the adsorbent to adsorb the solute from the solution. In simpler terms, a higher *Kf* suggests a more

efficient and effective adsorption process. The *Kf* values for BC300, BC600, BC300-LDH4, BC600-LDH4, and LDH4 were 25.209, 22.340, 18.347, 19.392, and 24.610 L mg^{-1}, respectively (Table 3). These high *Kf* values across all materials suggest their potential effectiveness in adsorbing P, highlighting their suitability for water treatment applications.

In the Freundlich model, there is also a qualitative relationship between the parameter *n* and the distribution of adsorption sites. Higher *n* values indicate greater heterogeneity of adsorption sites (Meroufel et al., 2013). Among the studied materials, the highest *n* value was observed for BC300 (9.199), followed by BC600 (5.478). The composites (BC300-LDH4 and BC600-LDH4) and LDH4 presented lower *n* values, suggesting a more uniform distribution of adsorption sites compared to the biochars alone.

Table 3. Isotherm parameters of Langmuir, Freundlich and Redlich-Peterson models for BC300, BC600, BC300-LDH4, BC600-LDH4 and LDH4.

Material	Langmuir			Freundlich			Redlich-Peterson			
	Q_m	K_L	R^2	K_F	n	R^2	K_R	ar	g	R^2
BC300	44.341	0.975	0.90	25.209	9.199	0.68	31.624	0.509	1.074	0.91
BC600	55.056	0.388	0.98	22.340	5.478	0.92	27.941	0.671	0.940	0.99
BC300-LDH4	74.903	0.175	0.93	18.347	3.306	0.91	21.863	0.562	0.856	0.96
BC600-LDH4	64.107	0.148	0.90	19.392	4.161	0.99	192.457	9.105	0.777	0.99
LDH4	272.530	0.016	0.79	24.610	2.541	0.73	3.703	0.006	1.150	0.75

Note: Q_m is the maximum adsorption capacity (mg g^{-1}); K_L (L mg^{-1}), K_F (mg g^{-1}), and K_R are Langmuir, Freundlich and Redlich-Peterson equilibrium constants; n is exponent related to the intensity of adsorption; ar Redlich-Peterson isotherm constant; g represents the Redlich-Peterson isotherm exponent; and R^2 are the R-squared values for each model fit.

In summary, it is known that the heterogeneity of adsorption sites, as indicated by *n* values, can influence the efficiency of P removal. Given that biochar-LDH composites and LDH4 had efficient adsorption capacities with relatively lower *n* values, this suggests a more uniform distribution of adsorption sites. However, the fact that the maximum adsorption capacity from the Langmuir isotherm model is higher for the composites (BC300-LDH4 and BC600-LDH4) than for the biochars alone (BC300 and BC600) suggests that higher overall capacity to adsorb P. This is likely due to the creation of higher-affinity sites provided by LDH, which leads to better performance in P removal. Thus, it is of primary importance to study the P desorption profile of biochar-LDH composites to evaluate their potential fertilizer value and assess the effectiveness of the impregnation method (ball milling) as an alternative approach to producing these types of materials.

The adsorption capacity of the materials studied in this work was generally lower than that of other biochar-LDH composites reported in the literature (Table 4). This variation in adsorption performance can be attributed to differences in the surface characteristics of biochar-LDH composites, which are influenced by factors such as biochar feedstocks, pyrolysis conditions, and preparation methods (e.g., hydrothermal synthesis, co-precipitation, and co-pyrolysis) (Zubair et al., 2021). Additionally, the pH of the adsorption solution plays a critical role in the performance of these composites. Optimal phosphate adsorption is typically achieved within a pH range of 3–8, where the availability of adsorption sites is maximized (Jung et al., 2017).

Table 4. Comparison of P adsorption capacity of various biochar/LDH composites.

Adsorbent	Langmuir Maximum P adsorption amount (mg/g)	
BC300-LDH4	74.9	This Study
BC600-LDH4	64.1	This Study
Corn stalks 600 °C - Mg/Al LDH composite	152.1	(Yang et al., 2019)
Palm derived biochar 700°C - MgAl–LDH	146.4	(Alagha et al., 2020)
Cotton wood biochar 600 °C - MgAl-LDH	410	(Zhang et al., 2019)
Calcined rape biochar 500 °C - MgAl-LDH	132.8	(Zhang et al., 2019)
Calcined cabagge biochar 500°C - MgAl-LDH	127.2	(Zhang et al., 2019)
Macadamia nutshell biochar 700 °C - Mg-Al LDH	43	(Ihsanullah et al., 2024)

4.2.3. XPS analysis

Survey spectra from X-ray Photoelectron Spectroscopy (XPS) analysis were used to understand the surface chemistry, considering the surface groups of biochar (e.g., carboxyl, hydroxyl) or LDH (e.g., metal hydroxides, metal-oxygen bonds) and how they interact with the adsorbed P species (Fig. S5 and S6). Normalized concentrations of C, O, Mg, Al, and P are presented in Table 5.

Table 5. Atomic carbon (C), oxygen (O), Magnesium (Mg) and Phosphorus (P) concentrations in biochars, LDH and biochar-LDH composites before and post P adsorption determined X-ray photoelectron spectroscopy (XPS).

Components	AM 1	AM 2	AM 3	AM 4	AM 5	AM 6	AM 7	AM 8	AM 9	AM 10
%										
C 1s	60.96	65.87	70.99	75.83	16.85	54.17	58.13	65.26	57.42	15.25
Mg 1s	3.75	3.04	2.64	2.03	15.93	4.68	5.57	2.87	3.38	10.57
O 1s	30.45	25.58	26.37	22.14	51.76	35.47	31.54	29.48	34.83	59.07
P 2p	-	-	-	-	-	2.61	2.25	2.39	4.37	6.01
Al 2p	4.84	5.51	-	-	15.46	3.07	2.51	-	-	9.10
C 1s										
					%					
C sp^2	69.83	70.89	67.86	80.97	52.02	67.69	70.39	65.34	66.42	55.19
C sp^3	16.84	15.39	14.99	10.77	4.09	16.35	14.59	17.08	16.65	2.17
C-OH	5.11	6.72	6.13	3.75	30.61	7.10	7.18	8.20	7.58	24.26
C=O	2.27	3.70	8.89	1.52	10.27	6.35	4.56	7.03	6.88	5.93
COOH	5.96	3.31	2.14	2.99	3.01	2.52	3.28	2.35	2.48	12.45
Mg 1s										
					%					
MgO	96.96	78.19	4.77	17.92	41.44	54.28	46.52	56.24	53.61	13.16
$Mg(OH)_2$	3.04	21.81	95.23	82.08	58.56	-	-	1.41	-	-
$MgHPO_4$	-	-	-	-	-	45.72	53.48	42.35	46.39	86.84
O 1s										
					%					
-OH	20.95	7.07	24.37	10.63	49.21	7.86	4.04	7.43	7.75	17.40
-O	69.47	67.76	75.35	57.79	18.83	88.45	83.73	66.07	30.25	74.25
=O	9.59	25.16	0.28	31.58	31.96	3.69	12.23	26.50	62.00	8.35
P 2p										
					%					
$MgHPO_4$ $2p_{1/2}$	-	-	-	-	-	72.07	52.05	33.97	25.34	26.80
$MgHPO_4$ $2p_{3/2}$	-	-	-	-	-	27.93	47.95	66.03	74.66	73.20

AM1: BC300-LDH4; AM2: BC600-LDH4; AM3: BC300; AM4: BC600; AM5: LDH4; AM6: BC300-LDH4-Post P adsorption; AM7: BC600-LDH4-Post P adsorption; AM8: BC300-Post P adsorption; AM9: BC600-Post P adsorption; AM10: LDH4-Post P adsorption.

The C-1s peak was deconvoluted into five components representing different carbon species: C sp^2 (284.5 eV), C sp^3 (285.9 eV), C-OH (287.2 eV), C=O (290.1 eV), and COOH (288.7 eV) (Fig. S7). In biochar samples, the dominant functional group was aromatic C=C (C sp^2), with a higher concentration in biochar prepared at 600 °C, followed by C-C/C-H (C sp^3). The polar groups (C=O, C-OH, and COOH) accounted for less than 10%, which is in agreement with studies on biochar samples (Singh et al., 2014). After P adsorption, the relative concentrations of C-OH and C=O increased, suggesting that P adsorption induces chemical modifications, such as oxidation and the exposure of new oxygenated functional groups. This change in surface chemistry is also reflected in the increase in the binding energy of the O-functional groups, indicating that the adsorbate interacts with these groups by coordinating with

the oxygen atoms (Huang et al., 2024). In contrast, LDH samples exhibited dominant C-OH and C=O groups (Li et al., 2023), and the phosphate adsorption mechanism likely involves the formation of inner-sphere monodentate and bidentate complexes, displacing water molecules or hydroxyl ions (Rahman et al., 2021).

The O-1s peak (Fig. S8) was deconvoluted into three components: one at a binding energy of 533.0 eV, corresponding to –OH (hydroxyl); the other at 531.6 eV, corresponding to O-; and the third at 530.1 eV, representing the oxygen-containing functional group =O (carbonyl). In biochar, the carbonyl groups increased after P adsorption, consistent with the C 1s results. Phosphate ions may interact with hydroxyl (-OH) or carboxyl (-COOH) groups, which are less involved in the adsorption process (Li et al., 2023), leading to their transformation into more oxidized (=O) groups (Yang et al., 2019). In contrast, LDH samples showed an increase in –O groups, which are likely more involved in electrochemical processes and may be more reactive than other oxygen-containing groups, favoring the formation of phosphate-oxygen complexes and enhancing P adsorption (Li et al., 2023).

Three components with binding energies at 1305.7 eV (MgO), 1303.7 eV [$Mg(OH)_3$], and 1303.9 eV ($MgHPO_3$) were identified after curve-fitting of the Mg 1s spectrum (Fig. S9). Additionally, two components with binding energies at 134.8 eV ($MgHPO_3$ 2p $_{1/2}$) and 133.8 eV ($MgHPO_3$ 2p $_{3/2}$) were observed after curve fitting of the P 2p spectrum (Fig. S10). MgO compounds on the Mg-biochar could release Mg^{2+} into the solution, which may then react with phosphate to form Mg–P precipitates. Furthermore, phosphate can be adsorbed on MgO via chemical bonding and electrostatic interaction with Mg-OH groups (Fang et al., 2022; Xu et al., 2018).

Conclusion

The use of pristine biochar (Mg impregnated biochar only) compared to biochar-LDH composites has significant implications for P adsorption and its environmental applications. The impregnation of biochar with LDHs enhanced its P adsorption capacity due to characteristics such as greater thermal stability, more uniform distribution of adsorption sites, greater presence of carbonyl and hydroxyl groups that probably promote complexation with functional groups on the LDH surface. This means that LDHs provide additional active sites and chemical functionalities that improve the affinity for phosphate ions, leading to higher adsorption efficiency.

On the other hand, lower temperatures (300 °C) resulted in the highest adsorption capacity among the biochar-LDH composites, leading to synergistic effects, where the presence

of LDH enhances the overall adsorption capacity beyond what could be achieved by biochar alone. Additionally, the addition of Mg in biochar and biochar-LDH composites resulted in the precipitation of Mg phosphates, which also contributed to P adsorption. These findings provide valuable insights into the efficiency and mechanisms of phosphate adsorption by the studied materials. Finally, the desorption characteristics of phosphorus from these materials, as well as their capacity to supply phosphorus as a fertilizer, should be investigated. This could indicate a viable option for recycling P-loaded materials.

Funding

This work was funded by the Minas Gerais State Research Support Foundation – FAPEMIG (Grant APQ-01159-21), The Brazilian National Council for Scientific and Technological Development - CNPQ (Grant 311634/2021-4), and The Brazilian Federal Agency for Support and Evaluation of Graduate Education – CAPES. The first author received a scholarship from the National Secretary of Science, Technology and Innovation of Panama (SENACYT).

Acknowledgments

The production of LDH and XRD experiments were conducted at the Federal University of Viçosa, Rio Paranaíba, Brazil. We are grateful to Roberta Prado for her assistance with LDH production and XRD analysis. The authors would like to thank The Brazilian Nanotechnology National Laboratory (LNNano - Proposal XPS-20233214) for the XPS analysis. Special thanks to Ângela Albuquerque for her support in analyzing the XPS data. We also thank the Central Analysis and Chemical Prospecting Laboratory of the Federal University of Lavras, as well as Finep, FAPEMIG, CNPq, and CAPES for providing the equipment and technical support for the FTIR analyses. We appreciate the assistance of the Electron Microscopy and Ultrastructural Analysis Laboratory, particularly Aline Norberto Ferreira for her help with the SEM-EDX analysis. We thank Carlos Silva for his collaboration and carbon analyses and Luciene P.R. Profeti and Demetrius Profeti from the Federal University of Espírito Santo for their assistance in interpreting the XPS analysis data. Lastly, we thank Elaine Paris for her help with the BET-N_2 analysis, and Livia Botelho, Mariene Duarte, and Geila Carvalho for their support in laboratory analyses in general.

Declarations

Ethics approval and consent to participate

Not applicable.

Consent for publication

Not applicable.

Competing interests

The authors declare that they have no known competing financial interests or personal relationships that could have influenced the work reported in this paper.

References

Akgül, G., Maden, T.B., Diaz, E., Jiménez, E.M., 2019. Modification of tea biochar with Mg, Fe, Mn and Al salts for efficient sorption of PO43− and Cd2+ from aqueous solutions. Journal of Water Reuse and Desalination 9, 57–66. https://doi.org/10.2166/WRD.2018.018

Associação Mineira da Indústria Florestal (AMIF), 2023. Área plantada por estado brasileiro. Available in: https://amif.org.br/. Accessed: February 24, 2025

Alagha, O., Manzar, M.S., Zubair, M., Anil, I., Mu'azu, N.D., Qureshi, A., 2020. Comparative Adsorptive Removal of Phosphate and Nitrate from Wastewater Using Biochar-MgAl LDH Nanocomposites: Coexisting Anions Effect and Mechanistic Studies. Nanomaterials 2020, Vol. 10, Page 336 10, 336. https://doi.org/10.3390/NANO10020336

Amaringo, F., Hormaza, A., 2013. Determination of the point of zero charge and isoelectric point of two agricultural wastes and their application in the removal of colorants. Journal of Agricultural and Environmental Research 4, 27–26.

Associação Nacional para Difusão de Adubos (ANDA), 2022. Available in: https://anda.org.br/. Accessed: December 2, 2023

Ben Salem, I., El Gamal, M., Sharma, M., Hameedi, S., Howari, F.M., 2021. Utilization of the UAE date palm leaf biochar in carbon dioxide capture and sequestration processes. J Environ Manage 299, 113644. https://doi.org/10.1016/J.JENVMAN.2021.113644

Benício, L.P.F., Constantino, V.R.L., Pinto, F.G., Vergütz, L., Tronto, J., Da Costa, L.M., 2017. Layered Double Hydroxides: New Technology in Phosphate Fertilizers Based on Nanostructured Materials. ACS Sustain Chem Eng 5, 399–409. https://doi.org/10.1021/ACSSUSCHEMENG.6B01784

Benício, L.P.F., Eulálio, D., de Moura Guimarães, L., Pinto, F.G., Da Costa, L.M., Tronto, J., 2018. Layered Double Hydroxides as Hosting Matrices for Storage and Slow Release of Phosphate Analyzed by Stirred-Flow Method. Materials Research 21, e20171004. https://doi.org/10.1590/1980-5373-MR-2017-1004

Benício, L.P.F., Silva, R.A., Lopes, J.A., Eulálio, D., dos Santos, R.M.M., De Aquino, L.A., Vergütz, L., Novais, R.F., Da Costa, L.M., Pinto, F.G., Tronto, J., 2015. Layered double hydroxides: Nanomaterials for applications in agriculture. Rev Bras Cienc Solo 39, 1–13. https://doi.org/10.1590/01000683rbcs2015081

Bian, H., Shen, C., Liu, W., Man, Y.B., Wong, M.H., Christie, P., Shan, S., Wang, M., Zhang, J., 2023. An improved method of MgFe-layered double hydroxide/ biochar composite synthesis. J Clean Prod 393, 136186. https://doi.org/10.1016/J.JCLEPRO.2023.136186

Bolbol, H., Fekri, M., Hejazi-Mehrizi, M., 2019. Layered double hydroxide–loaded biochar as a sorbent for the removal of aquatic phosphorus: behavior and mechanism insights. Arabian Journal of Geosciences 12, 1–11. https://doi.org/10.1007/S12517-019-4694-4

Bravo-Suárez, J.J., Páez-Mozo, E.A., Oyama, S.T., 2004. Review of the synthesis of layered double hydroxides: a thermodynamic approach. Quim Nova 27, 601–614. https://doi.org/10.1590/S0100-40422004000400015

Buates, J., Imai, T., 2021. Application of biochar functionalized with layered double hydroxides: Improved plant growth performance after use as phosphate adsorbent. Applied Sciences (Switzerland) 11. https://doi.org/10.3390/app11146489

Cavani, F., Trifirò, F., Vaccari, A., 1991. Hydrotalcite-type anionic clays: Preparation, properties and applications. Catal Today 11, 173–301. https://doi.org/10.1016/0920-5861(91)80068-K

Dan Luo, Nan, H., Zhang, Y., Sher, F., Wang, C., 2025. Phosphorus recovery from wastewater by Ca-Al layered double hydroxide/biochar as potential agricultural phosphorus for closed-loop phosphorus recycling. Process Safety and Environmental Protection 194, 1538–1548. https://doi.org/10.1016/j.psep.2024.12.110

Domingues, R.R., Trugilho, P.F., Silva, C.A., De Melo, I.C.N.A., Melo, L.C.A., Magriotis, Z.M., Sánchez-Monedero, M.A., 2017. Properties of biochar derived from wood and high-nutrient biomasses with the aim of agronomic and environmental benefits. PLoS One 12, e0176884. https://doi.org/10.1371/JOURNAL.PONE.0176884

Durango Padilla, E.R., Hansted, F.A.S., Luna, C.M.R., de Campos, C.I., Yamaji, F.M., 2024. Biochar derived from agricultural waste and its application as energy source in blast furnace. Renew Energy 220, 119688. https://doi.org/10.1016/J.RENENE.2023.119688

El Hassani, K., Beakou, B.H., Kalnina, D., Oukani, E., Anouar, A., 2017. Effect of morphological properties of layered double hydroxides on adsorption of azo dye Methyl Orange: A comparative study. Appl Clay Sci 140, 124–131. https://doi.org/10.1016/J.CLAY.2017.02.010

Enders, A., Lehmann, J., 2012. Comparison of Wet-Digestion and Dry-Ashing Methods for Total Elemental Analysis of Biochar. Commun Soil Sci Plant Anal 43, 1042–1052. https://doi.org/10.1080/00103624.2012.656167

Fang, Y., Ali, A., Gao, Y., Zhao, P., Li, R., Li, X., Liu, J., Luo, Y., Peng, Y., Wang, H., Liu, H., Zhang, Z., Pan, J., 2022. Preparation and characterization of MgO hybrid biochar and its mechanism for high efficient recovery of phosphorus from aqueous media. Biochar 4, 1–15. https://doi.org/10.1007/S42773-022-00171-0

Farobie, O., Amrullah, A., Bayu, A., Syaftika, N., Anis, L.A., Hartulistiyoso, E., 2022. In-depth study of bio-oil and biochar production from macroalgae Sargassum sp. via slow pyrolysis. RSC Adv 12, 9567–9578. https://doi.org/10.1039/d2ra00702a

Feitoza, U. dos S., Thue, P.S., Lima, E.C., dos Reis, G.S., Rabiee, N., de Alencar, W.S., Mello, B.L., Dehmani, Y., Rinklebe, J., Dias, S.L.P., 2022. Use of Biochar Prepared from the Açaí Seed as Adsorbent for the Uptake of Catechol from Synthetic Effluents. Molecules 27, 7570. https://doi.org/10.3390/MOLECULES27217570

Fernandes, B.C.C., Mendes, K.F., Júnior, A.F.D., Caldeira, V.P. da S., Teófilo, T.M. da S., Silva, T.S., Mendonça, V., de Freitas Souza, M., Silva, D.V., 2020. Impact of Pyrolysis Temperature on the Properties of Eucalyptus Wood-Derived Biochar. Materials 2020, Vol. 13, Page 5841 13, 5841. https://doi.org/10.3390/MA13245841

Forano, C., Hibino, T., Leroux, F., Taviot-Guého, C., 2006. Chapter 13.1 Layered Double Hydroxides. Dev Clay Sci 1, 1021–1095. https://doi.org/10.1016/S1572-4352(05)01039-1

Gao, D., Zhang, W., Dong, H., Yu, Y., Liu, W., Luo, H., Jing, Z., Liang, B., Peng, L., Wu, B., Huang, T., Cheng, H., 2025. Phosphorus removal from water by the layered double hydroxides (LDHs)-based adsorbents: A review for structure, mechanism, and current progress. Environmental Technology & Innovation 37, 104003. https://doi.org/10.1016/j.eti.2024.104003

Gao, L., Wang, R., Shen, G., Zhang, Jixu, Meng, G., Zhang, Jiguang, 2017. Effects of biochar on nutrients and the microbial community structure of tobacco-planting soils. J Soil Sci Plant Nutr 17, 884–896. https://doi.org/10.4067/S0718-95162017000400004

Gao, X., Peng, Y., Guo, L., Wang, Q., Guan, C.Y., Yang, F., Chen, Q., 2020. Arsenic adsorption on layered double hydroxides biochars and their amended red and calcareous soils. J Environ Manage 271, 111045. https://doi.org/10.1016/J.JENVMAN.2020.111045

Giudicianni, P., Cardone, G., Ragucci, R., 2013. Cellulose, hemicellulose and lignin slow steam pyrolysis: Thermal decomposition of biomass components mixtures. J Anal Appl Pyrolysis 100, 213–222. https://doi.org/10.1016/J.JAAP.2012.12.026

He, D., Luo, Y., Zhu, B., 2024. Feedstock and pyrolysis temperature influence biochar properties and its interactions with soil substances: Insights from a DFT calculation. Science of The Total Environment 922, 171259. https://doi.org/10.1016/J.SCITOTENV.2024.171259

He, H., Kang, H., Ma, S., Bai, Y., Yang, X., 2010. High adsorption selectivity of ZnAl layered double hydroxides and the calcined materials toward phosphate. J Colloid Interface Sci 343, 225–231. https://doi.org/10.1016/J.JCIS.2009.11.004

He, H., Zhang, N., Chen, N., Lei, Z., Shimizu, K., Zhang, Z., 2019. Efficient phosphate removal from wastewater by MgAl-LDHs modified hydrochar derived from tobacco stalk. Bioresour Technol Rep 8, 100348. https://doi.org/10.1016/J.BITEB.2019.100348

Heidari, A., Khaki, E., Younesi, H., Lu, H.R. 2019. Evaluation of fast and slow pyrolysis methods for bio-oil and activated carbon production from eucalyptus wastes using a life cycle assessment approach. J Clean Prod 241, 118394. https://doi.org/10.1016/J.JCLEPRO.2019.118394

Huang, J., Xu, C-C-., Ridoutt, B.G., Wang, X-C., Ren, P-A., 2017. Nitrogen and phosphorus losses and eutrophication potential associated with fertilizer application to cropland in China. J.Clean. Prod. 159, 171-179. https://doi.org/10.1016/j.jclepro.2017.05.008

Huang, W.H., Chang, Y.J., Lee, D.J., 2024. Layered double hydroxide loaded pinecone biochar as adsorbent for heavy metals and phosphate ion removal from water. Bioresour Technol 391, 129984. https://doi.org/10.1016/J.BIORTECH.2023.129984

Huang, Y., Lee, X., Grattieri, M., Yuan, M., Cai, R., Macazo, F.C., Minteer, S.D., 2020. Modified biochar for phosphate adsorption in environmentally relevant conditions. Chemical Engineering Journal 380, 122375. https://doi.org/10.1016/J.CEJ.2019.122375

Ihsanullah, I., Almanassra, I.W., Abushawish, A., 2024. Macadamia nut shell biochar/Mg-Al LDH composite: A sustainable solution for highly effective phosphate ion removal from water. Journal of Water Process Engineering 67, 106164. https://doi.org/10.1016/J.JWPE.2024.106164

Indústria Brasileira De Árvores (IBÁ), 2024. Anual Report. Available in: https://iba.org/datafiles/publicacoes/relatorios/relatorio2024.pdf. Accessed: February 24, 2025

Iwaniec, D.M., Metson, G.S., Cordell, D., 2016. P-FUTURES: towards urban food & water security through collaborative design and impact. Curr Opin Environ Sustain 20, 1–7. https://doi.org/10.1016/J.COSUST.2016.03.001

Janu, R., Mrlik, V., Ribitsch, D., Hofman, J., Sedláček, P., Bielská, L., Soja, G., 2021. Biochar surface functional groups as affected by biomass feedstock, biochar composition and pyrolysis temperature. Carbon Resources Conversion 4, 36–46. https://doi.org/10.1016/J.CRCON.2021.01.003

Jung, K.W., Lee, S., Lee, Y.L., 2017. Synthesis of novel magnesium ferrite (MgFe2O4)/biochar magnetic composites and its adsorption behavior for phosphate in aqueous solutions. Bioresour Technol 245, 751-759. https://doi.org/10.1016/J.BIORTECH.2017.09.035

Keyikoglu, R., Khataee, A., Yoon, Y., 2022. Layered double hydroxides for removing and recovering phosphate: Recent advances and future directions. Advances in Colloid and Interface Science 300, 102598. https://doi.org/10.1016/j.cis.2021.102598

Lehmann, J., Joseph, S., 2024. Biochar for environmental management: An introduction. Biochar for Environmental Management: Science, Technology and Implementation 1–14. https://doi.org/10.4324/9781003297673-1

Leite, A. do A., Melo, L.C.A., Hurtarte, L.C.C., Zuin, L., Piccolla, C. Dela, Werder, D., Shabtai, I., Lehmann, J., 2023. Magnesium-enriched poultry manure enhances phosphorus bioavailability in biochars. Chemosphere 331. https://doi.org/10.1016/j.chemosphere.2023.138759

Leng, L., Xiong, Q., Yang, L., Li, Hui, Zhou, Y., Zhang, W., Jiang, S., Li, Hailong, Huang, H., 2021. An overview on engineering the surface area and porosity of biochar. Science of The Total Environment 763, 144204. https://doi.org/10.1016/J.SCITOTENV.2020.144204

Li, G., Zhu, W., Zhu, L., Chai, X., 2016. Effect of pyrolytic temperature on the adsorptive removal of p-benzoquinone, tetracycline, and polyvinyl alcohol by the biochars from sugarcane bagasse. Korean Journal of Chemical Engineering 33, 2215–2221. https://doi.org/10.1007/s11814-016-0067-9

Li, H., Cui, S., Tan, Y., Peng, Y., Gao, X., Yang, X., Ma, Y., He, X., Fan, B., Yang, S., Chen, Q., 2022. Synergistic effects of ball-milled biochar-supported exfoliated LDHs on phosphate adsorption: Insights into role of fine biochar support. Environmental Pollution 294, 118592. https://doi.org/10.1016/J.ENVPOL.2021.118592

Li, P., Zhao, T., Zhao, Z., Tang, H., Feng, W., Zhang, Z., 2023. Biochar Derived from Chinese Herb Medicine Residues for Rhodamine B Dye Adsorption. ACS Omega 8, 4813–4825. https://doi.org/10.1021/ACSOMEGA.2C06968

Li, Y., Xing, B., Ding, Y., Han, X., Wang, S., 2020. A critical review of the production and advanced utilization of biochar via selective pyrolysis of lignocellulosic biomass. Bioresour Technol 312, 123614. https://doi.org/10.1016/J.BIORTECH.2020.123614

Luo X, Wang X, Bao S, Liu X, Zhang W, Fang T. 2016. Adsorption of phosphate in water using one-step synthesized zirconium-loaded reduced graphene oxide. Sci Rep. 6(1):1–13. https://doi.org/10.1038/srep39108

Ma, X., Li, S., Ren, H., Zhang, Y., Ma, Z., 2022. Egg White-Mediated Fabrication of Mg/Al-LDH-Hard Biochar Composite for Phosphate Adsorption. Molecules 2022, Vol. 27, Page 8951 27, 8951. https://doi.org/10.3390/MOLECULES27248951

Maia, C. M. B. De F., Guiotoku, M., Peixoto, R. T Dos G., Vargas, L. M. P. Biochar e o eucalipto. In: OLIVIERA, E. B. de, PINTO JUNIOR, J. E. (Embrapa). O eucalipto e a Embrapa: quatro décadas de pesquisa e desenvolvimento. Brasília, DF: Embrapa, 2021. P. 589-610.

Meroufel, B., Benali, O., Benyahia, M., Zenasni, M.A., Merlin, A., George, B., 2013. Removal of Zn (II) from Aqueous Solution onto Kaolin by Batch Design. J Water Resour Prot 05, 669–680. https://doi.org/10.4236/jwarp.2013.57067

Mu'azu, N.D., Zubair, M., Jarrah, N., Alagha, O., Al-harthi, M.A., Essa, M.H., 2020. Sewage sludge ZnCl2-activated carbon intercalated MgFe–LDH nanocomposites: Insight of the sorption mechanism of improved removal of phenol from water. Int J Mol Sci 21. https://doi.org/10.3390/ijms21051563

Muhammad, N., Ge, L., Chan, W.P., Khan, A., Nafees, M., Lisak, G., 2022. Impacts of pyrolysis temperatures on physicochemical and structural properties of green waste derived biochars for adsorption of potentially toxic elements. J Environ Manage 317, 115385. https://doi.org/10.1016/J.JENVMAN.2022.115385

Nardis, B.O., Santana Da Silva Carneiro, J., Souza, I.M.G. De, Barros, R.G. De, Azevedo Melo, L.C., 2021. Phosphorus recovery using magnesium-enriched biochar and its potential use as fertilizer. Arch Agron Soil Sci 67, 1017–1033. https://doi.org/10.1080/03650340.2020.1771699

Nguyen, T.T.H., Nguyen, X.C., Nguyen, D.L.T., Nguyen, D.D., Vo, T.Y.B., Vo, Q.N., Nguyen, T.D., Ly, Q.V., Ngo, H.H., Vo, D.V.N., Nguyen, T.P., Kim, I.T., Van Le, Q., 2023.

Converting biomass of agrowastes and invasive plant into alternative materials for water remediation. Biomass Convers Biorefin 13, 5391–5406. https://doi.org/10.1007/S13399-021-01526-6

Novais, S.V., Zenero, M.D.O., Tronto, J., Conz, R.F., Cerri, C.E.P., 2018. Poultry manure and sugarcane straw biochars modified with MgCl2 for phosphorus adsorption. J Environ Manage 214, 36–44. https://doi.org/10.1016/J.JENVMAN.2018.02.088

Pavan, P.C., Crepaldi, E.L., Valim, J.B., 2000. Sorption of Anionic Surfactants on Layered Double Hydroxides. J Colloid Interface Sci 229, 346–352. https://doi.org/10.1006/JCIS.2000.7031

Ponnusamy, V.K., Nagappan, S., Bhosale, R.R., Lay, C.H., Duc Nguyen, D., Pugazhendhi, A., Chang, S.W., Kumar, G., 2020. Review on sustainable production of biochar through hydrothermal liquefaction: Physico-chemical properties and applications. Bioresour Technol 310, 123414. https://doi.org/10.1016/J.BIORTECH.2020.123414

Rahman, S., Navarathna, C.M., Krishna Das, N., Alchouron, J., Reneau, P., Stokes, S., V.K.G. Thirumalai, R., Perez, F., Barbary Hassan, E., Mohan, D., Pittman, C.U., Mlsna, T., 2021. High capacity aqueous phosphate reclamation using Fe/Mg-layered double hydroxide (LDH) dispersed on biochar. J Colloid Interface Sci 597, 182–195. https://doi.org/10.1016/J.JCIS.2021.03.114

Rajkovich, S., Enders, A., Hanley, K., Hyland, C., Zimmerman, A.R., Lehmann, J., 2012. Corn growth and nitrogen nutrition after additions of biochars with varying properties to a temperate soil. Biol Fertil Soils 48, 271–284. https://doi.org/10.1007/S00374-011-0624-7

Ringeval, B., Demay, J., Goll, D.S., He, X., Wang, Y.P., Hou, E., Matej, S., Erb, K.H., Wang, R., Augusto, L., Lun, F., Nesme, T., Borrelli, P., Helfenstein, J., McDowell, R.W., Pletnyakov, P., Pellerin, S., 2024. A global dataset on phosphorus in agricultural soils. Scientific Data 2024 11:1 11, 1–34. https://doi.org/10.1038/s41597-023-02751-6

Robati, D., 2013. Pseudo-second-orders kinetic equations for modeling adsorption systems for removal of lead ions using multi-walled carbon nanotube. J Nanostructure Chem 3. https://doi.org/10.1186/2193-8865-3-55

Roy, E.D., Richards, P.D., Martinelli, L.A., Coletta, L. Della, Lins, S.R.M., Vazquez, F.F., Willig, E., Spera, S.A., VanWey, L.K., Porder, S., 2016. The phosphorus cost of agricultural intensification in the tropics. Nature Plants 2016 2:5 2, 1–6. https://doi.org/10.1038/nplants.2016.43

Scholz, R.W., Ulrich, A.E., Eilittä, M., Roy, A., 2013. Sustainable use of phosphorus: A finite resource. Science of The Total Environment 461–462, 799–803. https://doi.org/10.1016/J.SCITOTENV.2013.05.043

Shepherd, J.G., Sohi, S.P., Heal, K. V., 2016. Optimising the recovery and re-use of phosphorus from wastewater effluent for sustainable fertiliser development. Water Res 94, 155–165. https://doi.org/10.1016/J.WATRES.2016.02.038

Singh, B., Fang, Y., Cowie, B.C.C., Thomsen, L., 2014. NEXAFS and XPS characterisation of carbon functional groups of fresh and aged biochars. Org Geochem 77, 1–10. https://doi.org/10.1016/J.ORGGEOCHEM.2014.09.006

Soliemanzadeh, A., Fekri, M., Bakhtiary, S., Mehrizi, M.H., 2016. Biosynthesis of iron nanoparticles and their application in removing phosphorus from aqueous solutions. Chemistry and Ecology 32, 286–300. https://doi.org/10.1080/02757540.2016.1139091

Sun, J., He, F., Pan, Y., Zhang, Z., 2017. Effects of pyrolysis temperature and residence time on physicochemical properties of different biochar types. Acta Agric Scand B Soil Plant Sci 67, 12–22. https://doi.org/10.1080/09064710.2016.1214745

Takaya, C.A., Fletcher, L.A., Singh, S., Anyikude, K.U., Ross, A.B., 2016. Phosphate and ammonium sorption capacity of biochar and hydrochar from different wastes. Chemosphere 145, 518–527. https://doi.org/10.1016/J.CHEMOSPHERE.2015.11.052

Theiss, F.L., Ayoko, G.A., Frost, R.L., 2013. Thermogravimetric analysis of selected layered double hydroxides. J Therm Anal Calorim 112, 649–657. https://doi.org/10.1007/S10973-012-2584-Z

Thue, P.S., Lima, E.C., Sieliechi, J.M., Saucier, C., Dias, S.L.P., Vaghetti, J.C.P., Rodembusch, F.S., Pavan, F.A., 2017. Effects of first-row transition metals and impregnation ratios on the physicochemical properties of microwave-assisted activated carbons from wood biomass. J Colloid Interface Sci 486, 163–175. https://doi.org/10.1016/j.jcis.2016.09.070

Tian, J., Dunfield, K., Condron, L., 2024. Biological cycling of nitrogen and phosphorus in soils. Plant Soil 498, 1–4. https://doi.org/10.1007/S11104-024-06601-1/FIGURES/1

Vikrant, K., Kim, K.H., Ok, Y.S., Tsang, D.C.W., Tsang, Y.F., Giri, B.S., Singh, R.S., 2018. Engineered/designer biochar for the removal of phosphate in water and wastewater. Science of The Total Environment 616–617, 1242–1260. https://doi.org/10.1016/J.SCITOTENV.2017.10.193

Wan, S., Wang, S., Li, Y., Gao, B., 2017. Functionalizing biochar with Mg–Al and Mg–Fe layered double hydroxides for removal of phosphate from aqueous solutions. Journal of Industrial and Engineering Chemistry 47, 246–253. https://doi.org/10.1016/J.JIEC.2016.11.039

Wang, C., Zhou, Y., Yu, F., Zhu, X., Dong, M., Li, Q., 2024. Recovery of phosphate from aqueous solution by modified biochar with concentrated seawater and its potential application as fertilizer. J Environ Chem Eng 12, 112646. https://doi.org/10.1016/J.JECE.2024.112646

Wang, Q., Ohare, D., 2012. Recent advances in the synthesis and application of layered double hydroxide (LDH) nanosheets. Chem Rev 112, 4124–4155. https://doi.org/10.1021/CR200434V

Wang, W., Tan, J., Li, S., Guan, Y., Zhang, X., Wang, N., Liu, J., Jiang, X., 2022. Transport, retention and release of phytate in soil with addition of Mg–Al layered double hydroxides. J Clean Prod 379. https://doi.org/10.1016/j.jclepro.2022.134774

Wang, Y., Hu, Y., Zhao, X., Wang, S., Xing, G., 2013. Comparisons of Biochar Properties from Wood Material and Crop Residues at Different Temperatures and Residence Times. Energy and Fuels 27, 5890–5899. https://doi.org/10.1021/EF400972Z

Witek-Krowiak, A., Gorazda, K., Szopa, D., Trzaska, K., Moustakas, K., Chojnacka, K., 2022. Phosphorus recovery from wastewater and bio-based waste: an overview. Bioengineered. https://doi.org/10.1080/21655979.2022.2077894

Xu, K., Lin, F., Dou, X., Zheng, M., Tan, W., Wang, C., 2018. Recovery of ammonium and phosphate from urine as value-added fertilizer using wood waste biochar loaded with magnesium oxides. J Clean Prod 187, 205–214. https://doi.org/10.1016/J.JCLEPRO.2018.03.206

Yang, F., Zhang, S., Sun, Y., Tsang, D.C.W., Cheng, K., Ok, Y.S., 2019. Assembling biochar with various layered double hydroxides for enhancement of phosphorus recovery. J Hazard Mater 365, 665–673. https://doi.org/10.1016/J.JHAZMAT.2018.11.047

Yang, K., Yan, L.G., Yang, Y.M., Yu, S.J., Shan, R.R., Yu, H.Q., Zhu, B.C., Du, B., 2014. Adsorptive removal of phosphate by Mg–Al and Zn–Al layered double hydroxides: Kinetics, isotherms and mechanisms. Sep Purif Technol 124, 36–42. https://doi.org/10.1016/J.SEPPUR.2013.12.042

Yao, Y., Gao, B., Chen, J., Zhang, M., Inyang, M., Li, Y., Alva, A., Yang, L., 2013. Engineered carbon (biochar) prepared by direct pyrolysis of Mg-accumulated tomato tissues: Characterization and phosphate removal potential. Bioresour Technol 138, 8–13. https://doi.org/10.1016/J.BIORTECH.2013.03.057

Yao, Y., Gao, B., Inyang, M., Zimmerman, A.R., Cao, X., Pullammanappallil, P., Yang, L., 2011. Biochar derived from anaerobically digested sugar beet tailings: Characterization and phosphate removal potential. Bioresour Technol 102, 6273–6278. https://doi.org/10.1016/J.BIORTECH.2011.03.006

Yi, Y., Huang, Z., Lu, B., Xian, J., Tsang, E.P., Cheng, W., Fang, J., Fang, Z., 2020. Magnetic biochar for environmental remediation: A review. Bioresour Technol 298, 122468. https://doi.org/10.1016/J.BIORTECH.2019.122468

Zeng, Z., Zhang, S. Da, Li, T.Q., Zhao, F.L., He, Z.L., Zhao, H.P., Yang, X.E., Wang, H.L., Zhao, J., Rafiq, M.T., 2013. Sorption of ammonium and phosphate from aqueous solution by biochar derived from phytoremediation plants. J Zhejiang Univ Sci B 14, 1152–1161. https://doi.org/10.1631/jzus.B1300102

Zhang, K., Mao, J., Chen, B., 2019a. Reconsideration of heterostructures of biochars: Morphology, particle size, elemental composition, reactivity and toxicity. Environmental Pollution 254, 113017. https://doi.org/10.1016/J.ENVPOL.2019.113017

Zhang, L., Liu, J., Guo, X., 2018. Investigation on mechanism of phosphate removal on carbonized sludge adsorbent. Journal of Environmental Sciences 64, 335–344. https://doi.org/10.1016/J.JES.2017.06.034

Zhang, M., Gao, B., Yao, Y., Inyang, M., 2013. Phosphate removal ability of biochar/MgAl-LDH ultra-fine composites prepared by liquid-phase deposition. Chemosphere 92, 1042–1047. https://doi.org/10.1016/J.CHEMOSPHERE.2013.02.050

Zhang, Q., Xu, H., Lu, W., Zhang, D., Ren, X., Yu, W., Wu, J., Zhou, L., Han, X., Yi, W., Lei, H., 2020. Properties evaluation of biochar/high-density polyethylene composites: Emphasizing the porous structure of biochar by activation. Science of The Total Environment 737, 139770. https://doi.org/10.1016/J.SCITOTENV.2020.139770

Zhang, Y., Wang, X., Hu, Z. qiang, Xiao, Q. qing, Wu, Y., 2025. Capturing and recovering phosphorus in water via composite material: Research progress, future directions, and challenges. Sep Purif Technol 353, 128453. https://doi.org/10.1016/J.SEPPUR.2024.128453

Zhang, Z., Yan, L., Yu, H., Yan, T., Li, X., 2019b. Adsorption of phosphate from aqueous solution by vegetable biochar/layered double oxides: Fast removal and mechanistic studies. Bioresour Technol 284, 65–71. https://doi.org/10.1016/J.BIORTECH.2019.03.113

Zhu, D., Chen, Y., Yang, H., Wang, S., Wang, X., Zhang, S., Chen, H., 2020. Synthesis and characterization of magnesium oxide nanoparticle-containing biochar composites for efficient phosphorus removal from aqueous solution. Chemosphere 247, 125847. https://doi.org/10.1016/J.CHEMOSPHERE.2020.125847

Zubair, M., Ihsanullah, I., Abdul Aziz, H., Azmier Ahmad, M., Al-Harthi, M.A., 2021. Sustainable wastewater treatment by biochar/layered double hydroxide composites: Progress, challenges, and outlook. Bioresour Technol 319, 124128. https://doi.org/10.1016/J.BIORTECH.2020.124128

Zubair, M., Manzar, M.S., El-Qanni, A., Haroon, H., Alqahtani, H.A., Al-Ejji, M., Mu'azu, N.D., AlGhamdi, J.M., Haladu, S.A., Al-Hashim, D., Ahmed, S.Z., 2023. Biochar-layered double hydroxide composites for the adsorption of tetracycline from water: synthesis, process modeling, and mechanism. Environmental Science and Pollution Research 30, 109162–109180. https://doi.org/10.1007/S11356-023-29954-Z

Supplementary material

Table S1. Adsorption capacity of biochar as a function of pyrolysis temperature

Biochar (°C)	P Adsorption (%)	P adsorption (mg g^{-1})
300	92.1 ± 1.34	53.8 ± 0.6
600	96.8 ± 2.71	56.4 ± 1.58
900	81.2 ± 0.67	47.6 ± 0.38

Table S2. Properties of biochars at 300 °C, 600 °C and 900 °C impregnated with Mg^{2+}.

Properties	Material					
	BC300	**BC600**	**BC900**	**BC300-LDH4**	**BC600-LDH4**	**LDH4**
Ash (%)	14.8 ± 0.3	14.2 ± 0.3	14.0 ± 0.4	-	-	-
Moisture (%)	3.9 ± 0.3	3.7 ± 0.3	3.7 ± 0.2	-	-	-
Total C (%)	55.9 ± 0.4	70.2 ± 0.3	70.3 ± 0.4	42.6 ± 0.01	52.4 ± 0.35	-
pH	10.7 ± 0.0	11.1 ± 0.0	11.1 ± 0.0	10.0 ± 0.04	10.32 ± 0.03	9.73 ± 1.08
EC (μS cm^{-1})	1427.7 ± 53.9	413.3 ± 11.9	469.7 ± 13.5	-	-	
Yield (%)	35.9 ± 0.2	26.6 ± 0.7	25.0 ± 0.7	-	-	55.43 ± 0.2
PZC	10.5	10.3	-	-	-	13.0
Mg (g k^{-1})	4.29 ± 0.1	12.20 ± 0.2	11.89 ± 0.2	187.28 ± 0.0	194.12 ± 0.0	403.98 ± 0.0
Al (g k^{-1})	-	-	-	25.70 ± 1.3	24.10 ± 1.0	91.70 ± 0.7
P (g k^{-1})	0.05 ± 0.0	0.08 ± 0.0	0.08 ± 0.0	0.00 ± 0.0	0.07 ± 0.0	0.00 ± 0.0

Table S3. Phosphorus adsorption as a function of biochar dose and pyrolysis temperature.

Pyrolysis temperature (°C)	**Dose (g L^{-1})**	**P adsorption (mg g^{-1})**	**pH**
	1	6.7 ± 3.6	6.6 ± 0.6
	2	2.2 ± 1.2	7.1 ± 0.4
300	5	51.1 ± 3.4	8.0 ± 2.6
	10	53.8 ± 0.7	9.7 ± 1.3
	20	29.2 ± 0.0	10.5 ± 0.1
	1	24.0 ± 2.3	6.6 ± 0.3
	2	8.6 ± 4.3	7.1 ± 1.5
600	5	38.3 ± 4.6	8.2 ± 4.0
	10	56.4 ± 1.6	11.5 ± 2.71
	20	26.8 ± 0.9	11.9 ± 3.1
	1	5.2 ± 4.6	6.5 ± 0.8
	2	0.6 ± 0.0	7.0 ± 0.0
900	5	35.9 ± 0.8	7.9 ± 0.9
	10	47.6 ± 0.4	11.3 ± 0.7
	20	28.4 ± 0.1	11.8 ± 0.5

Table S4. Phosphorus adsorption as a function of LDH dose and Mg/Al ratios.

Mg/Al ratio LDH	Dose (g L^{-1})	P Adsorption (mg g^{-1})	pH
LDH 1:1	1	93.5 ± 7.5	7.5 ± 0.0
	2	95.8 ± 8.6	8.6 ± 0.0
	5	75.4 ± 9.9	9.9 ± 0.0
	10	41.3 ± 0.5	10.2 ± 0.0
LDH 2:1	1	140.0 ± 17.4	8.1 ± 0.0
	2	154.2 ± 5.0	8.5 ± 0.0
	5	77.8 ± 0.7	10.3 ± 0.0
	10	37.8 ± 0.1	10.7 ± 0.0
LDH 3:1	1	189.4 ± 5.6	8.6 ± 0.0
	2	178.2 ± 3.4	9.8 ± 0.1
	5	91.5 ± 0.9	11.3 ± 0.0
	10	53.0 ± 0.4	12.3 ± 0.0
LDH 4:1	1	271.5 ± 10.4	8.6 ± 0.1
	2	194.0 ± 1.1	10.8 ± 0.0
	5	104.4 ± 0.8	11.5 ± 0.0
	10	52.9 ± 0.2	12.0 ± 0.0

Table S5. Phosphorus adsorption as a function of biochar-LDH composites dose.

Composite	Dose (g L^{-1})	P Adsorption (mg g^{-1})	pH
BC300-LDH4	1	12.0 ± 3.3	7.0 ± 0.0
	2.5	37.9 ± 1.2	7.9 ± 0.0
	5	79.9 ± 0.4	9.9 ± 0.0
	10	46.9 ± 0.1	10.8 ± 0.0
BC600-LDH4	1	3.57 ± 1.1	6.9 ± 0.0
	2.5	9.31 ± 3.0	7.9 ± 0.0
	5	66.97 ± 0.7	10.3 ± 0.0
	10	43.36 ± 0.1	11.7 ± 0.0

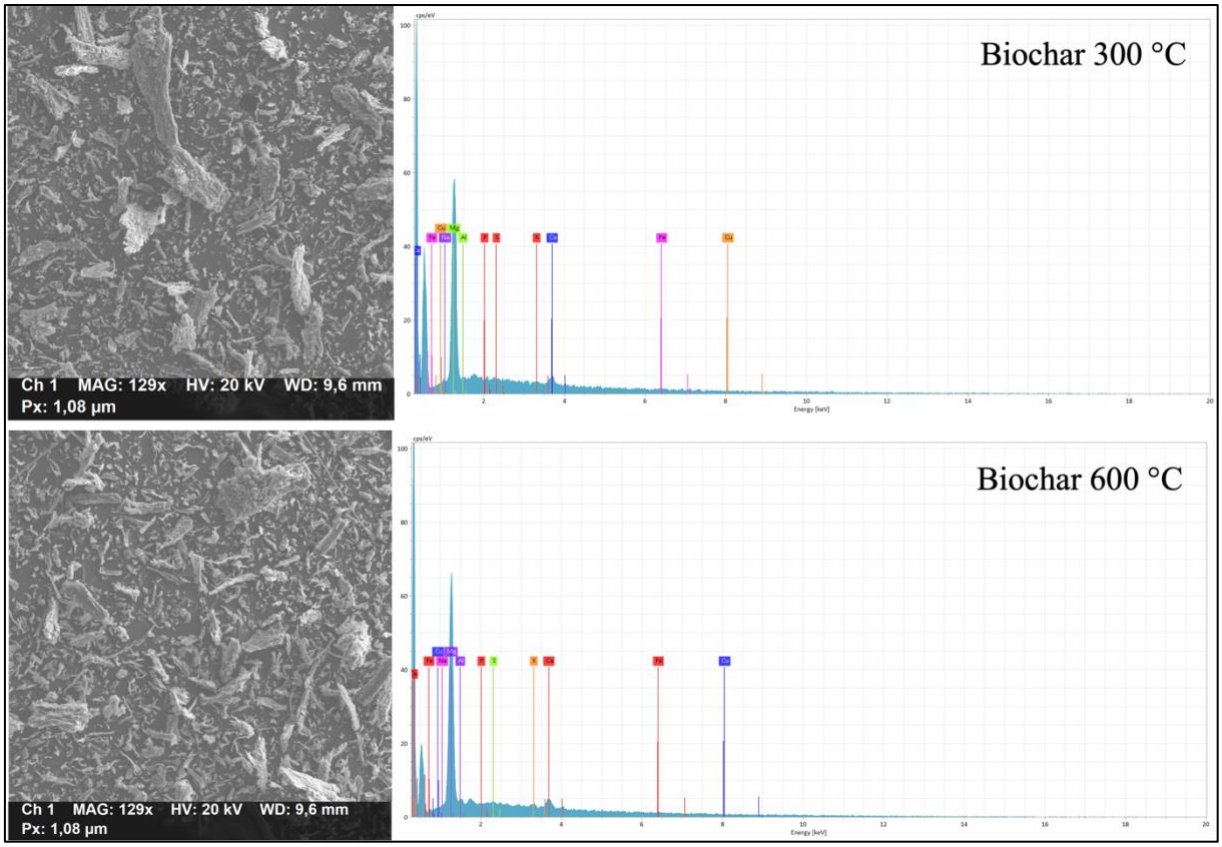

Figure S1. SEM (Scanning electron microscopy) and EDS (Energy dispersive spectroscopy) of biochars.

Table S6. EDS (Energy dispersive spectroscopy) of biochar.

Biochar at 300 °C							
Element	At. No.	Netto	Mass [%]	Mass Norm. [%]	Atom [%]	abs. error [%] (1 sigma)	rel. error [%] (1 sigma)
Phosphorus	15	91.4	0.09	1.35	1.13	0.05	76.82
Aluminium	13	515	0.65	11.54	11.05	0.09	14.35
Sulfur	16	84	0.07	1.09	0.88	0.03	44.63
Iron	26	38	0.08	1.35	0.63	0.06	64.02
Potassium	19	112.8	0.09	1.54	1.02	0.05	62.24
Magnesium	12	8262	4.45	75.76	80.58	0.29	6.45
Calcium	20	458	0.43	7.21	4.65	0.07	17.30
		Sum	5.87	100	100		
Biochar at 600 °C							
Element	At. No.	Netto	Mass [%]	Mass Norm. [%]	Atom [%]	abs. error [%] (1 sigma)	rel. error [%] (1 sigma)
Phosphorus	15	81	0.07	1.20	1.01	0.04	115.25
Aluminium	13	662	0.78	12.83	12.31	0.10	12.57
Sulfur	16	83	0.07	0.99	0.80	0.03	39.56
Iron	26	32	0.06	0.87	0.40	0.05	124.65
Potassium	19	152	0.11	1.76	1.17	0.05	61.81
Magnesium	12	9213	4.74	74.25	79.09	0.30	6.39
Calcium	20	571	0.51	8.05	5.20	0.07	14.71
		Sum	6.34	100	100		

Note: Average of 5 single points.

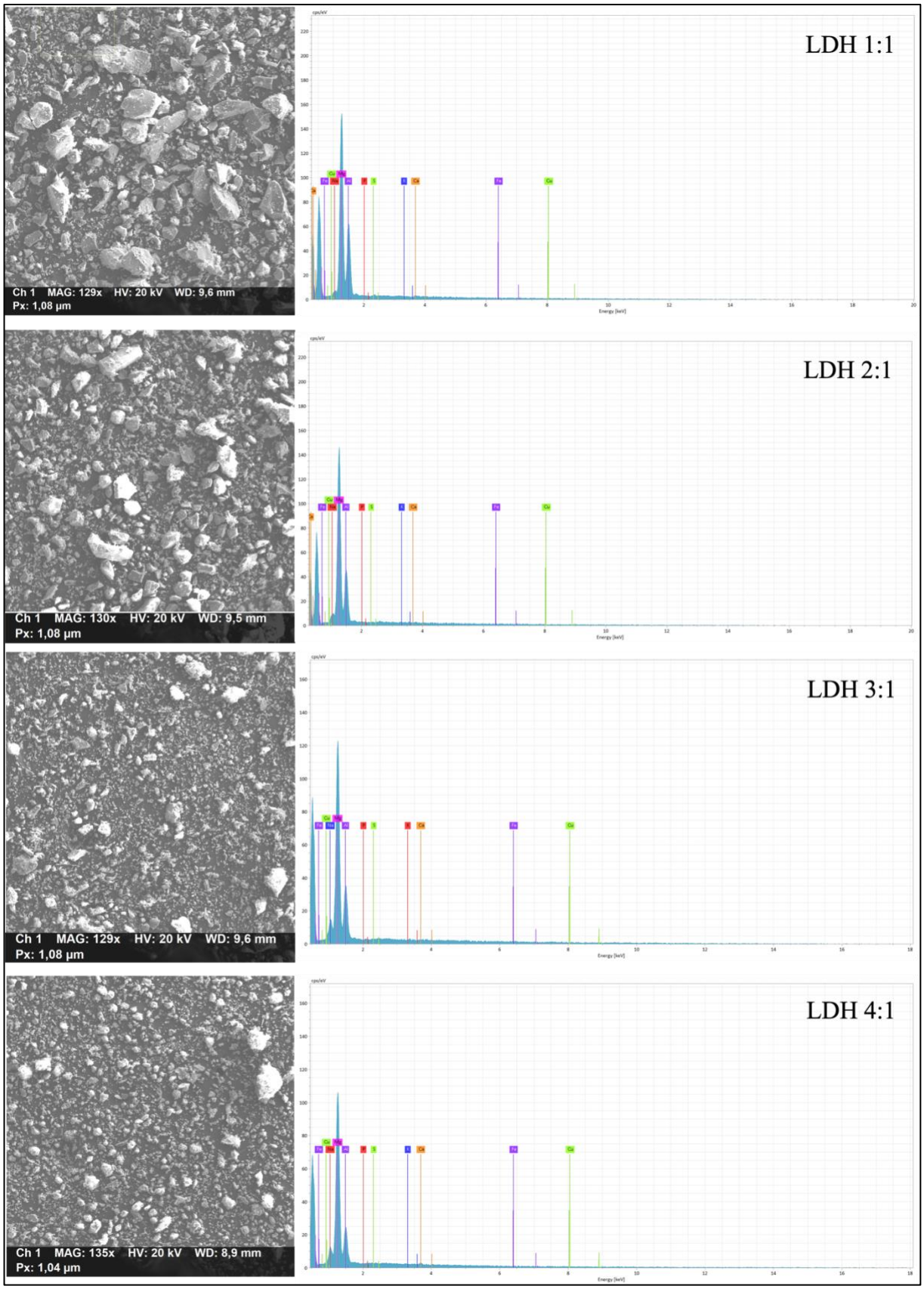

Figure S2. SEM (Scanning electron microscopy) and EDS (Energy dispersive spectroscopy) of LDH of different Mg/Al ratio.

Table S7. EDS (Energy dispersive spectroscopy) of LDH of different Mg/Al ratio

LDH 1:1							
Element	At. No.	Netto	Mass [%]	Mass Norm. [%]	Atom [%]	abs. error [%] (1 sigma)	rel. error [%] (1 sigma)
Phosphorus	15	30	0.04	0.14	0.11	0.04	80.47
Aluminium	13	10483	11.88	45.24	42.89	0.62	5.26
Sulfur	16	20	0.02	0.07	0.06	0.02	34.67
Sodium	11	0	-	-	-	-	4.43
Potassium	19	22	0.02	0.08	0.05	0.02	41.29
Magnesium	12	25014	14.06	53.57	56.37	0.81	5.76
Calcium	20	151	0.17	0.63	0.40	0.06	38.84
Iron	26	13	0.03	0.10	0.05	0.04	128.25
		Sum	26.21	100	100		
LDH 2:1							
Element	At. No.	Netto	Mass [%]	Mass Norm. [%]	Atom [%]	abs. error [%] (1 sigma)	rel. error [%] (1 sigma)
Phosphorus	15	15	0.02	0.09	0.08	0.02	131.07
Aluminium	13	7206	9.81	40.66	38.24	0.53	5.44
Sulfur	16	7	0.01	0.04	0.03	0.01	15.47
Sodium	11	180	0.15	0.57	0.63	0.05	36.18
Potassium	19	22	0.02	0.11	0.07	0.02	66.02
Magnesium	12	21929	14.06	58.23	60.80	0.81	5.78
Calcium	20	23	0.03	0.13	0.08	0.02	224.64
Iron	26	4	0.01	0.03	0.02	0.03	396.41
		Sum	24.10	100	100		
LDH 3:1							
Element	At. No.	Netto	Mass [%]	Mass Norm. [%]	Atom [%]	abs. error [%] (1 sigma)	rel. error [%] (1 sigma)
Phosphorus	15	43	0.05	0.28	0.23	0.04	71.11
Aluminium	13	5012	6.40	35.90	33.76	0.37	5.75
Sulfur	16	50	0.05	0.28	0.22	0.02	20.11
Sodium	11	724	0.52	2.89	3.20	0.09	16.87
Potassium	19	20	0.02	0.09	0.06	0.03	195.68
Magnesium	12	17073	10.58	59.35	61.97	0.62	5.88
Calcium	20	30	0.04	0.23	0.14	0.03	60.38
Iron	26	38	0.09	0.52	0.24	0.06	56.45
Copper	29	24	0.08	0.46	0.18	0.05	42.21
		Sum	11.38	100	100		
LDH 4:1							
Element	At. No.	Netto	Mass [%]	Mass Norm. [%]	Atom [%]	abs. error [%] (1 sigma)	rel. error [%] (1 sigma)
Phosphorus	15	63	0.06	0.30	0.25	0.03	33.38
Aluminium	13	5584	6.43	31.57	29.55	0.37	5.68
Sulfur	16	64	0.05	0.27	0.21	0.04	169.69
Potassium	19	22	0.02	0.10	0.06	0.02	114.03
Sodium	11	1114	0.70	3.37	3.70	0.09	14.01
Magnesium	12	23817	12.84	63.01	65.48	0.74	5.78
Calcium	20	179	0.17	0.84	0.53	0.06	37.42
Iron	26	18	0.03	0.17	0.08	0.04	141.54
Copper	29	27	0.08	0.38	0.15	0.05	49.12
		Sum	13.90	100	100		

Note: Average of 5 single points.

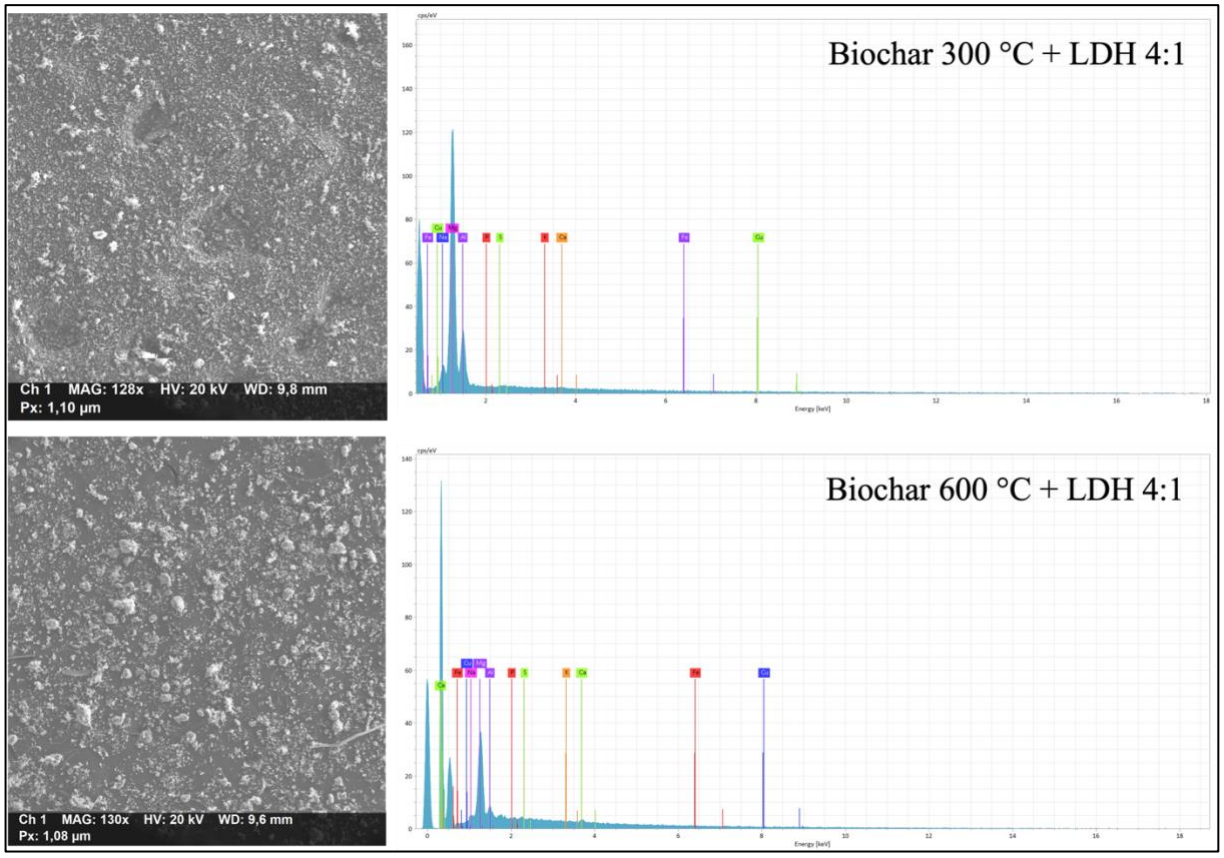

Figure S3. SEM (Scanning electron microscopy) and EDS (Energy dispersive spectroscopy) of biochar and LDH composites.

Table S8. EDS (Energy dispersive spectroscopy) of Biochar- LDH composites.

Biochar at 300 °C-LDH 4:1							
Element	At. No.	Netto	Mass [%]	Mass Norm. [%]	Atom [%]	abs. error [%] (1 sigma)	rel. error [%] (1 sigma)
Phosphorus	15	173	0.15	2.03	1.70	0.06	78.62
Sulfur	16	144	0.11	1.50	1.22	0.04	53.79
Aluminium	13	1864	1.88	26.46	25.28	0.14	7.72
Iron	26	30	0.05	0.72	0.33	0.05	76.04
Copper	29	9	0.02	0.31	0.13	0.02	13.76
Calcium	20	315	0.26	3.70	2.38	0.06	23.92
Magnesium	12	10054	4.58	64.61	68.52	0.29	6.33
Sodium	11	0	-	-	-	-	4.43
Potassium	19	64	0.05	0.68	0.45	0.04	102.03
		Sum	6.84	100	100		
Biochar at 600 °C-LDH 4:1							
Element	At. No.	Netto	Mass [%]	Mass Norm. [%]	Atom [%]	abs. error [%] (1 sigma)	rel. error [%] (1 sigma)
Phosphorus	15	171	0.14	2.42	1.98	0.04	93.28
Sulfur	16	96	0.07	1.32	1.10	0.02	37.54
Aluminium	13	1672	1.55	29.04	28.15	0.13	8.21
Iron	26	61	0.10	1.82	0.86	0.05	45.62
Copper	29	22	0.06	1.13	0.47	0.06	110.58
Calcium	20	229	0.18	3.20	2.09	0.06	36.37
Magnesium	12	7298	3.23	60.12	64.65	0.22	6.72
Sodium	11	0	-	-	-	-	4.43
Potassium	19	91	0.06	1.10	0.73	0.05	82.06
		Sum	5.25	100	100		

Note: Average of 5 single points.

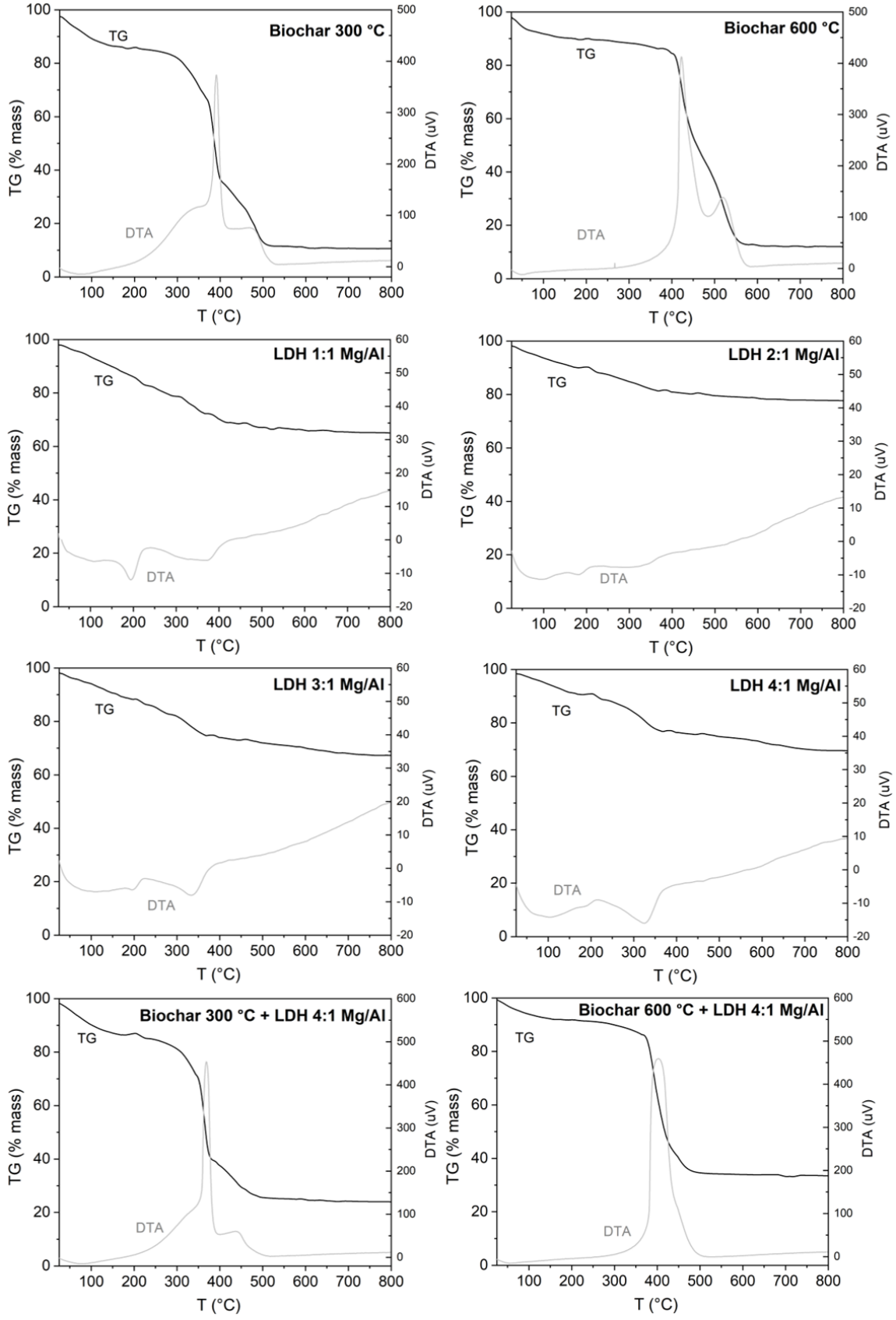

Figure S4. TG and DTA curves of biochars, LDH and biochar-LDH composites.

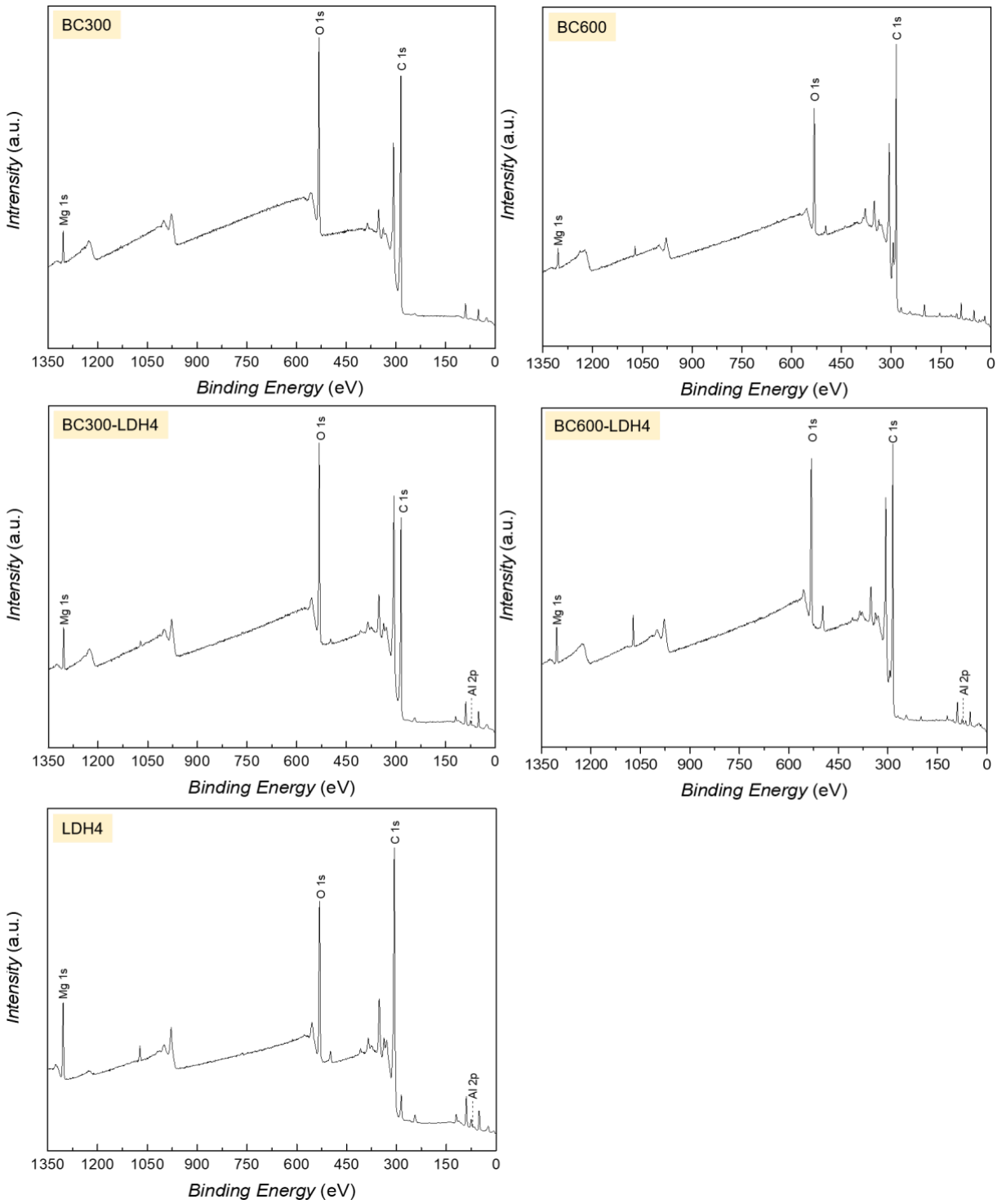

Figure S5. XPS survey of biochar, LDH and LDH-composites**.**

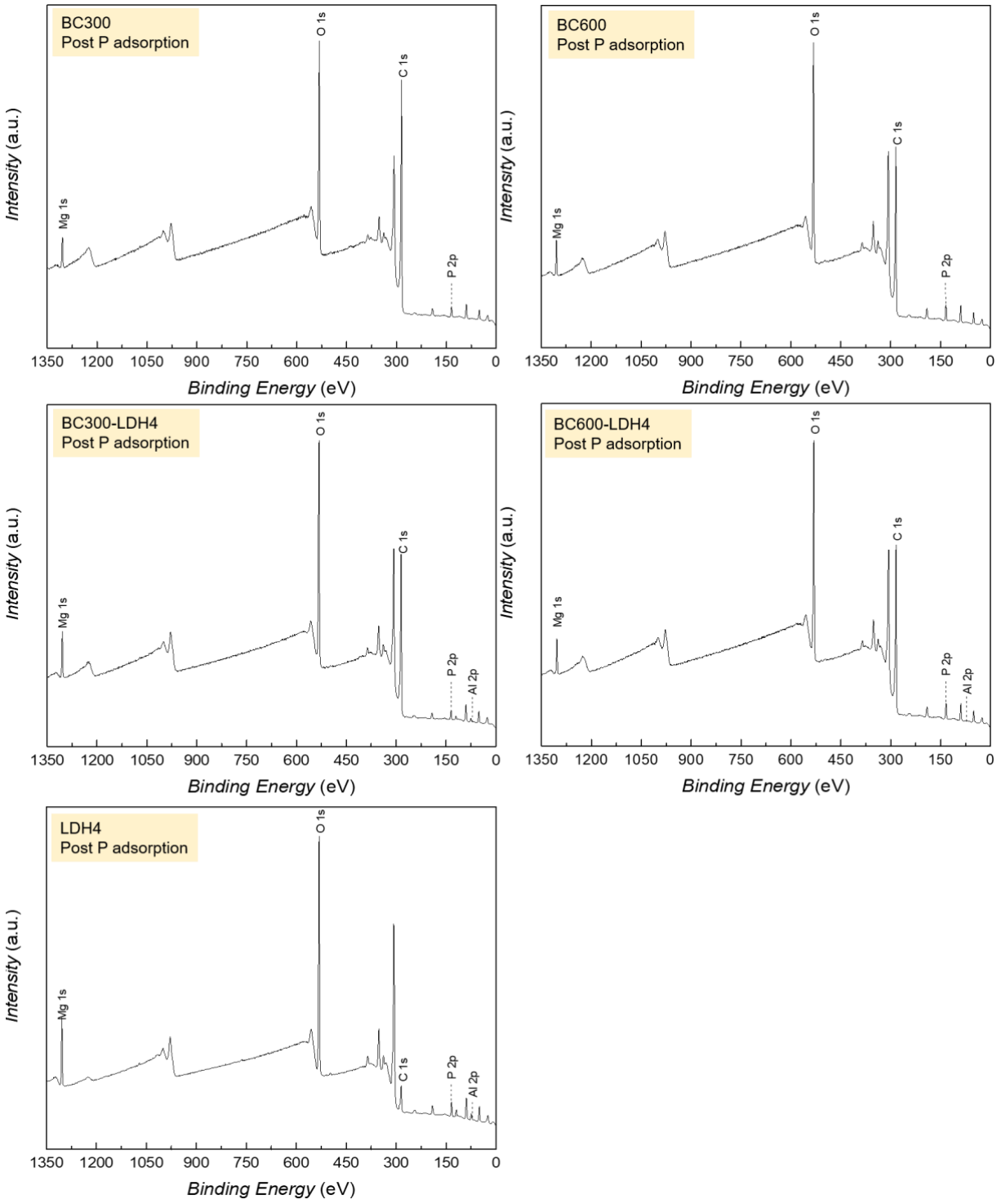

Figure S6. XPS survey of biochar, LDH and LDH-composites post P adsorption.

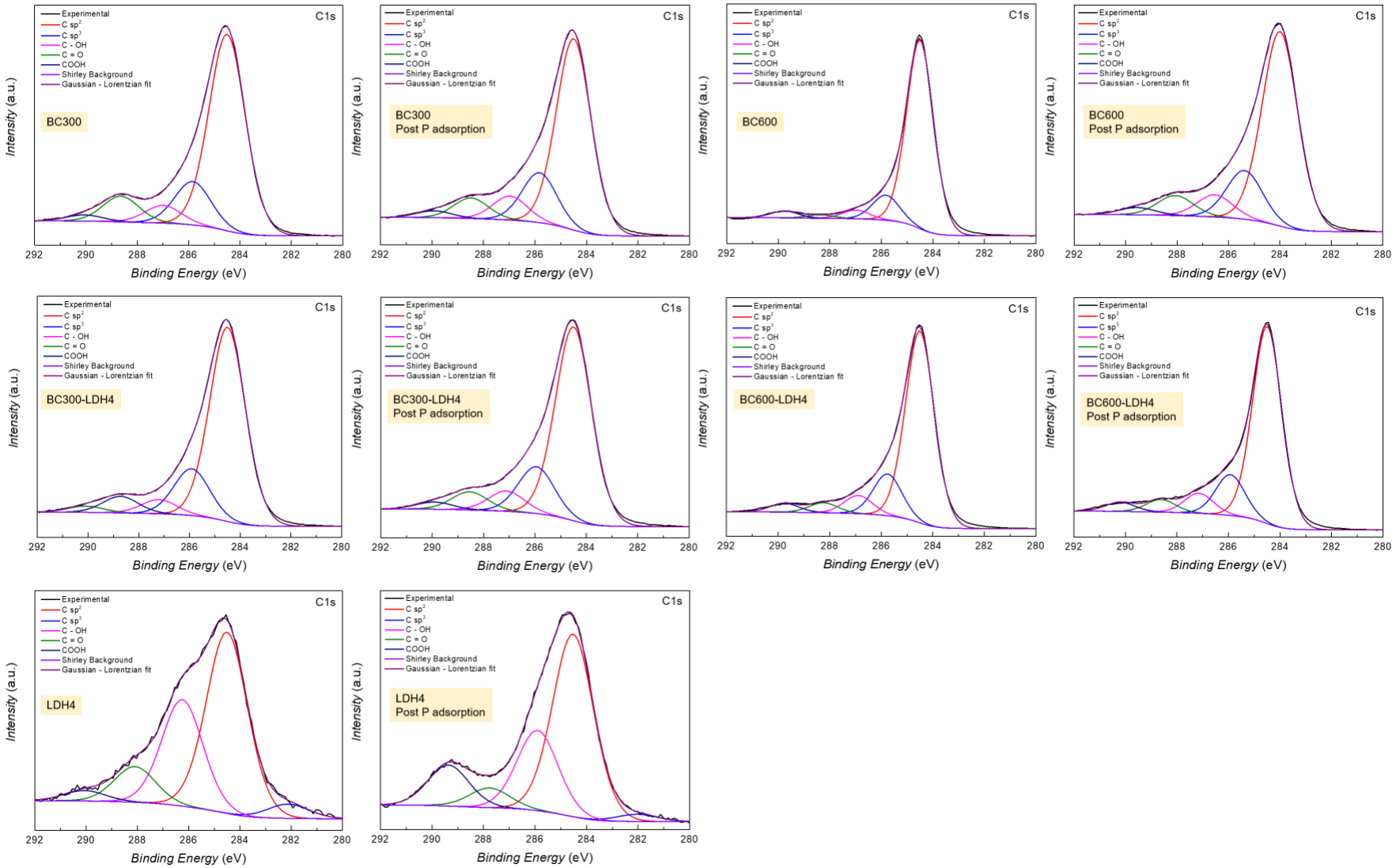

Figure S7. Deconvoluted peaks of C 1s of biochar, biochar-LDH composites and LDH before and post P adsorption.

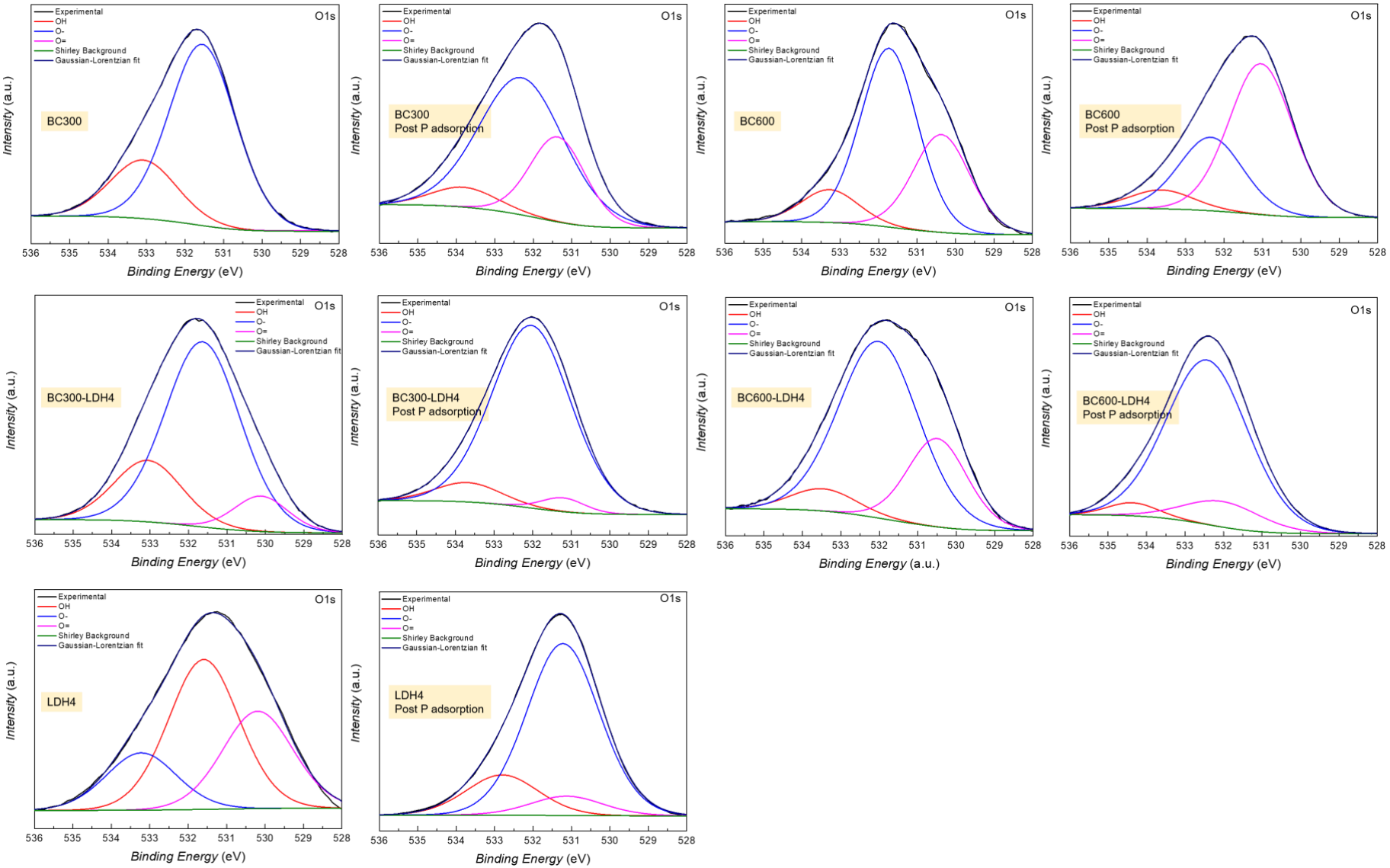

Figure S8. Deconvoluted peaks of O 1s of biochar, biochar-LDH composites and LDH before and post P adsorption.

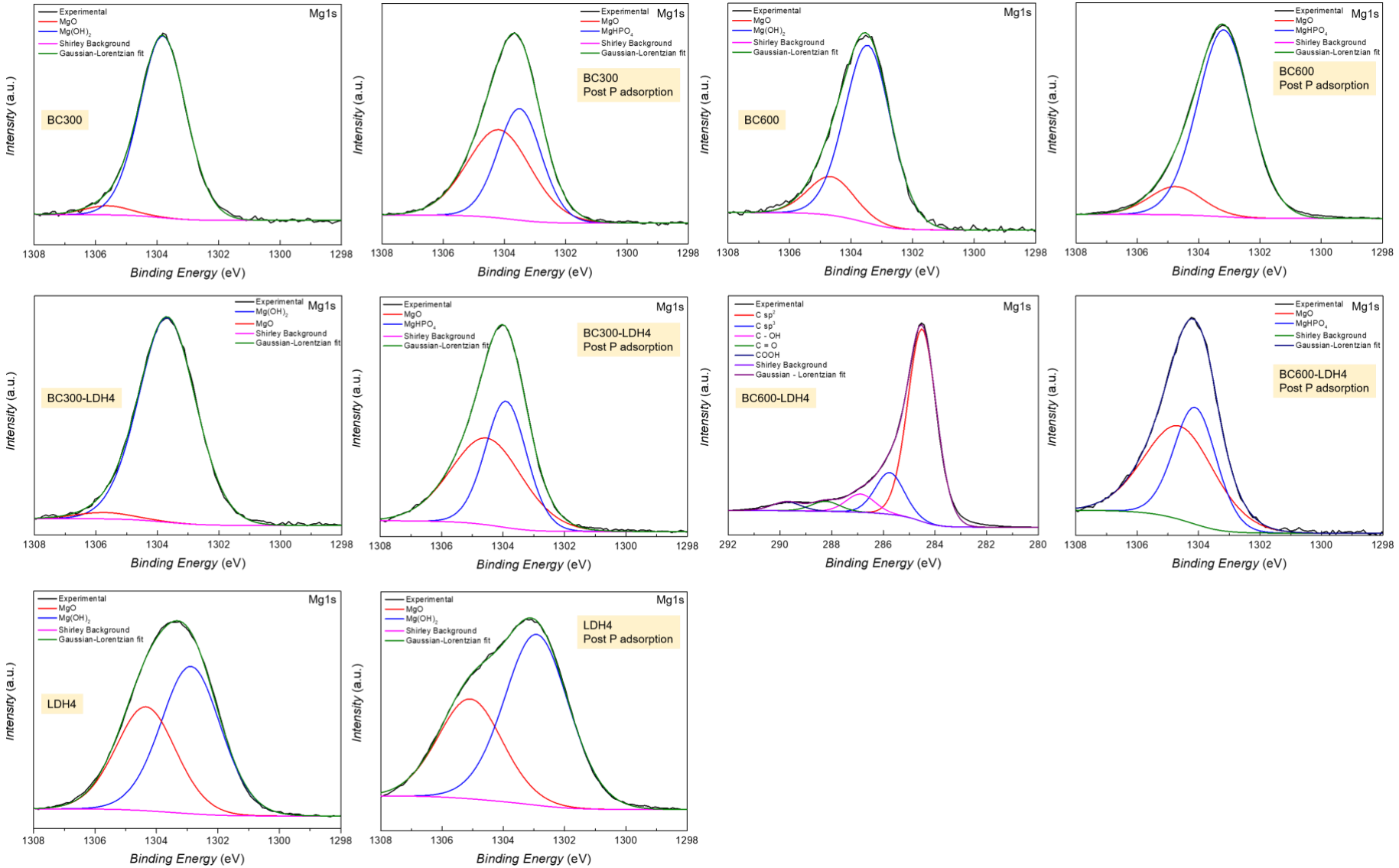

Figure S9. Deconvoluted peaks of Mg 1s of biochar, biochar-LDH composites and LDH before and post P adsorption.

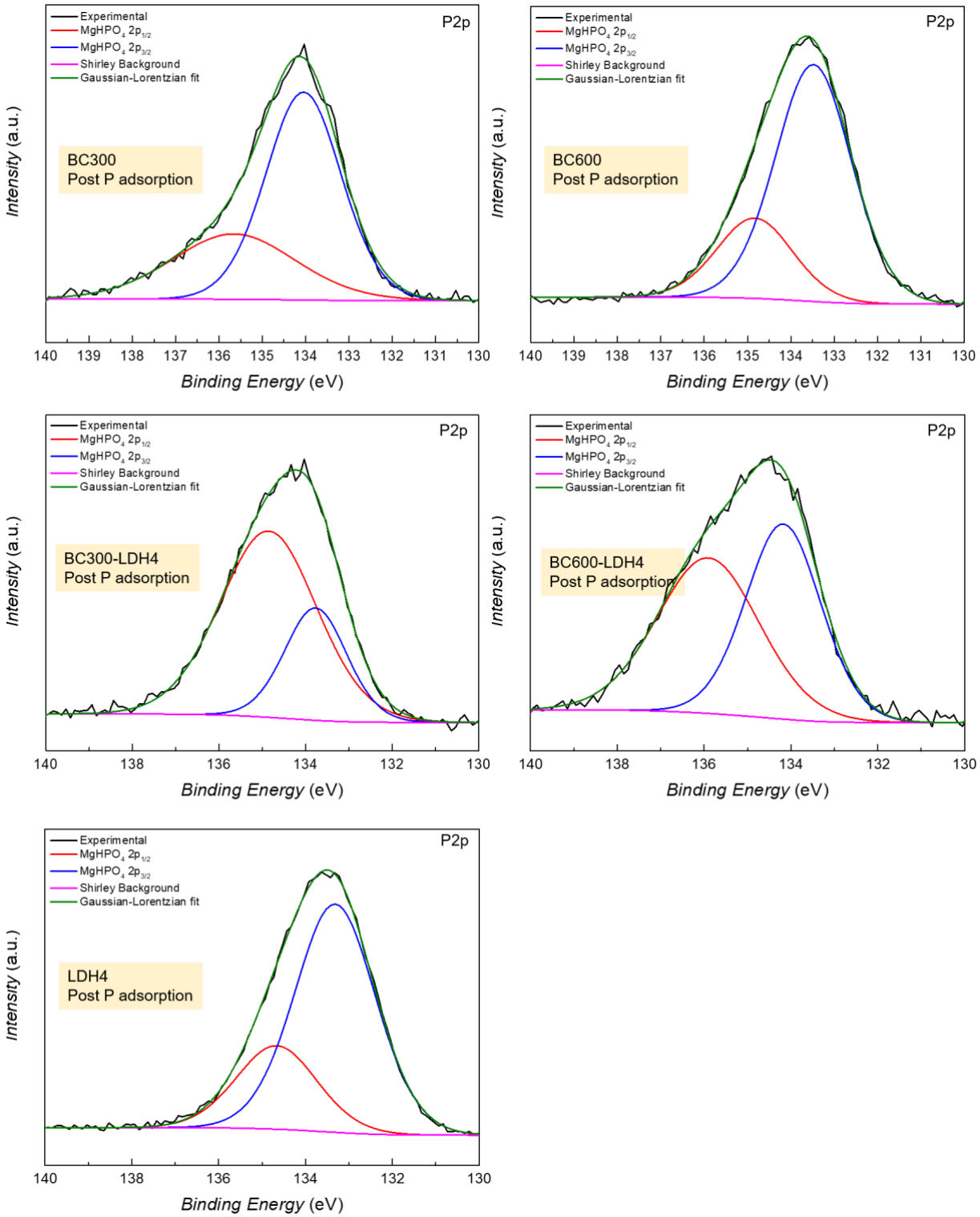

Figure S10. Deconvoluted peaks of P 2p of biochar, biochar-LDH composites and LDH before and post P adsorption.

CHAPTER 2

Phosphorus-loaded MgAl-LDH-biochar composites as a potential phosphate fertilizer for maize growth in acidic soil

To be submitted to Chemosphere journal

Phosphorus-loaded MgAl-LDH-biochar composites as a potential phosphate fertilizer for maize growth in acidic soil

Ana María Villarreal Barrera[a,b], Evanise Penido[a], Aline do Amaral Leite[a], Andres Olaya Montes[a,c], Thiago Costa Viana[a], Daniela Dourado Leal Quiroz[a], Giovana Pereira Nunes[a], Jairo Tronto[d], Leônidas Carrijo Azevedo Melo[a*].

[a] Federal University of Lavras/UFLA – Soil Science Dept., 37200-000, Lavras, Brazil
[b] University of Panama/UP – Soil and Water Dept., 772-9085, Chiriqui, Panama
[c] University of Amazon – Faculty of Engineering, 84358786, Caqueta, Colombia.
[d] Federal University of Viçosa / UFA - Institute of Exact and Technological Sciences, (34) 38559355, Viçosa, Brazil

*corresponding author: leonidas.melo@ufla.br

Abstract

Phosphorus (P) is an essential nutrient for plant development, but its low mobility and availability in many tropical soils limit agricultural productivity. In this study, it was evaluated the potential of MgAl layered double hydroxide (LDH) immobilized on biochar as a composite material for P loading and slow release. The LDH-biochar composites were synthesized and subsequently enriched with phosphate to create P-loaded materials. Their structural, chemical, and morphological characteristics were analyzed using XRD, FTIR, SEM-EDS, and BET surface area analysis. The materials demonstrated effective phosphate retention capacity, with the P-loaded LDH-biochar composites showing improved stability and surface properties compared to the individual components. A greenhouse experiment was conducted to assess the agronomic efficiency of the materials using maize (Zea mays L.) as a test crop. The application of P-loaded biochar and P-loaded LDH-biochar composites significantly improved maize growth compared to the P-loaded LDH treatment. Plants treated with the P-loaded LDH-biochar composite showed up to 58% higher shoot dry matter and up to 2.6 times greater P accumulation compared to the P-loaded LDH treatment, and had 12% higher shoot dry matter and 22% greater P accumulation than those treated with soluble P fertilizer. These results suggest enhanced P bioavailability and more efficient nutrient delivery to plants. The LDH-biochar composites also showed potential to reduce P fixation in soil, contributing to better nutrient use efficiency. In conclusion, the P-loaded MgAl-LDH-biochar composites represent a promising strategy for sustainable phosphorus management in agriculture, particularly in tropical soils with high P sorption capacity.

Keywords: adsorbent; recycling; alternative sources; sustainability.

Highlights

- Biochar–LDH composites show potential as slow-release P fertilizers.
- Biochar–LDH underperformed TSP in the first crop cycle but outperformed it in the second.

- BC300–LDH had a strong residual effect, enhancing growth in the second cycle.
- P-loaded biochar and LDH–biochar composites improved soil chemical properties.
- P-doped LDH alone had limited agronomic effectiveness in both crop cycles.

1. Introduction

Phosphorus (P) is an essential nutrient for plant growth and cannot be substituted by any other element (Neset and Cordell, 2012). It plays a critical role in crop growth and development, constituting 0.2–0.8% of plant tissue. Phosphorus is a key component of vital biomolecules such as nucleic acids, enzymes, ATP, ADP, and phospholipids (Nesme et al., 2018). Plants absorb P primarily as orthophosphates and the availability in soil is influenced by factors including soil pH, organic matter content, water availability, and the root microbiome (Matoso et al., 2023).

Globally, phosphate fertilizer sources are gradually being depleted especially because they are non-renewable and difficult to recover (Illakwahhi et al., 2024; Jupp et al., 2021; Niu et al., 2024). In tropical soils, high doses of readily soluble P fertilizers are often applied to maintain sufficient plant-available P. While this practice enhances plant nutrition, it significantly increases the cost of P fertilization (Ibrahim et al., 2022). Yet, low concentrations of P in water bodies can cause serious environmental problems (Liu et al., 2021; Akinnawo, 2023), which is costly to remediate and require the development of effective technologies that could be reused in agriculture. These challenges underscore the need for sustainable alternatives to manage P globally.

Recovering P from alternative sources offers a promising approach to recycling and reusing this essential nutrient, thereby reducing reliance on finite mineral reserves. Phosphorus contamination in water represents a significant environmental hazard that, if not properly managed, can lead to severe ecological consequences. Even a small excess of P in water as low as 0.02 mg L^{-1} can trigger eutrophication in aquatic ecosystems, causing harmful algal blooms and hypoxia. These blooms pose risks to human health due to the release of cyanotoxins and substantially increase water treatment costs (Li et al., 2016a).

Addressing the challenges of P fertilizer sustainability and mitigating its environmental impacts requires urgent and innovative solutions, including recovering P from water sources (Jahan et al., 2025; Zhang et al., 2025b). Adsorption of P from aqueous solutions is as an effective recovery method, valued for its high efficiency, operational simplicity, and potential

recycling (Biswas et al., 2024; Wang et al., 2024; Yi et al., 2024). However, despite the development of various adsorbents, practical implementation often encounters challenges, such as high production costs, limited reusability, and inefficiencies in recovery process (Wan et al., 2017; Xu et al., 2018). In this context, biochar has emerged as a promising and sustainable alternative. Studies have demonstrated its potential as an ecological and cost-effective adsorbent, offering great potential due to its favorable properties, such as a high surface area, ease of production, and straightforward application (Takaya et al., 2016).

Biochar has a porous and aromatic structure that provides biological resistance and thermal stability. Its large specific surface area and high thermal stability have made biochar a subject of extensive research for its adsorption potential (Yu et al., 2016; Son et al., 2018; Yang et al., 2018). The properties of biochar vary depending on the type of biomass used and other production factors, leading to differences in pH, elemental composition, aromaticity, and functional group content (Kloss et al., 2012; Munsanda et al., 2018). However, biochar generally exhibits a lower capacity for adsorbing anions compared to other adsorbents (Xu et al., 2018; Yin et al., 2018). Despite this limitation, biochar's versatility and ability to interact with other minerals offer pathways for improving its adsorption capacity. Surface modification to enhance anion adsorption has therefore emerged as a key challenge in advancing biochar as an efficient P adsorbent (Najafi et al., 2018).

Layered double hydroxides (LDHs) are multifunctional anionic minerals composed of positively charged metal hydroxide layers formed by divalent or trivalent cations, interlayer anions, and water molecules (Yang et al., 2019). In recent years, LDHs have gained attention as potential adsorbents due to their unique structure (Brahma et al., 2025; Gumus et al., 2024; Riaz et al., 2024). They consist of stacked, positively charged mixed-metal hydroxide layers intercalated with water molecules and various exchangeable anionic species. This structural arrangement makes LDHs highly efficient anion exchangers, capable of sequestering toxic anions from bulk solutions (Bernardo et al., 2018). Multiple mechanisms contribute to the removal of contaminants by LDHs, including van der Waals forces, electrostatic attraction, ion exchange, and hydrogen bonding (Yang et al., 2019). Studies developed by Ji et al., (2017) have demonstrated that LDH intercalates exhibit remarkable adsorption capacities for various anionic contaminants. Combining LDHs with biochar presents a promising strategy for creating biochar-mineral composites with enhanced adsorption performance.

The combination of biochar and LDH significantly increases the number of oxygen functional groups on the LDH sheets, enhancing hydrogen bonding interactions and improving the adsorption performance for anionic organic contaminants (Zhang et al., 2014). This approach also enhances phosphate adsorption by improving particle stability, pore characteristics, surface active sites, functional group density, and the recoverability of the resulting composites (Yang et al., 2019). Consequently, several studies have reported the synergistic effects of biochar-LDH modifications in enhancing phosphate removal from aqueous solutions (Huang et al., 2024; Ihsanullah et al., 2024; Qing et al., 2024). Given the challenges associated with reusing many adsorbents, recent research has focused on utilizing the material obtained from P removal by biochar-LDH composites (Najafi et al., 2018; Azimzadeh et al., 2021). However, in agricultural practices, extensive investigations into the role of such biochar-LDH composites after adsorption in promoting plant growth remain limited (Buates and Imai, 2021).

In this context, these composites could serve as potential fertilizers after removing P from aqueous solutions. However, while recent studies have focused on the primary mechanisms of P adsorption, fewer have examined P desorption or the efficiency of P-loaded biochar-LDH composites as fertilizers for plant growth. In our previous study (Villarreal et al., unpublished data), we investigated the preparation of various types of biochar-LDH composites, emphasizing the influence of biochar and LDH doses on the mechanisms of phosphate adsorption. Analyses were also carried out on the soil and the plant after each crop to determine the effect of the materials loaded with P on the physical-chemical and biological characteristics (phosphatase activity) with the aim of understanding the behaviour of these materials with respect to the release of P and its consequent release that intervenes in the development of the maize crop. Therefore, the present study aims to evaluate the desorption characteristics of P adsorbed by biochar-LDH composites and assess their potential as fertilizers for maize growth under tropical soil conditions.

2. Materials and Methods

2.1 Adsorbents preparation

For biochar production, eucalyptus sawdust was sourced from a local sawmill in Lavras, Minas Gerais, Brazil. The biomass was impregnated with 10% magnesium (w/w) using $Mg(OH)_3$, following the methods described by Li et al. (2016b) and Novais et al. (2018). Impregnation was carried out in a closed-chamber ball mill (Marconi MA350, Brazil) for 30 minutes. Further details on biomass preparation and impregnation can be found elsewhere (Villarreal et al. unpublished data). Biochar was produced by pyrolyzing the eucalyptus sawdust at two target temperatures: 300 °C and 600 °C, designated as BC300 and BC600, respectively. Pyrolysis was performed in an adapted laboratory-scale muffle furnace, with a heating rate of 5 °C per minute and a holding time of one hour at the target temperature. The samples were allowed to cool slowly to room temperature (25 °C) before the furnace was opened. After pyrolysis, the biochars were sieved through a 100-mesh screen and stored in a desiccator to prevent moisture absorption.

The LDH used in this study was synthesized as magnesium/aluminum layered double hydroxide intercalated with carbonate anions (Mg-Al-CO_3-LDH). Following the procedure described by Pavan et al. (2000), the salt solution was slowly dripped into a solution containing the interlayer anion and NaOH, employing the co-precipitation method. The synthesis was conducted under constant stirring at a controlled temperature of 35 °C and variable pH. The resulting solid samples were collected, washed with distilled water, and dried in a vacuum desiccator. The LDH prepared for the biochar-LDH composites was designated as LDH, corresponding to Mg-Al-CO_3-LDH with a molar ratio of M(II):M(III) = 4:1 (Mg/Al). After synthesis, LDH was calcined in the presence of molecular oxygen. This Mg/Al molar ratio was chosen based on our previous study (Villarreal et al. unpublished data), which indicated it as the most effective for P adsorption.

The biochar-LDH composites were synthesized via a dry method using a Marconi MA350 ball mill for 30 minutes. The composites were prepared in a ratio of 80% biochar (BC300 or BC600) and 20% LDH.

2.2 *Adsorption-Desorption study*

The adsorption-desorption of P was conducted following the procedure outlined by Li et al. (2016b), with modifications to quantify the P desorbed under laboratory conditions. Biochar,

LDH, and biochar-LDH composites were used to adsorb P from a solution containing 400 mg L^{-1} of P. The P concentration chosen for the adsorption/desorption experiment was based on the results of the adsorption isotherms, considering the maximum P adsorption capacity of the materials. The dosage for the biochars and composites was 5 g L^{-1} of solution, while for LDH the dosage was 1 g L^{-1} of solution. The mixtures were stirred at 120 rpm for 24 hours. After adsorption, the materials were separated from the solution by filtration using filter papers. The supernatants were analyzed for P concentration using inductively coupled plasma optical emission spectroscopy (ICP-OES, Spectro, Blue, Germany) to determine the levels of P adsorbed onto the materials. The filter papers containing the materials that had been in contact with the P solution (referred to as P-loaded) were oven-dried at 65 °C until constant mass to carry out the desorption study.

For de desorption experiments, 50 mg for P-loaded biochars and biochar-LDH composites, and 10 mg for P-loaded LDH were placed in contact with 10 mL of different solutions separately: Mehlich-1 solution (0.025 mol L^{-1} H_2SO_4 + 0.05 mol L^{-1} HCl), 2% citric acid, 0.01 mol L^{-1} $CaCl_2$, and deionized water. These amounts (mg) of the materials correspond to the results of the dose experiment for the adsorbent materials. The P released into each solution supernatant was measured using ICP-OES. The percentage of desorbed P was calculated by determining the difference between the initial and final P concentrations for each material. The desorption rate was then calculated by dividing the amount of P desorbed by the amount of P adsorbed.

2.3 Pot experiment

The pot experiment was carried out in a greenhouse at the Federal University of Lavras (Minas Gerais State, Brazil). The experiment involved soil fertilization with P-loaded biochar, LDH4, and biochar-LDH composites, resulting in seven treatments, including five P-loaded adsorbent materials (BC300, BC600, LDH, BC300-LDH, and BC600-LDH), and triple superphosphate (TSP) and a No-P control treatment, which served as positive and negative controls, respectively. These materials were applied to supply the recommended P dose for pot experiments (200 mg P kg^{-1}, as per Novais et al., 1991), calculated based on the P adsorbed in each material (Q_m) (Table S1), and total P content of TSP. The treatments were arranged in a completely randomized design with four replicates, totaling 28 experimental units.

Soil samples were collected from a depth of 0 to 30 cm in an Oxisol (sandy loam) from a native forest area in Itumirim, Minas Gerais, Brazil (21°17′16″ S, 44°48′07″ W). Prior to the experiment, the soil was air-dried and passed through a 2-mm sieve for chemical and physical characterization (Table S2) following the methods of analysis of AOAC international (Kane, 2023)

The soil was analyzed for available P, potassium (K), iron (Fe), zinc (Zn), manganese (Mn), and copper (Cu) using the Mehlich-1 method. The extractant used in Mehlich-1 method is a dilute acid mixture of 0.05 mol L^{-1} hydrochloric acid (HCl) and 0.0125 mol L^{-1} sulfuric acid (H_2SO_4).

Other chemical properties measured included pH in water (1:2.5 w/v), by agitating the samples for 30 minutes. Exchangeable calcium (Ca), magnesium (Mg), and aluminum (Al) using 1.0 mol L^{-1} KCl. A soil sample was mixed with the KCl solution and the mixture was shaken to allow potassium ions (K^+) to displace the exchangeable cations from the soil cation exchange sites. After shaking, the suspension was filtered to separate the liquid extract. The concentrations of Ca^{2+}, Mg^{2+}, and Al^{3+} in the filtrate were analyzed using ICP-OES.

Organic matter content determined with $Na_2Cr_2O_7$ and H_2SO_4, which involved oxidizing soil organic carbon with a dichromate solution in a highly acidic environment. The potential acidity (H + Al) was determined using the SMP-buffer solution method. Remaining P was quantified after reacting 60 mg L^{-1} of P with a 0.01 mol L^{-1} $CaCl_2$ solution in 2.5 g of soil. Boron (B) was measured colorimetrically following extraction with hot water, while sulfate ($S\text{-}SO_4$) as available sulfur was determined by ICP-OES after extraction with a 500 mg L^{-1} calcium phosphate solution.

Maize (simple hybrid seed) was used as plant test. Two cultivation cycles of 21 days were performed in the same pot, with an interval of 20 days considering the harvest of the first cycle and planting of the second cycle. The second cultivation cycle of maize was performed to assess the residual effects of the treatments from the first cultivation. A short cultivation cycle was established due to the small volume of soil used in the pots.

After soil characterization, pots were filled with 1 kg of soil. In the first plantting, each pot received the assigned treatments along with a basic fertilization regimen. A nutrient solution was applied to all treatments, providing the following nutrients per pot (in mg): N from KNO_3 and $(NH_4)_2SO_4$ (50 mg), S from $(NH_4)_2SO_4$ (40 mg), K from KNO_3 (50 mg), B from H_3BO_3 (0.8 mg), Cu from $CuSO_4 \cdot 5H_2O$ (1.5 mg), Fe from $FeCl_3$ (3 mg), Mn from $MnCl_2 \cdot 4H_2O$ (3.5 mg),

Mo from $Na_2MoO_4 \cdot 2H_2O$ (0.1 mg), and Zn from $ZnSO_4 \cdot 7H_2O$ (5 mg). Following fertilization, three maize seeds were sown in each pot. Five days after germination, one seedling was selected and allowed to grow for 21 days. At the end of this period, plant height and stem diameter were recorded, and the plants were harvested. After 20 days, the second planting cycle was established in the same pots for each treatment.

For both the first and second cultivations, shoots were harvested, oven-dried at 65 ºC for 72 hours, and then ground to a particle size of less than 1.0 mm for chemical analysis. Shoot dry matter – SDM (g) and P concentration in the shoot tissues (g kg^{-1} dry weight) were determined. Briefly, 200 mg of shoot tissue was digested using a block digestion system, with the temperature progressively increased to 200 ºC over approximately 4 hours. The digestion was performed with a mixture of 6 mL of nitric acid (HNO_3) and perchloric acid ($HClO_4$) in a 2:1 ratio (4 mL HNO_3 + 2 mL $HClO_4$). After digestion, the samples were diluted to 50 mL with deionized water, and P concentration (g kg^{-1}) was measured using ICP-OES following the method of Malavolta et al. (1997). Phosphorus accumulation in the shoots (g per plant) was calculated by multiplying the P concentration by the shoot dry matter produced in each treatment.

Soil samples from each treatment in both experiments were collected for chemical and biological analysis. The soil chemical properties were characterized as previously described, and acid phosphatase activity was measured following the method of Juma and Tabatabai (1988). Briefly, the acid phosphatase activity was determined using ρara-nitrophenyl phosphate as the analogue substrate. A 1.0 g soil sample was incubated at 37°C for 1 hour with 4.0 mL of a buffer solution (pH 6.5) and 1.0 mL of p-nitrophenyl phosphate (0.025 mol L^{-1}). The reaction was stopped by adding 1.0 mL of $CaCl_2$ (0.5 mol L^{-1}). Absorbance of the yellow color developed was measured at 410 nm using a standard calibration curve of p-nitrophenyl.

3. Data analysis and statistics

Before proceeding with further analyses, the dataset was tested for normality using the Shapiro–Wilk test and for homogeneity of variance. Subsequently, the data were subjected to analysis of variance (ANOVA), and when significant ($p \leq 0.05$) treatment means were compared using Tukey's test ($p \leq 0.05$). All data analyses and statistical procedures were performed using R software with the RStudio interface

4. Results and discussion

4.1 Desorption study

The desorption of P from the P-loaded tested materials was evaluated using Mehlich-1 solution, 2% citric acid, 0.01 mol L^{-1} $CaCl_2$ solution, and distilled water (Fig. 1). Mehlich-1 and 2% citric acid solutions showed the highest P desorption percentages for all materials, likely due to the partial dissolution of LDH and biochar particles (López-Rayo et al., 2017), which is influenced by pH (Halajnia et al., 2016). BC300-LDH exhibited the highest desorption values, at 97.6% and 81.2% for Mehlich-1 and 2% citric acid solutions, respectively, followed by BC600 and BC300. This study exclusively tested acidic solutions for desorption, as the materials were intended for use in tropical, acidic soils. These acidic solutions simulate the acidification processes that occur in the rhizosphere due to the release of organic acids and the acidifying effects of fertilizer applications (Li et al., 2008). However, previous studies have reported higher phosphate removal by LDH and biochar-LDH composites when desorption was tested with basic solutions (Alagha et al., 2020). For LDH in basic solutions (e.g., 0.1 and 1.0 mol L^{-1} NaOH), the electrostatic interactions between the adsorbent and phosphate weaken due to the removal of H^+ ions, leading to anion desorption from the adsorbent sites (Ngwabebhoh et al., 2016). This mechanism makes these composites more suitable as P-fertilizers for alkaline or calcareous environments.

In both Mehlich-1 and 2% citric acid solutions, LDH showed minimal P desorption, with average values of 29.6%. Generally, lower desorption values indicate strong interactions between the adsorbent and adsorbate, which can be attributed to the high P binding energy associated with LDH surface types (Li et al., 2016b; Novais et al., 2018). Interestingly, LDH exhibited better P desorption in distilled water compared to the 0.01 mol L^{-1} $CaCl_2$ solution. Furthermore, BC300-LDH demonstrated greater P desorption in distilled water than BC600-LDH, indicating that biochar prepared at lower pyrolysis temperatures may enhance desorption in neutral conditions.

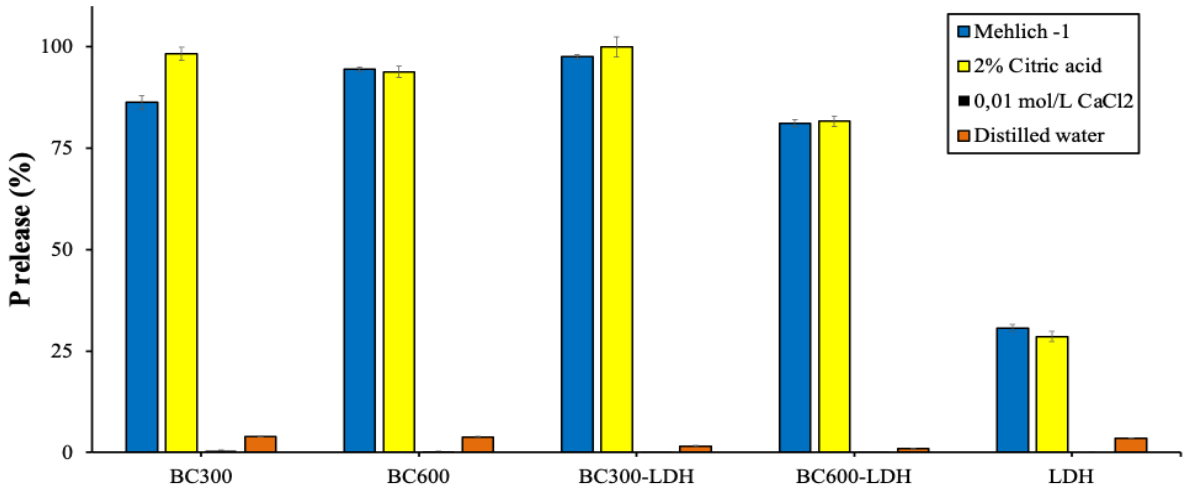

Figure 1. Percentage of desorption in Biochars, LDHs and composites. Mean values ± standard error; n= 3.

The desorption behavior of P in the composites differed in distilled water with lower percentages when compared with biochars. This suggests that only a small fraction of P is readily available, highlighting the potential of these composites for slow P release. The slow release of P from LDH and biochar-LDH composites has been previously reported in both water and acidic media (López-Rayo et al., 2017; Azimzadeh et al., 2021). Notably, the lower P availability in water does not necessarily diminish the fertilizer potential of these materials, as plants can enhance P dissolution and uptake through various mechanisms, particularly rhizosphere acidification. This process is especially beneficial in tropical soils, which have a high capacity for P adsorption (Morgan and Connolly, 2013), and, thus, less water-soluble P fertilizers might reduce the rapid P fixation in such soils.

Additionally, the percentage of P desorbed from LDH and biochar-LDH composites has been reported to decrease with successive desorption cycles, indicating the increasing difficulty of releasing P from these adsorbents over time (Hatami et al., 2018). Previous studies reported P desorption percentages for LDH-P composites ranging from 23% to 36%, suggesting that these synthesized materials could function as effective slow-release P fertilizers for soil applications (Hatami et al., 2018).

4.2 Greenhouse experiment

The potential reuse of P-loaded biochar, LDH, and biochar-LDH composites as phosphate fertilizers was evaluated in a pot experiment for the growth and nutrition of maize. In the first planting, the highest SDM production was observed in the positive control treatment using TSP, with a production of 5.6 g per plant (Fig. 2). This was followed by the biochars and biochar-LDH composites, which showed no significant differences, averaging 3.5 g of SDM per plant. This corresponds to approximately 60% of the SDM production achieved with TSP and 3.2 g higher than the production in the control without P addition. In contrast, the SDM production under LDH fertilization was the lowest among all P-loaded materials, with a production of 1.5 g per plant. This represents only 26% of the production recorded in the TSP treatment, highlighting the reduced efficacy of LDH as a P source for maize under the tested conditions. This behavior also reflects the low desorption rate observed for LDH in both neutral and acidic extractors.

P-loaded Mg-enriched biochar has been shown to be as efficient as TSP on acidic tropical soils (Nardis et al., 2021) despite containing much less soluble P. This suggests that Mg-doped biochar can function effectively as a slow-release fertilizer, making it more suitable for these soils. The preference for slow-release fertilizers in tropical soils arises from the strong interactions between the mineral fraction of the soil (Al and Fe oxides and hydroxides) and soluble P sources, which can limit the availability of P to plants (Roy et al., 2016).

In the second planting, the highest SDM production was recorded for BC300-LDH (yield of 4.2 g per plant), which was statistically equivalent to that verified for BC300, BC600, and TSP. Although statistically similar, this represents a 28% increase compared to the positive control (TSP), which produced 2.6 g. In contrast, BC600-LDH and LDH produced comparatively lower SDM values of 1.4 g and 1.9 g, respectively, being statistically similar to the negative control (without P). These outputs indicating their unsuitability as P fertilizers due to strong P retention and slow release, which limit plant growth. The biochar-LDH composites has demonstrated significant potential for efficiently removing contaminants from aqueous solutions, showing enhanced reusability compared to using biochar or LDH alone for adsorption. The porous surface characteristics of biochar provide an ideal support matrix for LDH particles, facilitating improved adsorption performance (He et al., 2019). Moreover, biochar-LDH composites are reported to possess a high water-holding capacity, which can

enhance water use efficiency in agricultural production by ensuring a consistent water supply to plants (Buates and Imai, 2021).

Aluminum, especially in its trivalent form (Al^{3+}), can be potentially toxic to crops, as excessive solubilization may lead to toxicity and reduced plant growth (Bojórquez-Quintal et al., 2017). Despite this, the current study observed low aluminum levels in plant tissues (both experiments), even without the application of P-loaded LDH materials (Tables S3 and S4). It suggests that aluminum toxicity was not a limiting factor in this experimental setup, and may be present in LDH structure within the hydroxide inlayers space (Novillo et al., 2014) and not available to plants.

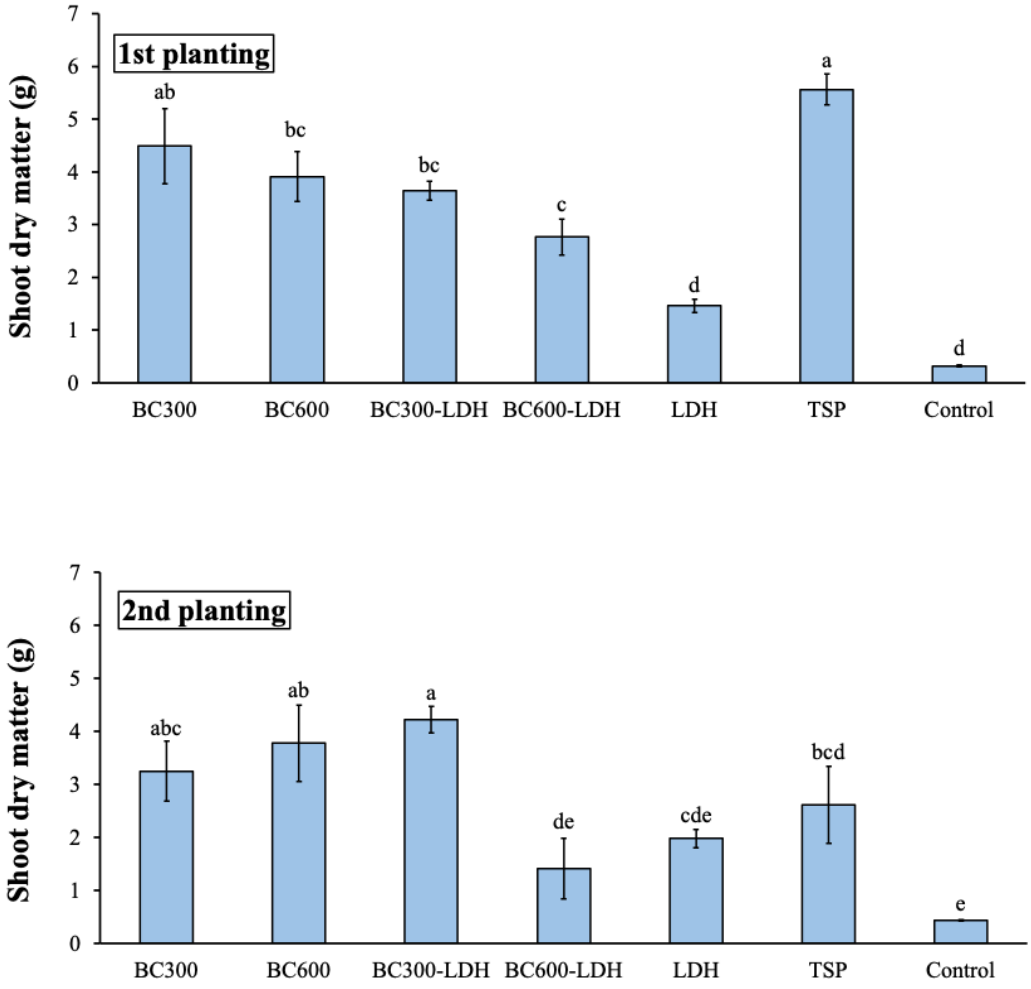

Figure 2. Maize shoot dry matter production (g) after P fertilization using biochar, biochar-LDH composites and LDH after maize growth for the first and second planting. Mean values ± standard error; n = 4. The letters above the bars compare the means of the treatments by the Tukey test ($p < 0.05$).

At first planting, significant differences ($p < 0.05$) were observed in P concentration between treatments (Fig. 3). A higher mean was observed for the TSP treatment, however differing statistically only from BC300, BC300-LDH and control. In the second planting, P concentration increased for all treatments. TSP recorded the highest P concentration at 2.4 g kg^{-1}, followed by BC600-LDH and BC300-LDH, with concentrations of 2.22 and 2.07 g kg^{-1}, respectively. BC300 and BC600 also demonstrated elevated P concentrations, at 1.79 and 1.87 g kg^{-1}, respectively. In contrast, LDH exhibited the lowest P concentration among the P-loaded materials, with a value of 1.6 g kg^{-1}, which corresponds to approximately 67% of the P concentration recorded for TSP. The consistently low efficiency of LDH observed in this study reaffirms its limited effectiveness in acidic soils.

This finding is consistent with previous research indicating that LDH performs better in calcareous soils. In such environments, the excess hydroxide ions (OH^-) in the basic soil solution weaken the interaction between the LDH adsorbent and the adsorbed phosphate, facilitating desorption of P from adsorption sites (Ngwabebhoh et al., 2016; Alagha et al., 2020). However, the present study highlights the synergistic benefits of combining biochar and LDH to form composites. These composites significantly enhanced plant productivity, particularly in treatments involving BC300-LDH. This suggests that incorporating biochar into LDH-based materials can address some of the limitations of reusing P-loaded LDH in acidic soils. Furthermore, biochar-LDH composites offer greater economic and environmental viability.

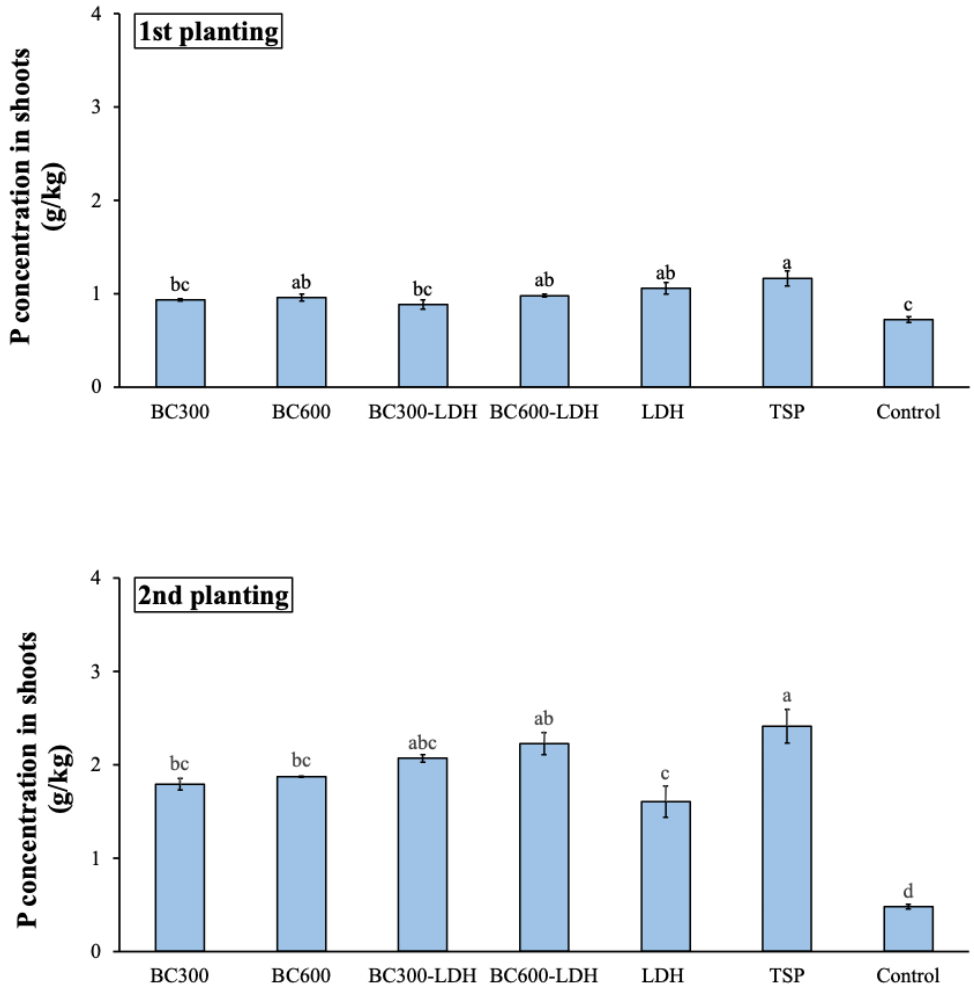

Figure 3. Phosphorus concentration (g kg^{-1}) in shoot dry matter after P fertilization using 3biochar, biochar-LDH composites and LDH after maize growth for the first and second planting. Mean values ± standard error; n = 4. The letters above the bars compare the means of the treatments by the Tukey test ($p < 0.05$). Concentration of other elements in shoot tissues are presented in tables S3 and S4.

Contrary to the P concentration in SDM, P accumulation in plants (g per plant) showed significant differences among the P-loaded materials (Fig. 4). In the first planting, the TSP treatment resulted in the highest P accumulation in maize plants at 6.5 mg per plant. Among the P-loaded materials, BC300 achieved the highest P accumulation, with 4.7 mg per plant, corresponding to 72% of the accumulation observed with TSP. This was followed by BC600 and BC300-LDH, with P accumulations of 3.7 and 3.2 mg per plant, respectively. The lowest P accumulations among the P-loaded treatments were recorded for BC600-LDH and LDH, with values of 2.5 and 1.5 mg per plant, respectively. Notably, P accumulation with LDH

corresponded to low percentage of that recorded for BC300 and BC300-LDH, underscoring its relatively lower efficiency as a P source under the conditions tested in this study.

In the second planting, the efficiency of TSP decreased, with P accumulation of 5.5 mg per plant, corresponding to 63% of the highest accumulation, which was observed for BC300-LDH with 8.7 mg per plant. Following BC300-LDH, the materials BC300, BC600, and BC600-LDH showed an average P accumulation of 5.4 mg per plant equivalent to 62% of the accumulation recorded for BC300-LDH. Notably, LDH exhibited the lowest P accumulation among all the P-loaded materials, with a value of 3.2 mg per plant. This represents only 37% of the P accumulation achieved with BC300-LDH and 58% of that observed with TSP, highlighting its relatively lower performance in the second planting as well.

The observed decrease in P accumulation during the second planting cycle for TSP compared to Mg-enriched biochars aligns with findings from previous studies (Lustosa-Filho et al., 2017). This highlights the efficiency of Mg-enriched biochars as slow-release P fertilizers, particularly in acidic and highly weathered soils, where their residual effect surpasses that of completely soluble P sources (Abdala et al., 2015). While initially effective, soluble P sources lose their efficiency over time very fast due to increased interaction with soil particles, necessitating more frequent more frequent applications at higher doses compared to biochar-based sources. Biochar also mimics the role of soil organic matter in influencing P dynamics. Studies have shown that biochar applications can reduce P sorption in soils by competing with soil minerals for P sorption sites through functional groups on the biochar surface (Ahmed et al., 2024; Qu et al., 2024). Additionally, soil P can be adsorbed by both physical and chemical mechanisms, with physically adsorbed P being more readily desorbed and thus more available to plants (Wang et al., 2021). The high porosity and large specific surface area of biochar enhance the physical adsorption of soil P, keeping it plant-accessible for extended periods (Matichenkov et al., 2017).

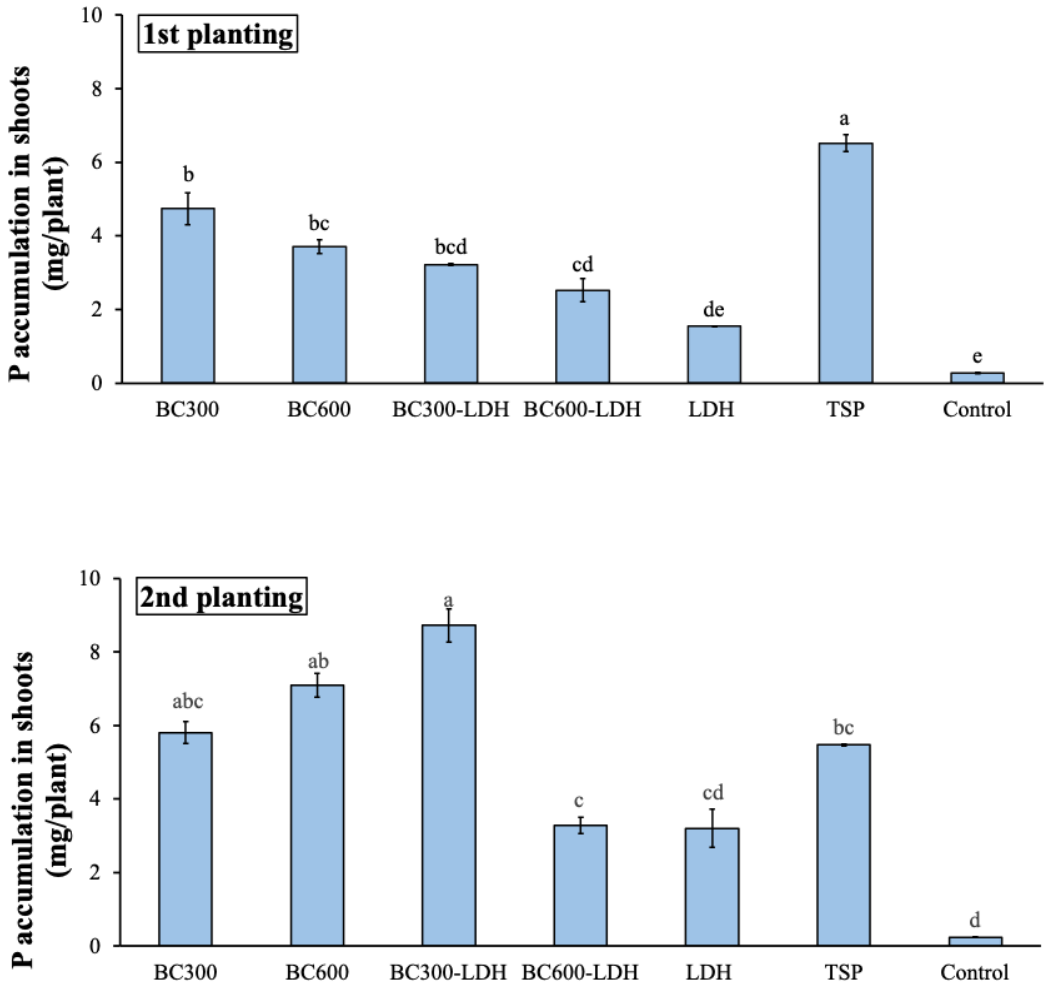

Figure 4. Phosphorus accumulation in shoot dry matter (mg per plant) after P fertilization using biochar, biochar-LDH composites and LDH after maize growth for the first and second planting. Mean values ± standard error; n = 4. The letters above the bars compare the means of the treatments by the Tukey test ($p < 0.05$).

In the first planting, soil chemical analysis revealed significant differences in available P (determined by Mehlich-1) among all treatments (Fig. 5), including the P-loaded materials and positive control (TSP). The highest P concentration in the soil was recorded for BC300, at 21.4 mg kg^{-1}, followed by BC600 and LDH, with concentrations of 15.0 and 12.9 mg kg^{-1}, respectively. BC600-LDH and BC300-LDH showed values of 11.0 and 10.4 mg kg^{-1}, respectively, while TSP recorded 11.9 mg kg^{-1}. The higher P availability from biochars can be attributed to the precipitation of Mg phosphates during biochar impregnation with Mg prior to pyrolysis (Leite et al., 2023). These Mg phosphates dissolve similarly to Ca-bound P

compounds, which are the main P forms targeted by Mehlich-1 extraction (Bortolon et al., 2011). They tipically exhibit low solubility in water but higher solubility under acidic conditions, such as the presence of citrate and other organic acids (Gu et al., 2021; Leite et al., 2024).

In contrast, available P in the soil after the second planting showed no significant differences across all treatments, including the P-loaded materials and positive control. The average P concentration across treatments was recorded as 20.6 mg kg^{-1}, indicating a stabilization of available P levels in the soil during the second planting, and resulting in higher P uptake and P concentration in maize shoots as recorded for the second cycle.

The deficiency of P in soils is a major factor to limit crop yields in many regions worldwide due to the strong sorption of P by soil minerals (Wang et al., 2021). While Mehlich-1 is widely recognized as an effective method for determining available P in soils, studies have shown that anion exchange resins often exhibit a stronger correlation with P accumulation in plants compared to Mehlich-1 (Nardis et al., 2021). This is because anion exchange resins extract P through ion-exchange reactions, closely mimicking the mechanisms by which plants acquire P. Moreover, resin-based extractors are less influenced by soil treatments, making them a more reliable option for evaluating available P in biochar-treated soils (Wang et al., 2014).

Mehlich-1, as an acidic extractor, has a reduced extraction capacity in soils with high buffering potential (Novais et al., 2015), particularly those treated with alkaline materials such as Mg-enriched biochars. The alkalinity of these materials can neutralize the acidity of the Mehlich-1 solution, diminishing its effectiveness in extracting P. This phenomenon is referred as the exhaustion of the extractor's capacity. This limitation might also have occurred in the present study in soils treated with Mg-enriched biochars.

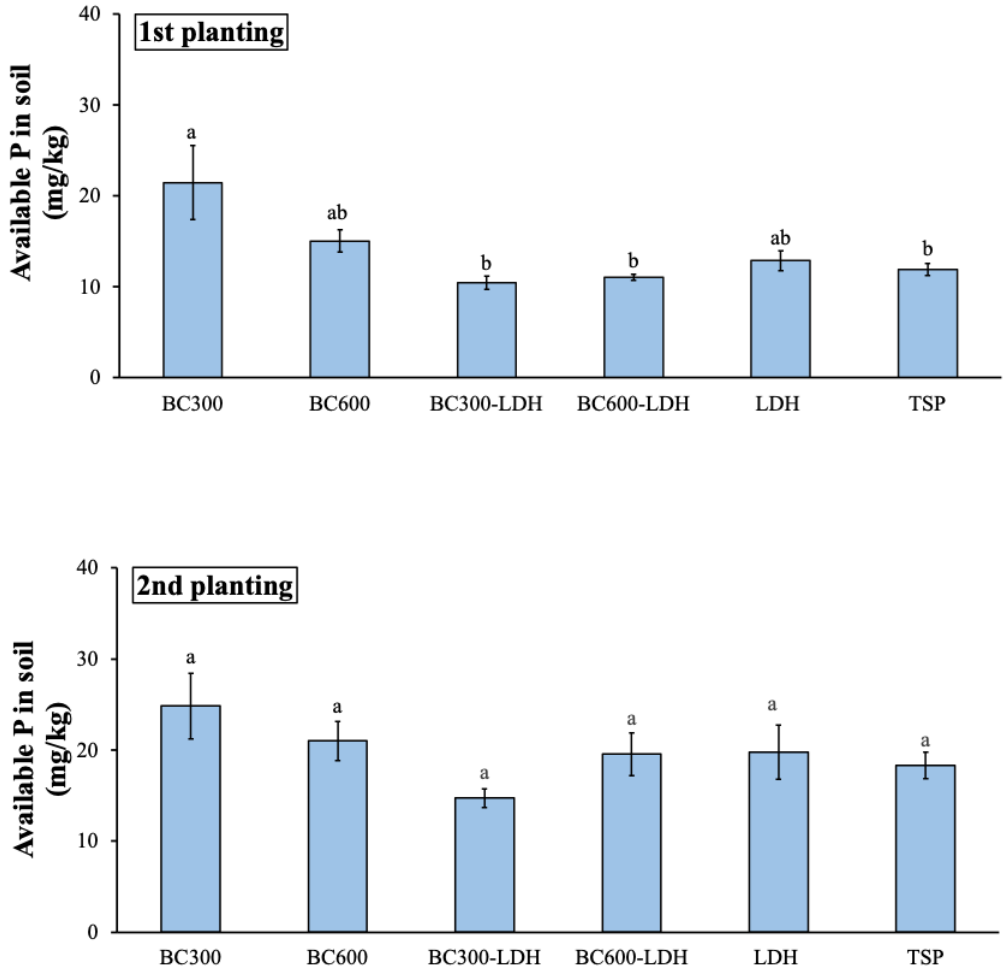

Figure 5. Available phosphorus in soil (mg/kg) after P fertilization using biochar, biochar-LDH composites and LDH and collected after maize growth for the first and second planting. Mean values ± standard error; n = 4. The letters above the bars compare the means of the treatments by the Tukey test ($p < 0.05$).

Acid phosphatase activity was highest during the first planting, with the greatest activity observed in the control treatment without P addition, reaching 760 µg PNF g^{-1} dry soil h^{-1} (Fig. 6). This was followed by the TSP and LDH treatments, which recorded 667 and 572 µg PNF g^{-1} dry soil h^{-11}, respectively. The lowest activity was observed for BC600-LDH, with a value of 311 µg PNF g^{-1} dry soil h^{-1}. Intermediate values were recorded for BC300, BC600, and BC300-LDH, which exhibited average activities of approximately 446 µg PNF g^{-11} dry soil h^{-1}.

In the second planting, acid phosphatase activity decreased across all treatments, regardless of the P source or its application. The highest activity was observed for the TSP

treatment, with 378 µg PNF g^{-1} dry soil h^{-1}, followed by the LDH treatment at 341 µg PNF g^{-1} dry soil h^{-1}. The lowest activity levels were recorded for the BC600-LDH and BC300-LDH composites, at 140 and 202 µg PNF g^{-1} dry soil h^{-1}, respectively. The biochar treatments exhibited intermediate activity levels, averaging 251 µg PNF g^{-1} dry soil h^{-1}.

Acid and alkaline phosphatases play a key role in converting organically bound P into soluble forms, thus enhancing P cycling in soils (Yang and Lu, 2022). In this study, the highest enzyme activity was observed in the TSP treatment, the fully soluble P source. This contrasts with findings from other research, where higher acid phosphatase activity was recorded for Mg-enriched biochar (Leite et al., 2024). The difference may be attributed to the presence of inorganic P in biochars and LDH, which can suppress the synthesis of phosphatases (Nannipieri et al., 2011; Janes-Bassett et al., 2022).

This suggests that other mechanisms may be contributing to the P desorption process, such as the production of organic acids and proton extrusion by plants or microorganisms. These mechanisms are more likely to occur in this study, since only inorganic P sources were loaded into the biochar, and the original biomass (eucalyptus sawdust) had low ash content, possibly contributing minimal organic P to the system.

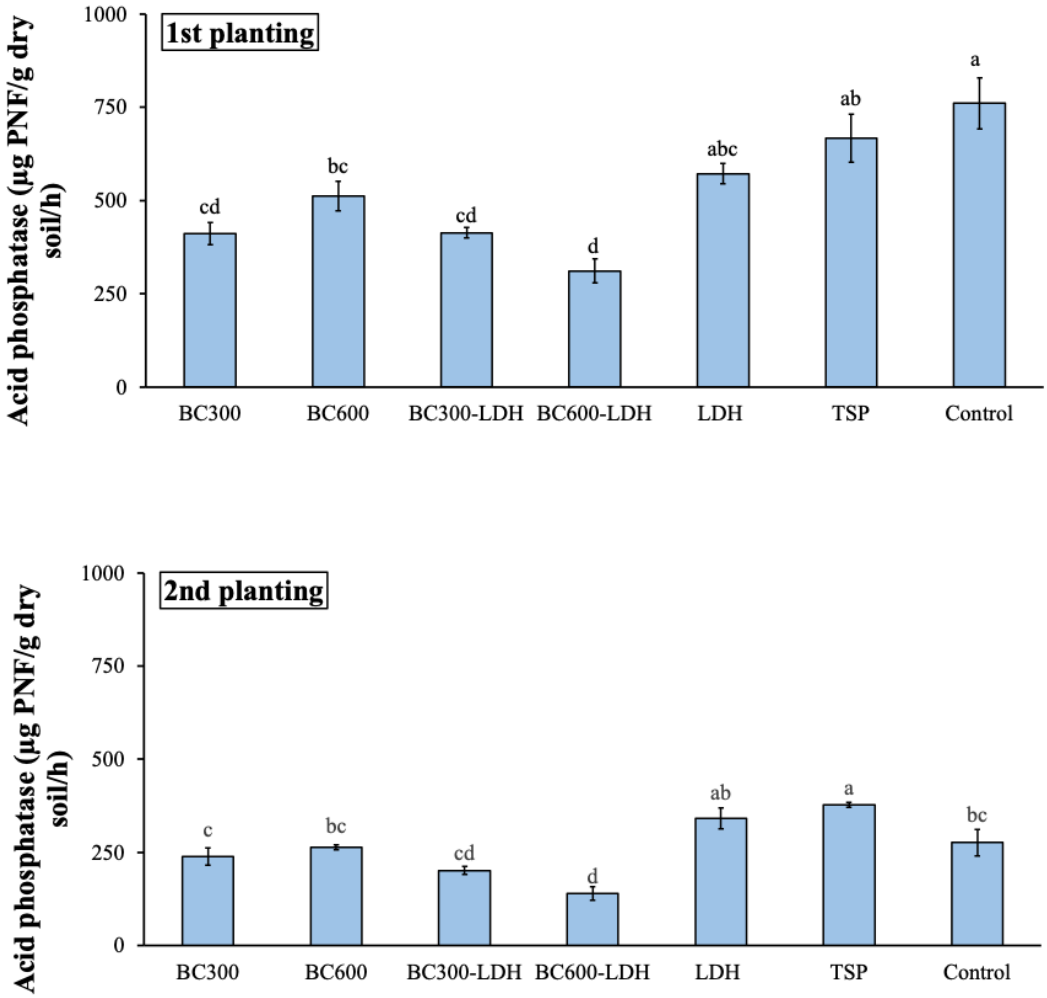

Figure 6. Phosphatase activity in soil (µg PNF g dry soil^{-1} h^{-1}) after P fertilization using biochar, biochar-LDH composites and LDH and collected after maize growth for the first and second planting. Mean values ± standard error; n = 4. The letters above the bars compare the means of the treatments by the Tukey test ($p < 0.05$).

At the beginning of the experiment, soil pH was around 5.7 (Table S2) and increased with the application of P-loaded materials, even after two cultivation cycles (Table 1). In the control treatment without P addition, soil pH remained stable at around 5.8 during the first planting but decreased to 5.1 in the second planting. In the positive control with TSP addition, soil pH increased to approximately 6.3 in both plantings. Among the P-loaded materials, the highest pH values in the first planting were observed for BC600-LDH and LDH, at 7.6 and 6.6, respectively. This trend persisted in the second planting, with both treatments maintaining the highest pH values at 6.8.

Soil pH is a critical factor influencing nutrient availability and absorption efficiency in plants, particularly in the application of phosphate fertilizers (Neina, 2019). In acidic soils (low pH), P tends to bind with elements such as Fe and Al, forming insoluble compounds that limit its availability to plants. Conversely, in alkaline soils (high pH), P can associate with Ca, similarly reducing its solubility (Johan et al., 2021; Lei et al., 2024). An optimal pH range, typically between 6 and 7, is ideal for maximizing the availability of P and other nutrients, thereby enhancing fertilizer efficiency (Bhardwaj et al., 2022; Barrow and Hartemink, 2023).

Biochar application has been shown to influence soil pH. Low-temperature biochars (300–400 °C) generally have lower ash content than high-temperature biochars (500–700 °C), as the former retain significant levels of volatile compounds and acidic functional groups, which can lower pH. In contrast, the higher ash content of high-temperature biochars is more effective in increasing soil pH (Zhang et al., 2015; Singh et al., 2022). When biochar is enriched with $Mg(OH)_2$, as in this study, its alkalizing properties are further enhanced, providing a dual benefit: pH correction and the addition of Mg to the soil (Li et al., 2022; Bolan et al., 2023).

Similar to their effect on soil pH, the application of P-loaded materials increased soil Mg levels when compared with the positive control and the control without P addition (Table S2 and Table 1). The highest Mg concentration was observed for BC600-LDH (up to 2.2 $cmol_c$ dm^{-3}), followed by LDH and BC300-LDH, both at 1.9 $cmol_c$ dm^{-3}, while the positive control recorded only 0.7 $cmol_c$ dm^{-3}. This trend persisted during the second planting for these materials. Magnesium is a critical element for photosynthesis, serving as the central component of the chlorophyll molecule. It also plays a vital role in various metabolic processes in plants, such as enzymatic activation, thereby enhancing overall soil fertility and plant health (Tränkner et al., 2018; Ishfaq et al., 2022). In tropical and acidic soils, Mg deficiency is a common issue, primarily due to high rainfall, which causes significant leaching of basic cations, including Mg^{2+}, from the soil profile (Wang et al., 2020; Chaudhry et al., 2021). Liming is a common practice in tropical soils to increase soil pH and supply Ca and Mg for plant growth. However, calcitic lime, which lacks Mg, is often applied repeatedly, neglecting Mg supplementation and inducing Mg deficiency (Li et al., 2019a; Leiva Soto et al., 2023). In this context, Mg-enriched P-biochar represents a promising alternative for these soils, addressing two critical nutrient imbalances: Mg deficiency and P limitation

Low Al levels were observed across all treatments in both plantings, with concentrations averaging approximately 0.1 cmolc dm^{-3} (Table 1). Aluminum in soil, particularly under acidic

conditions (pH < 5.5), poses significant risks to plant growth and nutrient availability. In such conditions, Al becomes soluble and can damage plant roots by inhibiting cell elongation, thereby reducing the plant's ability to access essential nutrients (Munyaneza et al., 2024; Ur Rahman et al., 2024). Regarding P availability in soil, Al can react with soluble phosphates, such as those from TSP, forming insoluble Al-P compounds. This reaction significantly reduces the effectiveness of phosphate fertilizers (Barrow et al., 2017; Zhu et al., 2021). Addressing this issue typically involves liming to raise soil pH, which reduces Al solubility. In this context, the application of P-loaded biochar-LDH composites could offer dual benefits by increasing soil pH, as observed in this study, and mitigating the negative impacts of Al on P availability.

The SB parameter increased significantly with the addition of P-loaded materials, particularly BC300-LDH, BC600-LDH, and LD, which recorded values of 3.3, 3.6, and 3.3 cmolc dm^{-3}, respectively, in the first planting (Table 1). This trend persisted in the second planting, with LDH and BC300-LDH reaching 3.9 and 3.7 cmolc dm^{-3}, respectively. The SB represents the total concentration of exchangeable base cations, primarily Ca, Mg, K, and Na, and is a critical indicator of soil fertility. Higher SB values generally indicate more fertile soils with improved nutrient availability (Havlin, 2005). In this study, the increase in SB observed with the application of LDH and biochar-LDH composites is likely attributable to the rise in Mg levels in the soil following their application.

The V% parameter also increased with the application of P-loaded materials. Before planting, V% was approximately 57%, and after the first planting, it rose to 78.9% for BC600-LDH, followed by 76.2% for LDH (Table 1). In contrast, the control treatment with TSP addition showed no change in the V% parameter, maintaining the same value of 57% as before planting. During the second planting, the V% parameter continued the same trend, with the highest value recorded for BC600-LDH of 79.6%. The V% parameter refers to the percentage of the soil cation exchange capacity that is occupied by base cations as previously mentioned. Similar to the SB parameter, V% is a critical indicator of soil fertility conditions. A higher V% reflects better nutrient availability and a more neutral soil pH, which is favorable for crop growth (Rawal et al., 2019; Kabala and Jedrzejewski, 2024). Furthermore, it has been reported that biochar can influence these parameters by interacting with soil nutrients, acting as a nutrient source, and altering nutrient cycling and reactions in the soil (Ghodake et al., 2021; Singh Yadav et al., 2023).

Remaining P also varied among treatments. In the first planting, the highest remaining P was recorded for BC600, with approximately 74.1 mg L^{-1}, followed by BC300 with 42.8 mg L^{-1} (Table 1). The lowest amount among the P-loaded treatments was observed for LDH, with concentration of 33.7 mg L^{-1}, which was similar to the control treatment without P addition, which had a remaining P value of 35.8 mg L^{-1}. In the second planting, remaining P levels were similar across all P-added treatments, ranging from 41 to 45 mg L^{-1}, except for LDH, which presented the lowest value (36.9 mg L^{-1}).

Remaining P is a soil parameter that indicates the capacity of the soil to retain P after a standard phosphate solution is added (Júlio et al., 2018). It represents the balance between P adsorption by soil particles and the amount that remains in the solution. High remaining P values suggest low P adsorption capacity, while low remaining P values indicate high adsorption capacity, where P is more likely to bind with soil components such as Fe and Al oxides (van Doorn et al., 2024). As previously discussed, the addition of biochar to soil can prevent P phosphates from being adsorbed onto soil mineral particles. Depending on the feedstock used to produce biochar, it can contain significant amounts of functional groups (e.g., carboxyl and phenolic groups) that compete with P ions for exchange sites in the soil, thereby affecting the adsorption-desorption process (Schneider and Haderlein, 2016; Li et al., 2019b; Alotaibi et al., 2021).

Table 1. Soil chemical analysis after the first maize cultivation under P dopped biochar, LDH and biochar-LDH composites.

1st Experiment							
	BC300	BC600	BC300-LDH	BC600-LDH	LDH	TSP	Control
pH	6.3 ± 0.2	6.2 ± 0.0	5.5 ± 0.0	7.6 ± 0.1	6.6 ± 0.1	6.3 ± 0.1	5.8 ± 0.0
P (mg/dm^3)	21.5 ± 4.1	15.0 ± 1.2	10.5 ± 0.7	11.0 ± 0.3	12.9 ± 1.1	11.9 ± 0.6	
Al ($cmol_c dm^3$)	0.1 ± 0.0	0.1 ± 0.0	0.1 ± 0.0	0.1 ± 0.0	0.1 ± 0.0	0.1 ± 0.0	0.1 ± 0.1
SB ($cmol_c dm^3$)	2.9 ± 0.1	3.0 ± 0.1	3.3 ± 0.1	3.6 ± 0.1	3.3 ± 0.1	2.2 ± 0.1	2.6 ± 0.1
t ($cmol_c dm^3$)	3.0 ± 0.1	3.1 ± 0.1	3.4 ± 0.1	3.7 ± 0.1	3.4 ± 0.1	2.3 ± 0.1	2.7 ± 0.1
T ($cmol_c dm^3$)	4.2 ± 0.1	4.2 ± 0.1	4.4 ± 0.1	4.5 ± 0.1	4.4 ± 0.1	3.9 ± 0.1	4.2 ± 0.2
V (%)	70.0 ± 0.9	72.2 ± 1.1	75.6 ± 1.3	78.9 ± 0.9	76.2 ± 1.0	57.2 ± 0.8	61.9 ± 0.7
M.O. ($dag\ kg^{-1}$)	1.5 ± 0.1	1.6 ± 0.1	1.8 ± 0.0	1.5 ± 0.1	1.9 ± 0.1	1.93 ± 0.2	2.3 ± 0.4
P-Rem ($mg\ L^{-1}$)	42.8 ± 3.2	74.1 ± 20.7	41.7 ± 0.6	40.6 ± 0.4	33.7 ± 1.1	42.6 ± 1.0	35.8 ± 0.3
2nd Experiment							
	BC300	BC600	BC300-LDH	BC600-LDH	LDH	TSP	Control
pH	6.4 ± 0.1	6.2 ± 0.0	5.5 ± 0.0	6.8 ± 0.1	6.8 ± 0.0	6.3 ± 0.1	5.1 ± 0.1
P (mg/dm^3)	24.8 ± 3.6	21.0 ± 2.2	14.7 ± 1.0	19.5 ± 2.3	19.8 ± 3.0	18.3 ± 1.5	
Al ($cmol_c dm^3$)	0.1 ± 0.0	0.1 ± 0.0	0.1 ± 0.0	0.1 ± 0.0	0.1 ± 0.0	0.1 ± 0.0	0.1 ± 0.0
SB ($cmol_c dm^3$)	2.9 ± 0.1	3.2 ± 0.1	3.4 ± 0.0	3.9 ± 0.1	3.7 ± 0.3	2.3 ± 0.1	3.4 ± 0.3

t ($cmol_c dm^3$)	3.0 ± 0.1	3.3 ± 0.1	3.5 ± 0.0	4.0 ± 0.1	3.8 ± 0.3	2.4 ± 0.1	3.5 ± 0.3
T ($cmol_c dm^3$)	4.1 ± 0.2	4.4 ± 0.0	4.4 ± 0.1	4.9 ± 0.2	4.8 ± 0.3	3.9 ± 0.2	5.1 ± 0.4
V (%)	70.7 ± 0.6	72.8 ± 1.6	76.2 ± 0.5	79.7 ± 1.4	76.8 ± 1.2	59.9 ± 1.2	66.9 ± 2.0
M.O. (dag kg^{-1})	2.6 ± 0.4	1.8 ± 0.1	1.8 ± 0.1	1.4 ± 0.1	1.6 ± 0.1	1.7 ± 0.1	1.4 ± 0.1
P-Rem (mg L^{-1})	44.9 ± 1.1	41.6 ± 1.2	41.5 ± 1.9	42.2 ± 2.1	36.9 ± 2.0	42.6 ± 0.8	46.4 ± 0.8

Mean values ± standard error; n= 4

Conclusion

The findings of this study suggest that both P-loaded biochar and P-loaded biochar-LDH composites produced by adsorbing P from aqueous solutions have potential as phospahte fertilizers for plant growth under tropical soil conditions. Although the composites resulted in lower dry matter production in the first crop compared to triple superphosphate (TSP), this difference was eliminated in the second crop, particularly for those made with biochar produced at a lower temperature (300 ºC). Thus, there are less production costs due to the lower energy requirements for its synthesis while providing a superior residual effect that improves soil fertility for futher cultivations considering the effects on soil pH, base saturation, nutrient inputs, among other soil attributes. Thus, these sources represent an option to partially substitute completely soluble P sources in crop fertilization, offering the additional benefit of recycling P-loaded materials. In contrast, P-loaded LDH demonstrated lower efficacy, likely due to the stronger interaction between P and LDH particles. Thus, it has potential as a slow-release P fertilizer under the conditions tested in this study. Long-term field studies are recommended to validate these materials as phosphate fertilizers in soil.

Funding

This work was funded in part by FAPEMIG, CNPQ and CAPES. The first author received a scholarship from the National Secretary of Science, Technology and Innovation of Panama (SENACYT).

Acknowledgments

The LDH's production was performed on Federal University of Viçosa, Rio Paranaiba, Brasil. We are grateful to Roberta Prado for providing assistance with the production of LDH's. We thank Silvia M. de Oliveira Longatti for her support in the soil phosphatase analysis. We thank Livia Botelho, Mariene Duarte and Geila Carvalho to assist with the analyses.

References

Abdala, D.B., Northrup, P.A., Arai, Y., Sparks, D.L., 2015. Surface loading effects on orthophosphate surface complexation at the goethite/water interface as examined by extended X-ray Absorption Fine Structure (EXAFS) spectroscopy. J Colloid Interface Sci 437, 297–303. https://doi.org/10.1016/J.JCIS.2014.09.057

Ahmed, N., Deng, Lifang, Wang, C., Shah, Z.U.H., Deng, Lansheng, Li, Y., Li, J., Chachar, S., Chachar, Z., Hayat, F., Bozdar, B., Ansari, F., Ali, R., Gong, L., Tu, P., 2024. Advancements in Biochar Modification for Enhanced Phosphorus Utilization in Agriculture. Land 2024, Vol. 13, Page 644 13, 644. https://doi.org/10.3390/LAND13050644

Akinnawo, S.O., 2023. Eutrophication: Causes, consequences, physical, chemical and biological techniques for mitigation strategies. Environmental Challenges, 12, 100733. https://doi.org/10.1016/j.envc.2023.100733.

Alagha, O., Manzar, M.S., Zubair, M., Anil, I., Mu'azu, N.D., Qureshi, A., 2020. Comparative Adsorptive Removal of Phosphate and Nitrate from Wastewater Using Biochar-MgAl LDH Nanocomposites: Coexisting Anions Effect and Mechanistic Studies. Nanomaterials 2020, Vol. 10, Page 336 10, 336. https://doi.org/10.3390/NANO10020336

Alotaibi, K.D., Arcand, M., Ziadi, N., 2021. Effect of biochar addition on legacy phosphorus availability in long-term cultivated arid soil. Chemical and Biological Technologies in Agriculture 8, 1–11. https://doi.org/10.1186/S40538-021-00249-0

Azimzadeh, Y., Najafi, N., Reyhanitabar, A., Oustan, S., Khataee, A., 2021. Effects of phosphate loaded LDH-biochar/hydrochar on maize dry matter and P uptake in a calcareous soil. Arch Agron Soil Sci 67, 1649–1664. https://doi.org/10.1080/03650340.2020.1802012

Barrow, N.J., 2017. The effects of pH on phosphate uptake from the soil. Plant Soil 410, 401–410. https://doi.org/10.1007/S11104-016-3008-9

Barrow, N.J., Hartemink, A.E., 2023. The effects of pH on nutrient availability depend on both soils and plants. Plant Soil 487, 21–37. https://doi.org/10.1007/S11104-023-05960-5

Bernardo, M.P., Guimarães, G.G.F., Majaron, V.F., Ribeiro, C., 2018. Controlled Release of Phosphate from Layered Double Hydroxide Structures: Dynamics in Soil and Application as Smart Fertilizer. ACS Sustain Chem Eng 6, 5152–5161. https://doi.org/10.1021/ACSSUSCHEMENG.7B04806

Bhardwaj, A.K., Arya, G., Kumar, R., Hamed, L., Pirasteh-Anosheh, H., Jasrotia, P., Kashyap, P.L., Singh, G.P., 2022. Switching to nanonutrients for sustaining agroecosystems and environment: the challenges and benefits in moving up from ionic to particle feeding. Journal of Nanobiotechnology 2021 20:1 20, 1–28. https://doi.org/10.1186/S12951-021-01177-9

Biswas, B., Adhikari, S., Jahromi, H., Ammar, M., Baltrusaitis, J., Torbert, A., Linhoss, J., Lamba, J., 2024. Magnesium doped biochar for simultaneous adsorption of phosphate and nitrogen ions from aqueous solution. Chemosphere 358, 142130. https://doi.org/10.1016/J.CHEMOSPHERE.2024.142130

Bojórquez-Quintal, E., Escalante-Magaña, C., Echevarría-Machado, I., Martínez-Estévez, M., 2017. Aluminum, a friend or foe of higher plants in acid soils. Front Plant Sci 8, 271596. https://doi.org/10.3389/FPLS.2017.01767

Bolan, N., Sarmah, A.K., Bordoloi, S., Bolan, S., Padhye, L.P., Van Zwieten, L., Sooriyakumar, P., Khan, B.A., Ahmad, M., Solaiman, Z.M., Rinklebe, J., Wang, H., Singh, B.P., Siddique, K.H.M., 2023. Soil acidification and the liming potential of biochar. Environmental Pollution 317, 120632. https://doi.org/10.1016/J.ENVPOL.2022.120632

Bortolon, L., Gianello, C., Welter, S., Almeida, R.G.O., Giasson, E., 2011. Simultaneous Extraction of Phosphorus, Potassium, Calcium and Magnesium from Soils and Potassium Recommendations for Crops in Southern Brazil. Pedosphere 21, 365–372. https://doi.org/10.1016/S1002-0160(11)60137-9

Brahma, D., Barman, M.P., Basak, D., Saikia, H., 2025. Prospects of layered double hydroxide (LDH)-based adsorbents for the remediation of environmental inorganic pollutants from wastewater: a critical review. Environ Sci (Camb) 11, 830–875. https://doi.org/10.1039/D4EW01039F

Buates, J., Imai, T., 2021. Application of biochar functionalized with layered double hydroxides: Improved plant growth performance after use as phosphate adsorbent. Applied Sciences (Switzerland) 11, 6489. https://doi.org/10.3390/APP11146489

Chaudhry, A.H., Nayab, S., Hussain, S.B., Ali, M., Pan, Z., 2021. Current Understandings on Magnesium Deficiency and Future Outlooks for Sustainable Agriculture. International Journal of Molecular Sciences 2021, Vol. 22, Page 1819 22, 1819. https://doi.org/10.3390/IJMS22041819

Ghodake, G.S., Shinde, S.K., Kadam, A.A., Saratale, R.G., Saratale, G.D., Kumar, M., Palem, R.R., AL-Shwaiman, H.A., Elgorban, A.M., Syed, A., Kim, D.Y., 2021. Review on biomass feedstocks, pyrolysis mechanism and physicochemical properties of biochar: State-of-the-art framework to speed up vision of circular bioeconomy. J Clean Prod 297, 126645. https://doi.org/10.1016/J.JCLEPRO.2021.126645

Gu, C., Zhou, Q., Cusick, R.D., Margenot, A.J., 2021. Evaluating agronomic soil phosphorus tests for soils amended with struvite. Geoderma 399, 115093. https://doi.org/10.1016/J.GEODERMA.2021.115093

Gumus, Z.P., Erbas, Z., Soylak, M., 2024. Layered Double Hydroxides (LDHs) for the Treatment and Determination of Pollutants in Water and Wastewater. Anal Lett 57, 1646–1665. https://doi.org/10.1080/00032719.2023.2264423

Halajnia, A., Oustan, S., Najafi, N., Khataee, A.R., Lakzian, A., 2016. Effects of Mg-Al Layered Double Hydroxide on Nitrate Leaching and Nitrogen Uptake by Maize in a Calcareous Soil. Commun Soil Sci Plant Anal 47, 1162–1175. https://doi.org/10.1080/00103624.2016.1165825

Hatami, H., Fotovat, A., Halajnia, A., 2018. Comparison of adsorption and desorption of phosphate on synthesized Zn-Al LDH by two methods in a simulated soil solution. Appl Clay Sci 152, 333–341. https://doi.org/10.1016/J.CLAY.2017.11.032

Havlin, J.L., 2005. FERTILITY. Encyclopedia of Soils in the Environment 4, 10–19. https://doi.org/10.1016/B0-12-348530-4/00228-9

He, H., Zhang, N., Chen, N., Lei, Z., Shimizu, K., Zhang, Z., 2019. Efficient phosphate removal from wastewater by MgAl-LDHs modified hydrochar derived from tobacco stalk. Bioresour Technol Rep 8, 100348. https://doi.org/10.1016/J.BITEB.2019.100348

Huang, W.H., Chang, Y.J., Lee, D.J., 2024. Layered double hydroxide loaded pinecone biochar as adsorbent for heavy metals and phosphate ion removal from water. Bioresour Technol 391, 129984. https://doi.org/10.1016/J.BIORTECH.2023.129984

Ibrahim, M., Iqbal, M., Tang, Y.T., Khan, S., Guan, D.X., Li, G., 2022. Phosphorus Mobilization in Plant–Soil Environments and Inspired Strategies for Managing Phosphorus: A Review. Agronomy 2022, Vol. 12, Page 2539 12, 2539. https://doi.org/10.3390/AGRONOMY12102539

Ihsanullah, I., Almanassra, I.W., Abushawish, A., 2024. Macadamia nut shell biochar/Mg-Al LDH composite: A sustainable solution for highly effective phosphate ion removal from water. Journal of Water Process Engineering 67, 106164. https://doi.org/10.1016/J.JWPE.2024.106164

Illakwahhi, D.T., Vegi, M.R., Srivastava, B.B.L., 2024. Phosphorus' future insecurity, the horror of depletion, and sustainability measures. International Journal of Environmental Science and Technology 21, 9265–9280. https://doi.org/10.1007/S13762-024-05664-Y/METRICS

Ishfaq, M., Wang, Y., Yan, M., Wang, Z., Wu, L., Li, C., Li, X., 2022. Physiological Essence of Magnesium in Plants and Its Widespread Deficiency in the Farming System of China. Front Plant Sci 13, 802274. https://doi.org/10.3389/FPLS.2022.802274

Jahan, N., Mahmud, U., Khan, Md.Z., 2025. Sustainable plant-soil phosphorus management in agricultural systems: challenges, environmental impacts and innovative solutions. Discover Soil 2025 2:1 2, 1–8. https://doi.org/10.1007/S44378-025-00039-2

Janes-Bassett, V., Blackwell, M.S.A., Blair, G., Davies, J., Haygarth, P.M., Mezeli, M.M., Stewart, G., 2022. A meta-analysis of phosphatase activity in agricultural settings in response to phosphorus deficiency. Soil Biol Biochem 165, 108537. https://doi.org/10.1016/J.SOILBIO.2021.108537

Ji, H., Wu, W., Li, F., Yu, X., Fu, J., Jia, L., 2017. Enhanced adsorption of bromate from aqueous solutions on ordered mesoporous Mg-Al layered double hydroxides (LDHs). J Hazard Mater 334, 212–222. https://doi.org/10.1016/J.JHAZMAT.2017.04.014

Johan, P.D., Ahmed, O.H., Omar, L., Hasbullah, N.A., 2021. Phosphorus Transformation in Soils Following Co-Application of Charcoal and Wood Ash. Agronomy 2021, Vol. 11, Page 2010 11, 2010. https://doi.org/10.3390/AGRONOMY11102010

Júlio, A.D.L., Fernandes, R. de C.R., Costa, M.D., Neves, J.C.L., Rodrigues, E.M., Tótola, M.R., 2018. A new biostimulation approach based on the concept of remaining P for soil bioremediation. J Environ Manage 207, 417–422. https://doi.org/10.1016/J.JENVMAN.2017.11.061

Juma, N.G., Tabatabai, M.A., 1988. Comparison of kinetic and thermodynamic parameters of phosphomonoesterases of soils and of corn and soybean roots. Soil Biol Biochem 20, 533–539. https://doi.org/10.1016/0038-0717(88)90069-7

Jupp, A.R., Beijer, S., Narain, G.C., Schipper, W., Slootweg, J.C., 2021. Phosphorus recovery and recycling-closing the loop. Chem Soc Rev. https://doi.org/10.1039/d0cs01150a

Kabala, C., Jedrzejewski, S., 2024. Comparison of cation exchange capacity extraction methods for soil data harmonization and soil classification in Central and East Europe. Geoderma 450, 117044. https://doi.org/10.1016/J.GEODERMA.2024.117044

Kane PF (ed) (2023) Soils. In: Latimer GW Jr. (ed) Official methods of analysis of AOAC International (22nd ed, Subchapter 8). New York: AOAC Publications. https://doi.org/10.1093/9780197610

Kloss, S., Zehetner, F., Dellantonio, A., Hamid, R., Ottner, F., Liedtke, V., Schwanninger, M., Gerzabek, M.H., Soja, G., 2012. Characterization of Slow Pyrolysis Biochars: Effects of Feedstocks and Pyrolysis Temperature on Biochar Properties. J Environ Qual 41, 990–1000. https://doi.org/10.2134/JEQ2011.0070

Lei, J., Yin, J., Chen, S., Fenton, O., Liu, R., Chen, Q., Fan, B., Zhang, S., 2024. Understanding phosphorus mobilization mechanisms in acidic soil amended with calcium-silicon-magnesium-potassium fertilizer. Science of The Total Environment 916, 170294. https://doi.org/10.1016/J.SCITOTENV.2024.170294

Leite, A. do A., Melo, L.C.A., Hurtarte, L.C.C., Zuin, L., Piccolla, C. Dela, Werder, D., Shabtai, I., Lehmann, J., 2023. Magnesium-enriched poultry manure enhances phosphorus bioavailability in biochars. Chemosphere 331, 138759. https://doi.org/10.1016/J.CHEMOSPHERE.2023.138759

Leite, A.C.A.L.R., Villarreal, A., Queiroz, D., Viana, T., de Oliveira-Longatti, S., Silva, C., de Souza Moreira, F., Lehmann, J., Melo, L., 2024. Phosphate-solubilizing bacteria increase maize phosphorus uptake from magnesium-enriched poultry manure biochar. Biol Fertil Soils 60, 421–436. https://doi.org/10.1007/S00374-024-01808-X

Leiva Soto, A., Culman, S.W., Herms, C., Sprunger, C., Doohan, D., 2023. Managing soil acidity vs. soil Ca:Mg ratio: What is more important for crop productivity? Crop, Forage & Turfgrass Management 9, e20210. https://doi.org/10.1002/CFT2.20210

Li, H., Shen, J., Zhang, F., Clairotte, M., Drevon, J.J., Le Cadre, E., Hinsinger, P., 2008. Dynamics of phosphorus fractions in the rhizosphere of common bean (Phaseolus vulgaris L.) and durum wheat (Triticum turgidum durum L.) grown in monocropping and intercropping systems. Plant Soil 312, 139–150. https://doi.org/10.1007/S11104-007-9512-1

Li, R., Wang, J.J., Zhou, B., Awasthi, M.K., Ali, A., Zhang, Z., Lahori, A.H., Mahar, A., 2016a. Recovery of phosphate from aqueous solution by magnesium oxide decorated magnetic biochar and its potential as phosphate-based fertilizer substitute. Bioresour Technol 215, 209–214. https://doi.org/10.1016/J.BIORTECH.2016.02.125

Li, G., Zhu, W., Zhu, L., Chai, X. 2016b. Effect of pyrolytic temperature on the adsorptive removal of p-benzoquinone, tetracycline, and polyvinyl alcohol by the biochars from sugarcane bagasse. Korean J. Chem. Eng., 33(7), 2215-2221. https://doi.org/10.1007/s11814-016-0067-9

Li, Y., Cui, S., Chang, S.X., Zhang, Q., 2019a. Liming effects on soil pH and crop yield depend on lime material type, application method and rate, and crop species: a global meta-analysis. J Soils Sediments 19, 1393–1406. https://doi.org/10.1007/S11368-018-2120-2

Li, F., Liang, X., Niyungeko, C., Sun, T., Liu, F., Arai, Y., 2019b. Effects of biochar amendments on soil phosphorus transformation in agricultural soils. Advances in Agronomy 158, 131–172. https://doi.org/10.1016/BS.AGRON.2019.07.002

Li, A., Ge, W., Liu, L., Qiu, G., 2022. Preparation, adsorption performance and mechanism of MgO-loaded biochar in wastewater treatment: A review. Environ Res 212, 113341. https://doi.org/10.1016/J.ENVRES.2022.113341

Liu, L., Zheng, X., Wei, X., Wei, X., Xu, Y., 2021. Excessive application of chemical fertilizer and organophosphorus pesticides induced total phosphorus loss from planting causing surface water eutrophication. Sci Rep 11, 23015. https://doi.org/10.1038/s41598-021-02521-7

López-Rayo, S., Imran, A., Hansen, H.C.B., Schjoerring, J.K., Magid, J., 2017. Layered Double Hydroxides: Potential Release-on-Demand Fertilizers for Plant Zinc Nutrition. J Agric Food Chem 65, 8779–8789. https://doi.org/10.1021/ACS.JAFC.7B02604

Lustosa Filho, J.F., Penido, E.S., Castro, P.P., Silva, C.A., Melo, L.C.A., 2017. Co-Pyrolysis of Poultry Litter and Phosphate and Magnesium Generates Alternative Slow-Release Fertilizer Suitable for Tropical Soils. ACS Sustain Chem Eng 5, 9043–9052. https://doi.org/10.1021/ACSSUSCHEMENG.7B01935

Malavolta, E., Vitti, G.C., Oliveira, S.A. de, 1997. Avaliação do estado nutricional das plantas: princípios e aplicações.

Matichenkov, V. V., Bocharnikova, E.A., Pakhnenko, E.P., Khomiakov, D.M., 2017. Effect of Si-rich substances on phosphorous adsorption by sandy soils. Environmental Science and Pollution Research 24, 24311–24317. https://doi.org/10.1007/S11356-017-0051-X

Matoso, S.C.G., Wadt, P.G.S., de Souza Júnior, V.S., Otero Pérez, X.L., 2023. Soil mineralogy-controlled phosphorus availability in soils mixed with phosphate fertiliser and biochar. Environ Technol 44, 3820–3833. https://doi.org/10.1080/09593330.2022.2074318

Morgan, J., Connolly, E., 2013. Plant-Soil Interactions: Nutrient Uptake [WWW Document]. URL https://www.nature.com/scitable/knowledge/library/plant-soil-interactions-nutrient-uptake-105289112/ (accessed 1.2.25).

Munsanda, N., Alice, M.M., Elijah, P., Samuel, C.M.N., Hendrix, C., Victor, S., Rick, L.B., 2018. Effects of biochar and gypsum soil amendments on groundnut (Arachis hypogaea L.) dry matter yield and selected soil properties under water stress. Afr J Agric Res 13, 1080–1090. https://doi.org/10.5897/AJAR2018.13123

Munyaneza, V., Zhang, W., Haider, S., Xu, F., Wang, C., Ding, G., 2024. Strategies for alleviating aluminum toxicity in soils and plants. Plant and Soil 2024 504:1 504, 167–190. https://doi.org/10.1007/S11104-024-06617-7

Najafi, N., Azimzadeh, Y., Reyhanitabar, A., Oustan, S., Khataee, A. 2018. Effects of Phosphate-Loaded LDH-Biochar and LDH-Hydrochar on Soil pH, EC and Available-P, and Maize Dry Matter and P Uptake in a Calcareous Soil. Proceedings of the International Soil Science Congress on "Environment and Soil Resources Conservation". Almaty, Kazakhstan, October 17–19.

Nannipieri, P., Giagnoni, L., Landi, L., Renella, G., 2011. Role of Phosphatase Enzymes in Soil 215–243. https://doi.org/10.1007/978-3-642-15271-9_9

Nardis, B.O., Santana Da Silva Carneiro, J., Souza, I.M.G. De, Barros, R.G. De, Azevedo Melo, L.C., 2021. Phosphorus recovery using magnesium-enriched biochar and its potential use as fertilizer. Arch Agron Soil Sci 67, 1017–1033. https://doi.org/10.1080/03650340.2020.1771699

Neina, D., 2019. The Role of Soil pH in Plant Nutrition and Soil Remediation. Appl Environ Soil Sci 2019, 5794869. https://doi.org/10.1155/2019/5794869

Neset, T.S.S., Cordell, D., 2012. Global phosphorus scarcity: identifying synergies for a sustainable future. J Sci Food Agric 92, 2–6. https://doi.org/10.1002/JSFA.4650

Nesme, T., Metson, G.S., Bennett, E.M., 2018. Global phosphorus flows through agricultural trade. Global Environmental Change 50, 133–141. https://doi.org/10.1016/J.GLOENVCHA.2018.04.004

Ngwabebhoh, F.A., Gazi, M., Oladipo, A.A., 2016. Adsorptive removal of multi-azo dye from aqueous phase using a semi-IPN superabsorbent chitosan-starch hydrogel. Chemical Engineering Research and Design 112, 274–288. https://doi.org/10.1016/J.CHERD.2016.06.023

Niu, K., Li, M., Lenzen, M., Wiedmann, T., Han, X., Jin, S., Malik, A., Gu, B., 2024. Impacts of global trade on cropland soil-phosphorus depletion and food security. Nature Sustainability 2024 7:9 7, 1128–1140. https://doi.org/10.1038/s41893-024-01385-9

Novais, R.F., Neves, J.C.L., Barros, N., de Oliveira, A.P., Garrido, W., Araujo, J., Lourenco, S., 1991. Métodos de pesquisa em fertilidade do solo [WWW Document]. URL https://www.scienceopen.com/document?vid=b3303b23-8fb4-4c2b-adff-69afa534337e (accessed 1.10.24).

Novais, S.V., Mattiello, E.M., Vergutz, L., Melo, L.C.A., de Freitas, Í.F., Novais, R.F., 2015. Loss of extraction capacity of Mehlich-1 and Monocalcium phosphate as a variable of remaining P and its relationship to critical levels of soil phosphosrus andsulfur. Rev Bras Cienc Solo 39, 1079–1087. https://doi.org/10.1590/01000683RBCS20140551

Novais, S.V., Zenero, M.D.O., Tronto, J., Conz, R.F., Cerri, C.E.P., 2018. Poultry manure and sugarcane straw biochars modified with MgCl2 for phosphorus adsorption. J Environ Manage 214, 36–44. https://doi.org/10.1016/J.JENVMAN.2018.02.088

Novillo, C., Guaya, D., Allen-Perkins Avendaño, A., Armijos, C., Cortina, J.L., Cota, I., 2014. Evaluation of phosphate removal capacity of Mg/Al layered double hydroxides from aqueous solutions. Fuel 138, 72–79. https://doi.org/10.1016/J.FUEL.2014.07.010

Pavan, P.C., Crepaldi, E.L., Valim, J.B., 2000. Sorption of Anionic Surfactants on Layered Double Hydroxides. J Colloid Interface Sci 229, 346–352. https://doi.org/10.1006/JCIS.2000.7031

Qing, Z., Qin, Q., Wang, L., Jiang, C., Yang, Z., Liu, Y., Zhang, S., Chen, J., 2024. Rapid and efficient removal of phosphate by La-doped layered double hydroxide/biochar from aqueous solution. New Journal of Chemistry 48, 3208–3220. https://doi.org/10.1039/D3NJ05213C

Qu, J., Peng, W., Wang, M., Cui, K., Zhang, J., Bi, F., Zhang, G., Hu, Q., Wang, Y., Zhang, Y., 2024. Metal-doped biochar for selective recovery and reuse of phosphate from water: Modification design, removal mechanism, and reutilization strategy. Bioresour Technol 407, 131075. https://doi.org/10.1016/J.BIORTECH.2024.131075

Rawal, A., Chakraborty, S., Li, B., Lewis, K., Godoy, M., Paulette, L., Weindorf, D.C., 2019. Determination of base saturation percentage in agricultural soils via portable X-ray fluorescence spectrometer. Geoderma 338, 375–382. https://doi.org/10.1016/J.GEODERMA.2018.12.032

Riaz, S., Rehman, A. ur, Akhter, Z., Najam, T., Hossain, I., Karim, M.R., Assiri, M.A., Shah, S.S.A., Nazir, M.A., 2024. Recent advancement in synthesis and applications of layered double hydroxides (LDHs) composites. Materials Today Sustainability 27, 100897. https://doi.org/10.1016/J.MTSUST.2024.100897

Roy, E.D., Richards, P.D., Martinelli, L.A., Coletta, L. Della, Lins, S.R.M., Vazquez, F.F., Willig, E., Spera, S.A., VanWey, L.K., Porder, S., 2016. The phosphorus cost of agricultural intensification in the tropics. Nature Plants 2016 2:5 2, 1–6. https://doi.org/10.1038/nplants.2016.43

Schneider, F., Haderlein, S.B., 2016. Potential effects of biochar on the availability of phosphorus — mechanistic insights. Geoderma 277, 83–90. https://doi.org/10.1016/J.GEODERMA.2016.05.007

Singh, H., Northup, B.K., Rice, C.W., Prasad, P.V.V., 2022. Biochar applications influence soil physical and chemical properties, microbial diversity, and crop productivity: a meta-analysis. Biochar 4, 1–17. https://doi.org/10.1007/S42773-022-00138-1

Singh Yadav, S.P., Bhandari, S., Bhatta, D., Poudel, A., Bhattarai, S., Yadav, P., Ghimire, N., Paudel, Prava, Paudel, Pragya, Shrestha, J., Oli, B., 2023. Biochar application: A sustainable approach to improve soil health. J Agric Food Res 11, 100498. https://doi.org/10.1016/J.JAFR.2023.100498

Son, E.B., Poo, K.M., Mohamed, H.O., Choi, Y.J., Cho, W.C., Chae, K.J., 2018. A novel approach to developing a reusable marine macro-algae adsorbent with chitosan and ferric oxide for simultaneous efficient heavy metal removal and easy magnetic separation. Bioresour Technol 259, 381–387. https://doi.org/10.1016/J.BIORTECH.2018.03.077

Takaya, C.A., Fletcher, L.A., Singh, S., Anyikude, K.U., Ross, A.B., 2016. Phosphate and ammonium sorption capacity of biochar and hydrochar from different wastes. Chemosphere 145, 518–527. https://doi.org/10.1016/J.CHEMOSPHERE.2015.11.052

Tränkner, M., Tavakol, E., Jákli, B., 2018. Functioning of potassium and magnesium in photosynthesis, photosynthate translocation and photoprotection. Physiol Plant 163, 414–431. https://doi.org/10.1111/PPL.12747

Ur Rahman, S., Han, J.C., Ahmad, M., Ashraf, M.N., Khaliq, M.A., Yousaf, M., Wang, Y., Yasin, G., Nawaz, M.F., Khan, K.A., Du, Z., 2024. Aluminum phytotoxicity in acidic environments: A comprehensive review of plant tolerance and adaptation strategies. Ecotoxicol Environ Saf 269, 115791. https://doi.org/10.1016/J.ECOENV.2023.115791

van Doorn, M., van Rotterdam, D., Ros, G., Koopmans, G.F., Smolders, E., de Vries, W., 2024. The phosphorus saturation degree as a universal agronomic and environmental soil P test. Crit Rev Environ Sci Technol 54, 385–404. https://doi.org/10.1080/10643389.2023.2240211

Wan, S., Wang, S., Li, Y., Gao, B., 2017. Functionalizing biochar with Mg–Al and Mg–Fe layered double hydroxides for removal of phosphate from aqueous solutions. Journal of Industrial and Engineering Chemistry 47, 246–253. https://doi.org/10.1016/J.JIEC.2016.11.039

Wang, C., Zhou, Y., Yu, F., Zhu, X., Dong, M., Li, Q., 2024. Recovery of phosphate from aqueous solution by modified biochar with concentrated seawater and its potential application as fertilizer. J Environ Chem Eng 12, 112646. https://doi.org/10.1016/J.JECE.2024.112646

Wang, Q., Xu, L., Guo, D., Wang, G., Song, X., Ma, Y., 2021. The continuous application of biochar in field: effects on P fraction, P sorption and release. Chemosphere 263, 128084. https://doi.org/10.1016/J.CHEMOSPHERE.2020.128084

Wang, T., Camps-Arbestain, M., Hedley, M., 2014. The fate of phosphorus of ash-rich biochars in a soil-plant system. Plant Soil 375, 61–74. https://doi.org/10.1007/S11104-013-1938-Z

Wang, Z., Hassan, M.U., Nadeem, F., Wu, L., Zhang, F., Li, X., 2020. Magnesium Fertilization Improves Crop Yield in Most Production Systems: A Meta-Analysis. Front Plant Sci 10, 495191. https://doi.org/10.3389/FPLS.2019.01727

Xu, K., Lin, F., Dou, X., Zheng, M., Tan, W., Wang, C., 2018. Recovery of ammonium and phosphate from urine as value-added fertilizer using wood waste biochar loaded with magnesium oxides. J Clean Prod 187, 205–214. https://doi.org/10.1016/J.JCLEPRO.2018.03.206

Yang, C., Lu, S., 2022. Straw and straw biochar differently affect phosphorus availability, enzyme activity and microbial functional genes in an Ultisol. Science of The Total Environment 805, 150325. https://doi.org/10.1016/J.SCITOTENV.2021.150325

Yang, F., Zhang, S., Sun, Y., Tsang, D.C.W., Cheng, K., Ok, Y.S., 2019. Assembling biochar with various layered double hydroxides for enhancement of phosphorus recovery. J Hazard Mater 365, 665–673. https://doi.org/10.1016/J.JHAZMAT.2018.11.047

Yang, Yan, Sun, K., Han, L., Jin, J., Sun, H., Yang, Yu, Xing, B., 2018. Effect of minerals on the stability of biochar. Chemosphere 204, 310–317. https://doi.org/10.1016/J.CHEMOSPHERE.2018.04.057

Yi, Y., Fu, Y., Wang, Y., Xu, Z., Diao, Z., 2024. Lanthanum/iron co-modified biochar for highly efficient adsorption of low-concentration phosphate from aqueous solution. J Environ Chem Eng 12, 111876. https://doi.org/10.1016/J.JECE.2024.111876

Yin, Q., Wang, R., Zhao, Z., 2018. Application of Mg–Al-modified biochar for simultaneous removal of ammonium, nitrate, and phosphate from eutrophic water. J Clean Prod 176, 230–240. https://doi.org/10.1016/J.JCLEPRO.2017.12.117

Yu, J., Bi, X., Yu, B., Chen, D., 2016. Isoflavones: Anti-Inflammatory Benefit and Possible Caveats. Nutrients 2016, Vol. 8, Page 361 8, 361. https://doi.org/10.3390/NU8060361

Zhang, H., Voroney, R.P., Price, G.W., 2015. Effects of temperature and processing conditions on biochar chemical properties and their influence on soil C and N transformations. Soil Biol Biochem 83, 19–28. https://doi.org/10.1016/J.SOILBIO.2015.01.006

Zhang, M., Yao, Q., Lu, C., Li, Z., Wang, W., 2014. Layered double hydroxide-carbon dot composite: High-performance adsorbent for removal of anionic organic dye. ACS Appl Mater Interfaces 6, 20225–20233. https://doi.org/10.1021/AM505765E

Zhang, Y., Wang, X., Hu, Z. qiang, Xiao, Q. qing, Wu, Y., 2025. Capturing and recovering phosphorus in water via composite material: Research progress, future directions, and challenges. Sep Purif Technol 353, 128453. https://doi.org/10.1016/J.SEPPUR.2024.128453

Zhu, X., Fang, X., Wang, L., Xiang, W., Alharbi, H.A., Lei, P., Kuzyakov, Y., 2021. Regulation of soil phosphorus availability and composition during forest succession in subtropics. For Ecol Manage 502, 119706. https://doi.org/10.1016/J.FORECO.2021.119706

Supplementary material

Table S1. Amount of biochar, biochar-LDH and LDH4 used in the greenhouse experiment.

	Total P content (% of mass)	total mass added for each pot (g)
BC300	5	2
BC600	2.5	4
BC300 - LDH4	5.6	1.8
BC600 - LDH4	3.3	3
LDH4	11.0	0.9

Table S2. Physicochemical properties of the studied soil.

pH	5.7	T	4.14 $cmolc/dm^3$
P	0.01 mg/dm^3	V	59.84%
Al	0.10 $cmolc/dm^3$	m	3.89 %
H+Al	1.67 $cmolc/dm^3$	M.O	1.98 %
SB	2.48 $cmolc/dm^3$	P-rem	34.83 mg L^{-1}
t	2.58 $cmolc/dm^3$	Mg	0.48 $cmolc/dm^3$

Table S3. Nutrients concentration in shoot dry matter of maize plants (g kg^{-1}) from the first planting under P dopped biochar, LDH and biochar-LDH composites.

Nutrient (g kg^{-1})	1st Experiment						
	BC300	BC600	BC300-LDH	BC600-LDH	LDH	TSP	Control
Al	0.05 ± 0.02	0.02 ± 0.00	0.03 ± 0.00	0.03 ± 0.00	0.04 ± 0.00	0.03 ± 0.00	0.08 ± 0.01
B	0.02 ± 0.00	0.02 ± 0.00	0.02 ± 0.00	0.02 ± 0.00	0.02 ± 0.00	0.02 ± 0.00	0.04 ± 0.00
Ca	2.42 ± 0.49	2.18 ± 0.19	1.94 ± 0.06	2.05 ± 0.12	4.14 ± 0.38	3.10 ± 0.15	8.01 ± 0.46
Cu	0.00 ± 0.00	0.00 ± 0.00	0.003 ± 0.00	0.003 ± 0.00	0.004 ± 0.00	0.003 ± 0.00	0.008 ± 0.00
Fe	0.10 ± 0.04	0.06 ± 0.00	0.06 ± 0.00	0.06 ± 0.00	0.08 ± 0.00	0.05 ± 0.00	0.11 ± 0.01
K	27.5 ± 3.01	29.9 ± 2.84	29.4 ± 1.11	31.0 ± 3.51	43.9 ± 1.14	21.5 ± 1.13	35.7 ± 3.89
Mg	3.36 ± 0.45	3.44 ± 0.28	4.41 ± 0.11	4.79 ± 0.29	5.61 ± 0.24	2.55 ± 0.11	4.09 ± 0.19
Mn	0.04 ± 0.00	0.04± 0.00	0.04 ± 0.00	0.04 ± 0.00	0.07 ± 0.00	0.05 ± 0.00	0.23 ± 0.03
P	1.06 ± 0.12	0.96 ± 0.05	0.88 ± 0.05	0.92 ± 0.06	1.06 ± 0.06	1.16 ± 0.08	0.83 ± 0.11
S	1.43 ± 0.09	1.49 ± 0.15	1.64 ± 0.04	1.51 ± 0.24	2.29 ± 0.08	1.59 ± 0.04	2.99 ± 0.22
Zn	0.01 ± 0.00	0.01 ± 0.00	0.01 ± 0.00	0.01 ± 0.00	0.04 ± 0.00	0.03 ± 0.00	0.09 ± 0.00

Mean values ± standard error; n= 4

Table S4. Nutrients concentration in shoot dry matter of maize plants (g kg^{-1}) from the second planting under P dopped biochar, LDH and biochar-LDH composites.

Nutrient (g kg^{-1})	2nd Experiment						
	BC300	BC600	BC300-LDH	BC600-LDH	LDH	TSP	Control
Al	0.02 ± 0.00	0.05 ± 0.01	0.04 ± 0.00	0.02 ± 0.00	0.04 ± 0.01	0.04 ± 0.01	0.06 ± 0.02
B	0.02 ± 0.00	0.02 ± 0.00	0.04 ± 0.01	0.02 ± 0.00	0.02 ± 0.00	0.03 ± 0.00	0.02 ± 0.00
Ca	1.81 ± 0.45	1.43 ± 0.17	0.93 ± 0.10	1.17 ± 0.13	1.96 ± 0.21	3.30 ± 0.26	3.83 ± 0.52
Cu	0.00 ± 0.00	0.01 ± 0.00	0.01 ± 0.00	0.00 ± 0.00	0.01 ± 0.00	0.01 ± 0.00	0.00 ± 0.00
Fe	0.06 ± 0.00	0.06 ± 0.00	0.06 ± 0.00	0.05 ± 0.00	0.08 ± 0.00	0.09 ± 0.01	0.08 ± 0.01
K	35.9 ± 3.49	32.3 ± 2.57	28.3 ± 2.05	37.7 ± 2.49	43.5 ± 3.69	40.2 ± 0.99	34.8 ± 2.56
Mg	3.32 ± 0.40	3.40 ± 0.31	3.22 ± 0.19	4.35 ± 0.20	4.11 ± 0.17	2.80 ± 0.23	2.25 ± 0.15
Mn	0.04 ± 0.00	0.03 ± 0.00	0.03 ± 0.00	0.03 ± 0.00	0.04 ± 0.00	0.06 ± 0.00	0.09 ± 0.00
P	1.79 ± 0.06	1.87 ± 0.01	2.07 ± 0.04	2.80 ± 0.58	1.61 ± 0.17	2.17 ± 0.30	0.57 ± 0.09
S	1.37 ± 0.16	1.58 ± 0.04	1.58 ± 0.03	1.18 ± 0.43	1.90 ± 0.19	2.08 ± 0.16	1.14 ± 0.06
Zn	0.02 ± 0.00	0.03 ± 0.00	0.03 ± 0.00	0.02 ± 0.00	0.03 ± 0.00	0.06 ± 0.00	0.05 ± 0.00

Mean values ± standard error n= 4

CONCLUDING REMARKS

- This study demonstrates the clear advantages of LDH-impregnated biochar over pristine biochar for phosphate adsorption, mainly due to increased active sites and enhanced interactions with functional groups.
- Lower pyrolysis temperatures (e.g., 300 °C) improved the phosphate adsorption efficiency of Mg-enriched biochar more effectively than higher temperatures.
- P-loaded biochar and biochar–LDH composites have potential as alternative phosphate fertilizers for tropical soils. Although their slow-release behavior results in lower short-term efficiency compared to soluble fertilizers (e.g., TSP), they outperform in subsequent cropping cycles. Long-term field validation is still needed.
- LDH materials offer limited immediate P availability but are promising for slow-release applications. Despite their high P sorption capacity, their practical use is constrained by synthesis costs. Incorporating small amounts of LDH into biochar may provide a more feasible approach for P recovery and reuse in agriculture.
- Future studies should focus on long-term P desorption in soil and on optimizing field application strategies. Mg-enriched biochar also shows potential to reduce nutrient leaching, particularly nitrate and phosphate, and should be explored further for soil management applications.